TECHNISCHE
UNIVERSITÄT
WIEN
Vienna University of Technology

INSTITUT FÜR
MECHANIK UND
MECHATRONIK
Mechanics & Mechatronics

DISSERTATION

Predictive energy management of fuel cell electric trucks

ausgeführt zum Zwecke der Erlangung des akademischen Grades
eines Doktors der technischen Wissenschaften
unter der Leitung von

Associate Prof. Dipl.-Ing. Dr.techn. Christoph Hametner

am Institut für Mechanik und Mechatronik
Abteilung für Regelungstechnik und Prozessautomatisierung

eingereicht an der Technischen Universität Wien,
Fakultät für Maschinenwesen und Betriebswissenschaften

von

Alessandro Ferrara

[redacted]

Wien, am 16. März 2023

E quindi uscimmo a riveder le stelle.

– Inferno, Dante Alighieri.

Eidesstattliche Erklärung

Ich erkläre eidesstattlich, dass ich die Arbeit selbständig angefertigt, keine anderen als die angegebenen Hilfsmittel benutzt und alle aus ungedruckten Quellen, gedruckter Literatur oder aus dem Internet im Wortlaut oder im wesentlichen Inhalt übernommenen Formulierungen und Konzepte gemäß den Richtlinien wissenschaftlicher Arbeiten zitiert, durch Fußnoten gekennzeichnet bzw. mit genauer Quellenangabe kenntlich gemacht habe.

Wien, am 16. März 2023 Alessandro Ferrara

Abstract

In fuel cell electric trucks, the energy management strategy controls the operation of the fuel cell and battery systems. Besides the considerable impact on fuel consumption and driving range, properly designing this control function is essential to ensure that the powertrain components meet the lifetime requirements of long-haul transportation. Even though the literature on energy management strategies for fuel cell electric vehicles is vast, there is a fundamental research gap in studies focused on long-haul trucks, nowadays considered the most promising fuel cell application in the automotive sector.

During his doctoral studies, the author has conducted state-of-the-art investigations and addressed this gap in several publications, significantly contributing to the research on energy management strategies for fuel cell electric trucks. The present doctoral thesis describes his research on the topic and summarizes the most relevant findings. In particular, it proposes innovative energy management strategies to reduce the fuel consumption and component degradation of fuel cell electric trucks and foster their market penetration.

The main focus of this thesis is predictive energy management, a topic that will play a critical role in the development of intelligent fuel cell electric trucks. Indeed, the thesis demonstrates that implementing predictive strategies is the only effective way to achieve optimal vehicle performance in high-demanding driving cycles (for example, due to the heavy truckloads on mountain routes). In particular, considering long-term elevation forecasts is essential to anticipate driving conditions that are challenging from an energy management standpoint and achieve optimal performance.

One of the main contributions of this thesis is the development of a dual-stage control structure for predictive energy management strategies that enables achieving optimal performance even in challenging route topographies. The dual-stage structure has two advantageous characteristics. First, it can consider the elevation profile of the entire route in the energy management optimization with low computational complexity. Second, it allows the implementation of dynamic programming to find globally optimal solutions, overcoming the well-known barriers of non-causality and high computational complexity.

Moreover, the proposed predictive energy management strategy has high flexibility regarding the optimization targets. Initially, it is implemented to optimize only the fuel consumption while controlling the battery state of charge. Then, an innovative formula-

tion is presented for the simultaneous and multi-objective optimization of fuel consumption, fuel cell degradation, and battery degradation. The benefits of this predictive and health-conscious energy management strategy are assessed in real-world driving scenarios, also considering different battery sizes and degradation states. Eventually, the simulation results demonstrate the absolute superiority of the proposed strategy against standard approaches.

The thesis also proposes innovative solutions to establish synergies between the energy management strategy and other control functions from a holistic standpoint. Novel concepts are presented to significantly reduce degradation by exploiting the interaction with battery thermal management and the intelligent activation of multi-module fuel cell systems. Moreover, the co-optimization of vehicle speed and energy management using dynamic programming is proposed for optimal eco-driving, substantially reducing fuel consumption and enabling longer driving ranges to cope with the limited hydrogen refueling infrastructure.

Eventually, the innovative strategies proposed in this thesis can significantly contribute to the development and market penetration of fuel cell electric trucks thanks to lower fuel consumption and component degradation. Indeed, by adopting these strategies, truck manufacturers can achieve better performance and lower ownership costs, closing the gap with conventional diesel trucks for long-haul transportation.

Kurzfassung

In Brennstoffzellen-Elektro-Lkws regelt die Energiemanagementstrategie den Betrieb der Brennstoffzellen- und Batteriesysteme. Neben den beträchtlichen Auswirkungen auf den Kraftstoffverbrauch und die Reichweite ist die richtige Auslegung dieser Steuerungsfunktion von entscheidender Bedeutung, um sicherzustellen, dass die Komponenten des Antriebsstrangs die Anforderungen an die Lebensdauer im Fernverkehr erfüllen. Obwohl die Literatur über Energiemanagementstrategien für Brennstoffzellen-Elektrofahrzeuge sehr umfangreich ist, gibt es eine grundlegende Forschungslücke bei Studien zum Thema Langstrecken-Lkw, welcher heutzutage als die vielversprechendste Brennstoffzellenanwendung im Automobilsektor gilt.

Während seines Promotionsstudiums hat der Autor Untersuchungen nach dem neuesten Stand der Technik durchgeführt und die Forschungslücke in mehreren Veröffentlichungen aufgegriffen, wodurch er einen wesentlichen Beitrag zur Erforschung von Energiemanagementstrategien für Brennstoffzellen-Elektro-Lkw geleistet hat. Die vorliegende Dissertation beschreibt seine Forschungen zu diesem Thema und fasst die wichtigsten Erkenntnisse zusammen. Insbesondere werden innovative Energiemanagementstrategien vorgeschlagen, um den Kraftstoffverbrauch und die Bauteildegradation von Brennstoffzellen-Elektrofahrzeugen zu reduzieren und deren Marktdurchdringung zu fördern.

Das Hauptaugenmerk dieser Arbeit liegt auf dem prädiktiven Energiemanagement, einem Thema, das bei der Entwicklung von intelligenten Brennstoffzellen-Elektrofahrzeugen eine entscheidende Rolle spielen wird. In dieser Arbeit wird veranschaulicht, dass die Implementierung von prädiktiven Strategien der einzige effektive Weg ist, um eine optimale Fahrzeugleistung in anspruchsvollen Fahrzyklen, wie etwa aufgrund einer vollen Lkw-Ladung auf Bergstrecken, zu erreichen. Insbesondere die Berücksichtigung langfristiger Höhenprognosen ist von entscheidender Bedeutung, um Fahrbedingungen zu antizipieren, die aus Sicht des Energiemanagements schwierig sind, und um eine optimale Leistung zu erzielen.

Einer der Hauptbeiträge dieser Arbeit ist die Entwicklung einer zweistufigen Regelstruktur für prädiktive Energiemanagementstrategien, die es ermöglicht, auch bei anspruchsvollen Streckentopographien eine optimale Leistung zu erzielen. Die zweistufige Struktur hat zwei vorteilhafte Eigenschaften. Erstens kann sie das Höhenprofil der gesamten Strecke bei der Optimierung des Energiemanagements mit geringem

Rechenaufwand berücksichtigen. Zweitens ermöglicht sie die Implementierung der dynamischen Programmierung, um global optimale Lösungen zu finden, und überwindet damit die bekannten Hindernisse der Nicht-Kausalität und der hohen Rechenkomplexität.

Darüber hinaus bietet die vorgeschlagene prädiktive Energiemanagementstrategie eine hohe Flexibilität in Bezug auf die Optimierungsziele. Zunächst wird sie so implementiert, dass nur der Kraftstoffverbrauch optimiert wird, während der Ladezustand der Batterie geregelt wird. Anschließend wird eine innovative Formulierung für die gleichzeitige und mehrzielorientierte Optimierung des Kraftstoffverbrauchs, der Degradation der Brennstoffzelle und der Degradation der Batterie vorgestellt. Die Vorteile dieser vorausschauenden und Energiemanagementstrategie werden in realen Fahrszenarien bewertet, wobei auch unterschiedliche Batteriegrößen und Degradationszustände berücksichtigt werden. Schließlich zeigen die Simulationsergebnisse die absolute Überlegenheit der vorgeschlagenen Strategie gegenüber Standardansätzen.

In dieser Arbeit werden auch innovative Lösungen vorgeschlagen, um Synergien zwischen der Energiemanagementstrategie und anderen Regelfunktionen aus einem ganzheitlichen Blickwinkel heraus zu schaffen. Es werden neuartige Konzepte vorgestellt, um durch Ausnutzung des Zusammenspiels vom Thermomanagement der Batterie und der intelligenten Ansteuerung von Mehrmodul-Brennstoffzellensystemen die Degradation deutlich zu reduzieren. Darüber hinaus wird die Ko-Optimierung von Fahrzeuggeschwindigkeit und Energiemanagement mittels dynamischer Programmierung für ein optimales ökologisches Fahrkonzept vorgeschlagen. Dies ermöglicht eine erhebliche Reduzierung des Kraftstoffverbrauchs sowie eine Erhöhung der Reichweite, wodurch das Problem der begrenzten Infrastruktur für die Wasserstoffbetankung bewältigt wird.

Letztendlich können die in dieser Arbeit vorgeschlagenen innovativen Strategien dank des geringeren Kraftstoffverbrauchs und der geringeren Abnutzung der Komponenten erheblich zur Entwicklung und Marktdurchdringung von Elektro-Lkw mit Brennstoffzellen beitragen. Durch die Anwendung dieser Strategien können Lkw-Hersteller niedrigere Betriebskosten erzielen und so die Lücke zu herkömmlichen Diesel-Lkw im Fernverkehr schließen.

Acknowledgment

The author gratefully acknowledges the financial support of the Austrian Federal Ministry for Digital and Economic Affairs, and the National Foundation for Research, Technology and Development. This work has been created in cooperation with the Austrian research projects “HyTruck” (grant no. 868790) and “FC4HD” (grant no. 885044).

Contents

List of Figures

List of Tables

Chapter 1

Introduction

This chapter provides an overview of fuel cell electric trucks and their role in the decarbonization of the transport sector. It describes what energy management strategies are and why using predictive strategies is essential in heavy-duty vehicles to ensure optimal performance. Lastly, it summarizes the main contributions of this doctoral thesis, followed by its outline and a list of publications.

1.1 Overview

Climate change is the single biggest health threat to humankind because it affects the main determinants of health: clean air, safe drinking water, sufficient food, and secure shelter [1]. Air pollution is undoubtedly the leading cause of climate change. Indeed, over the past century, the increasing concentration of greenhouse gases in the atmosphere caused a steady growth of the average temperature on Earth.

The transport sector is among the leading contributors to air pollution, so a massive global effort is ongoing to develop zero-emission vehicles and decarbonize the entire sector. In this context, the decarbonization of heavy-duty commercial vehicles is the most urgent and, at the same time, the most challenging task. In particular, heavy-duty trucks massively contribute to air pollution, representing less than one-tenth of all vehicles but roughly 40% of their carbon emissions [2]. This issue will worsen in the future, considering that freight activity will double within the next two decades [3].

The good news is that the development and commercialization of electric vehicles have significantly accelerated in the last few years, mainly thanks to the decrease in Lithium-ion battery costs. However, since the transport sector is vast and diverse, there is no one-solution-fits-all technology that will dominate the market of electric vehicles. For example, the low-cost, long-range, and high-utilization transportation markets are not served well by Lithium-ion-powered electric vehicles [4].

Fuel cell technologies will likely lead the long-range and high-utilization heavy-duty transportation markets in the near future. Indeed, fuel cell electric vehicles offer the

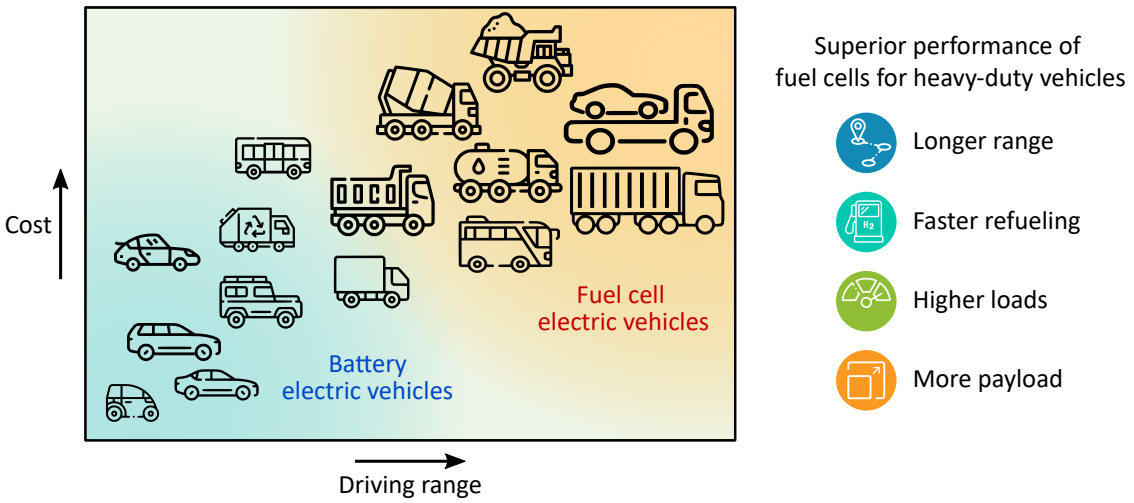

Figure 1.1: Electrification prospects and advantages of fuel cell electric vehicles.

same operational experience as conventional vehicles while maintaining the benefits of electrification, including zero tailpipe emissions, low noise, low vibration, and fast acceleration [5].

Fuel cells are electrochemical devices that use hydrogen to generate electricity through redox reactions. The hydrogen stored in the on-board tank system can usually satisfy the daily energy requirements thanks to its high gravimetric energy density. Moreover, the tank can be rapidly refueled once it is empty. The powertrain of fuel cell electric vehicles always includes batteries as a buffer between the fuel cells and the electric loads to increase efficiency and reduce degradation. However, unlike battery electric vehicles (BEVs), there is no need to plug the vehicle into the grid to recharge the batteries.

Several studies acknowledged the superior performance of fuel cells for heavy-duty vehicles compared with batteries [2]–[16]. The main advantages of fuel cell electric trucks are more extended and cost-effective range, faster refueling, supply of higher loads, and ability to carry more payload. For these reasons, fuel cell electric vehicles (FCEVs) are ideal for high-utilization and long-range transportation markets. Examples of applications are long-haul delivery, drayage, refuse, cement, utility, and mining trucks. Figure 1.1 summarizes the main prospects and advantages of FCEVs.

The insufficient hydrogen refueling infrastructure is the most limiting barrier to the market penetration of fuel cell electric trucks. However, the recent hydrogen economy roadmaps established by several countries are pushing to promote hydrogen utilization in the transport, industrial, and energy sectors, increasing the research and development investments for hydrogen production, storage, and refueling infrastructure [6]. A key factor for the advancement of such policies is that hydrogen is the most convenient way to store renewable energy. Therefore, fuel cell electric trucks can be the cleanest option for a sustainable transport sector.

Recently, the California Fuel Cell Partnership released a vision document calling for additional investments in fuel cell electric trucks, which are essential to achieve California's ambitious energy, environmental, and transportation policy goals. In particular, the document envisions that, with adequate policy support, 70.000 fuel cell electric trucks and 200 hydrogen stations can be achieved by 2035. This scenario would determine a tipping point for the self-sustainability of the market without the need for government financial incentives [17]. Similar calls for action are happening all around the world. In Europe, for example, a consortium called HyTrucks has been formed by Air Liquide, DATS 24, and the ports of Rotterdam, Antwerp, and Duisburg, pledging to deploy 1.000 fuel cell trucks and 25 hydrogen refueling stations by 2025 [18]. Two truck manufacturers, Scania and Hyzon Motors, recently joined the consortium, committing to deliver their class 8 fuel cell electric trucks.

Several truck manufacturers have chosen fuel cell technologies for their long-haul vehicle markets. The most notable are Hyzon Motors, Hyundai, Nikola Motor, Mercedes-Benz, Quantron, Scania, and Volvo. Table 1.1 lists the fuel cell electric trucks already on the market (or close-to-be), along with the key characteristics of the fuel cell powertrain. Notably, some manufacturers claim that their fuel cell electric trucks will have a driving range of up to 1.500 kilometers (similar to diesel trucks) with a refueling time of around 20 minutes, thanks to high-capacity tanks [19, 20].

Table 1.1: Powertrain characteristics of fuel cell electric trucks and prototypes.

Manufacturer/Vehicle	FCS power (kW)	Hydrogen tank (kg)	Battery capacity (kWh)	Gross weight (tons)
Hyzon HyMax 24 [21]	80	30	70	24
Hyzon HyMax 46 [21]	240	70	140	46
Hyzon HyMax 70 [21]	240	95	140	70
Hyundai XCIENT Fuel Cell [22]	190	32	73	36
Mercedes-Benz GENH2 Truck [23]	300	80	70	40
Nikola Tre FCEV [19]	200	60-100	140	37
Nikola Two FCEV [19]	300	60-100	250	42
Quantron QHM FCEV [20]	240	54-116	118	42
Scania [24]	90	33	56	27
Volvo [25]	300	-	-	42-65
Project FC4HD [26]	310	30	72	42

Figure 1.2: Prototype of the 42-ton fuel cell electric truck under development within the Austrian research project FC4HD.

The last entry of Table 1.1 refers to the 42-ton fuel cell electric truck (depicted in Figure 1.2) under development within the Austrian research project FC4HD, which aims at building a prototype to demonstrate the benefits of fuel cells for heavy-duty long-haul transportation [26]. The FC4HD consortium is led by AVL List GmbH and includes several partners from the automotive industry, universities, logistics, green hydrogen production and refueling. Among these partners, the Institute of Mechanics and Mechatronics of TU Wien contributed by developing predictive control strategies for innovative and intelligent energy and thermal management of the fuel cell powertrains. This doctoral thesis contains research conducted by the author in FC4HD [26] and the predecessor project HyTruck [27].

1.2 Motivation

A recent review study identified six central research areas for fuel cell electric trucks: public policies, hydrogen supply chain, environmental impact, powertrain technology, fuel cell technology, and hydrogen tank system [12]. Among these topics, research on powertrain technology is essential to ensure that fuel cell electric trucks meet the durability and efficiency requirements of heavy-duty vehicles.

Fuel cell powertrains are *hybrid*, meaning that multiple power sources work together to satisfy the load demanded by the driver. In particular, fuel cell powertrains include batteries to assist the fuel cells during fast load changes, which are common in vehicular

applications. Therefore, as in all hybrid vehicles, a supervisory controller is required to distribute the load between the power sources. This supervisory control task is usually called *energy management* or *power-split*, and it significantly impacts the overall efficiency and durability of the powertrain components [28].

The literature on energy management strategies for hybrid vehicles is vast. Over the last decade, several studies have been conducted considering different methods, targets, and powertrain configurations. Historically, the first investigations focused on hybrid electric vehicles (HEVs), in which battery-powered electric motors assist internal combustion engines in acceleration and regenerate braking energy in deceleration. However, the rapid growth of the electric vehicle market then pushed the research interest away from HEVs and towards zero-emission FCEVs, which have the same advantages as BEVs but also the long-range and fast refueling typical of conventional vehicles.

Comprehensive reviews of energy management strategies for HEVs can be found in [29], for FCEVs in [30]–[32], and for fuel cell-ultracapacitor-battery vehicles in [33]. Since a one-solution-fits-all energy management strategy does not exist, several approaches have been studied in the literature. Relevant works focused on fuel cell vehicles for light-duty applications are [34]–[45], for heavy-duty [46]–[53], and for long-haul transportation [54]–[65]. The most relevant methods and results from the literature are analyzed in more detail in Section 3.1. However, the literature survey identified a fundamental research gap in energy management strategies for long-haul fuel cell trucks. This gap indicates that the academic world did not swiftly follow the industrial one in the shift from passenger to long-haul applications. Indeed, besides the author's works [57]–[65], only a few recent studies focused on this topic [54]–[56].

The energy management strategies developed for light-duty vehicles are usually less effective for long-haul trucks. For example, most works on EMS design for fuel cell passenger cars neglect the elevation profile of the route. However, this assumption is unreasonable in long-haul transportation due to the substantial vehicle weight, which greatly impacts the electric load demands. On the contrary, using long-term route elevation forecasts for predictive control can be highly beneficial for fuel consumption.

Research on predictive energy management strategies with long-term load forecasts has already been conducted for other vehicular applications in [66]–[69], and for fuel cell electric trucks in the author's work [60]. Figure 1.3 provides a concept visualization of predictive energy management strategies for an intuitive demonstration of their benefits. In particular, if the predictive EMS ensures that the battery is fully discharged before a long downhill, it maximizes the amount of regenerative braking energy that can be absorbed. On the other hand, if the battery is fully charged before a long uphill, the predictive EMS can use the stored energy to assist the fuel cell in delivering the load, avoiding fuel cell high-power operation, which is less efficient. Therefore, predictive strategies can be highly beneficial for fuel consumption, especially on hilly or mountain routes. Moreover, they can prevent the worst-case scenario in which the vehicle must

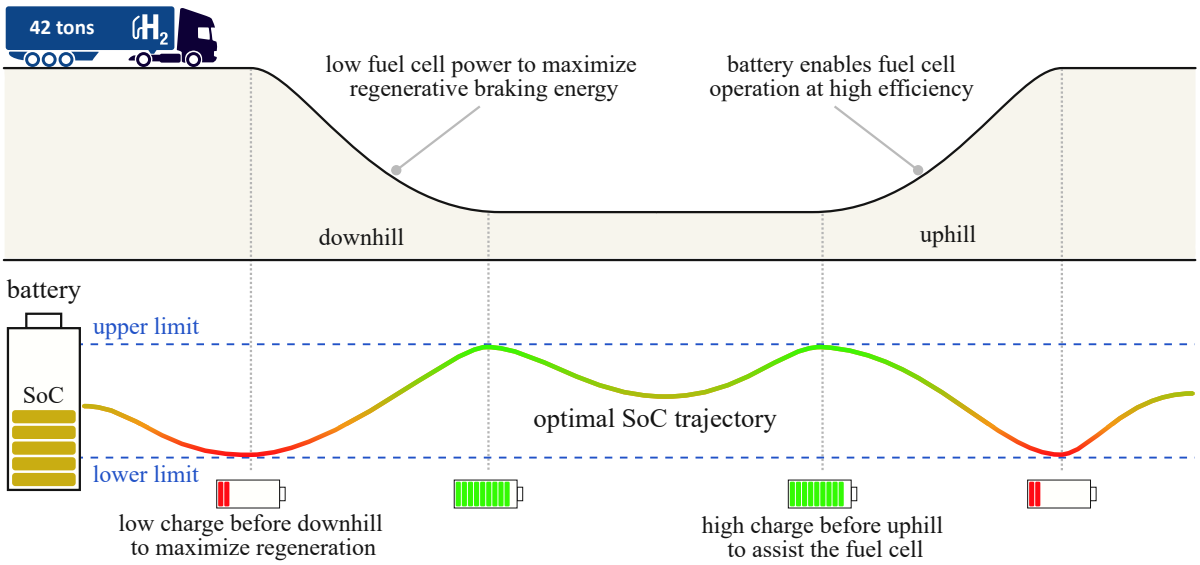

Figure 1.3: Concept visualization of predictive energy management strategies.

slow down or even stop because the battery is fully discharged and the fuel cell cannot sustain the load demand on its own.

As mentioned, the energy management strategy defines how the fuel cell and battery systems operate. Therefore, properly designing this supervisory control task is critical in ensuring that the powertrain components meet the lifetime requirements of long-haul transportation. Health-conscious energy management strategies have been developed for light-duty fuel cell vehicles, including component degradation within the optimization targets [40]–[44]. However, the trend shift from passenger cars to trucks exacerbates the durability challenges for fuel cells and calls for more research on the topic.

In particular, the energy management design in fuel cell electric trucks must consider fuel consumption, component degradation, and battery charge sustaining (or SoC control). Since these targets are often contrasting (e.g. fuel consumption versus degradation), the power-split task is a challenging control issue in hybrid vehicles. Such a high complexity makes it an exciting topic for academic research. Several methods can be adopted from the optimal control theory to find the better suited for on-board implementation and to yield the best trade-off between the optimization targets.

Among all methods, dynamic programming has been extensively adopted in the literature because it can find the global optimum solution to the optimal energy management problem. This method has been almost exclusively used as a benchmark for EMS design. Indeed, dynamic programming cannot be directly implemented in the vehicle for on-board control because it requires complete and apriori knowledge of the driving cycle. Moreover, another barrier to on-board implementations is its computational complexity, which is too high for real-time applications.

1.3 Contribution

This doctoral thesis focuses on predictive energy management strategies for fuel cell electric trucks, addressing the efficiency and durability challenges for long-haul transportation in realistic driving scenarios.

The main contributions of this thesis are summarized as follows.

- It conducts novel investigations to fill the research gaps on energy management of fuel cell electric trucks for long-haul transportation. Additionally, it develops control-oriented models from measurement data to design optimization-based control strategies and simulate vehicle performances in real-world driving cycles.
- It proposes a dual-stage control structure for predictive energy management strategies to meet the high-performance driving requirements of fuel cell electric trucks in challenging route topographies. The dual-stage structure favors the implementation of dynamic programming for optimal energy management with a computational complexity that is adequate for real-time control. The simulation results demonstrate that using long-term speed and elevation forecasts for predictive energy management significantly improves the overall performance in fuel consumption, component degradation, and SoC control.
- It develops a novel health-conscious energy management strategy for the simultaneous optimization of fuel consumption, fuel cell degradation, battery degradation, and SoC control. A detailed analysis of the Pareto fronts between the optimization targets demonstrates the goodness and flexibility of the proposed strategy. For example, assuming that the fuel cell and battery systems cannot be individually replaced, the health-conscious EMS can ensure balanced degradation, considerably extending the component life compared to the optimal fuel consumption solution.
- It assesses the benefits of predictive energy management strategies for the total cost of ownership of fuel cell electric trucks depending on the battery size. Moreover, it is the first work in the literature that shows how the progressive fuel cell and battery degradation impacts the overall vehicle performance.
- Lastly, it proposes innovative solutions to establish synergies between the energy management strategy and other control functions from a holistic standpoint. In particular, the degradation can be significantly reduced by exploiting the interaction with battery thermal management and the intelligent activation of multi-module fuel cell systems. Moreover, an eco-driving strategy that co-optimize vehicle speed and power-split can substantially reduce fuel consumption, enabling longer driving ranges to cope with the limited refueling infrastructure.

1.4 Thesis outline

The thesis is structured as follows.

Chapter 2 provides an overview of modeling for heavy-duty fuel cell electric vehicles and realistic driving scenarios, which are the basis for the present study. Moreover, it describes the main characteristics of dynamic programming: the method adopted from optimal control theory for developing predictive energy management strategies.

Chapter 3 describes the robust design of a novel dual-stage predictive energy management strategy for optimal fuel consumption and SoC control of fuel cell electric trucks after analyzing the benefits and drawbacks of typical methods in the literature.

Chapter 4 focuses on the multi-objective optimization of fuel consumption and component degradation, developing a health-conscious predictive energy management strategy based on dynamic programming. Moreover, it establishes the significant impact of battery size on fuel consumption, component degradation, and predictive energy management. Lastly, this chapter studies the impact of progressive component degradation on the performance of fuel cell electric trucks.

Chapter 5 describes an adaptive energy management strategy to improve the battery thermal management. Moreover, it proposes a health-conscious activation strategy for vehicles with multi-module fuel cell systems to mitigate fuel cell degradation. Lastly, a novel method to co-optimize the vehicle speed and power-split is proposed for eco-driving strategies based on the route elevation profile.

Chapter 6 summarizes the main conclusions and outlines future research directions.

1.5 List of publications

The scientific quality of the research presented in this thesis is already demonstrated by the twelve publications that the author produced during his doctoral studies. In particular, the thesis includes contents, methods, and results deriving from the following publications:

1. **Alessandro Ferrara**, Michael Okoli, Stefan Jakubek, and Christoph Hametner. Energy management of heavy-duty fuel cell electric vehicles: Model predictive control for fuel consumption and lifetime optimization. *IFAC-PapersOnLine*, 53(2):14205–14210, 2020. [57]

2. **Alessandro Ferrara** and Christoph Hametner. Rule-based energy management strategy of fuel cell ultracapacitor battery vehicles: winner of the IEEE VTS motor vehicles challenge 2020. In *2020 IEEE Vehicle Power and Propulsion Conference (VPPC)*. IEEE, November 2020. [70]

3. **Alessandro Ferrara**, Stefan Jakubek, and Christoph Hametner. Energy management of heavy-duty fuel cell vehicles in real-world driving scenarios: Robust design of strategies to maximize the hydrogen economy and system lifetime. *Energy Conversion and Management*, 232:113795, March 2021. [58]

4. **Alessandro Ferrara**, Saeid Zendegan, Hans-Michael Koegeler, Sajin Gopi, Martin Huber, Johannes Pell, and Christoph Hametner. Calibration of adaptive energy management strategies for fuel cell trucks using real-world driving scenarios. In *International Simulation Conference*. AVL, June 2021. [59]

5. Saeid Zendegan, **Alessandro Ferrara**, Stefan Jakubek, and Christoph Hametner. Predictive battery state of charge reference generation using basic route information for optimal energy management of heavy-duty fuel cell vehicles. *IEEE Transactions on Vehicular Technology*, 70(12):12517–12528, December 2021. [60]

6. **Alessandro Ferrara**, Saeid Zendegan, Hans-Michael Koegeler, Sajin Gopi, Martin Huber, Johannes Pell, and Christoph Hametner. Optimal calibration of an adaptive and predictive energy management strategy for fuel cell electric trucks. *Energies*, 15(7):2394, March 2022. [61]

7. **Alessandro Ferrara** and Christoph Hametner. Impact of energy management strategies on hydrogen consumption and start-up/shut-down cycles in fuel cell ultracapacitor battery vehicles. *IEEE Transactions on Vehicular Technology*, 71(6):5692–5703, June 2022. [71]

8. **Alessandro Ferrara**, Matthias Hütter, and Christoph Hametner. Adaptive energy management strategy to avoid battery temperature peaks in fuel cell electric trucks. *IFAC-PapersOnLine*, 55(24):311–316, 2022. [62]

9. Julian Kölbl, **Alessandro Ferrara**, and Christoph Hametner. Impact of energy management strategy calibration on component degradation and fuel economy of heavy-duty fuel cell vehicles. *IFAC-PapersOnLine*, 55(24):317–322, 2022. [63]

10. Banu Cicek Büyüker, **Alessandro Ferrara**, and Christoph Hametner. Predictive Battery Cooling in Heavy-Duty Fuel Cell Electric Vehicles. *IFAC-PapersOnLine*, 55(24):304–310, 2022. [72]

11. **Alessandro Ferrara** and Christoph Hametner. Eco-driving of fuel cell electric trucks: optimal speed planning combining dynamic programming and pontryagin's minimum principle. In *2022 IEEE 96th Vehicular Technology Conference* (VTC2022-Fall). IEEE, September 2022. [64]

12. **Alessandro Ferrara**, Stefan Jakubek, and Christoph Hametner. Cost-optimal design and energy management of fuel cell electric trucks. Article accepted for publication in *International Journal of Hydrogen Energy*, January 2023. [65]

Chapter 2

Technical background

This chapter provides the theoretical background for simulating heavy-duty fuel cell electric vehicles in real-world driving cycles and formulating predictive energy management strategies. In particular, the chapter details the vehicle dynamics and powertrain component modeling, the real-world driving scenarios, and the method adopted from the optimal control theory to develop the predictive control strategy.

2.1 Modeling of fuel cell electric vehicles

This section presents a detailed description of the vehicle model developed within the Austrian research projects FC4HD [26] and HyTruck [27], in collaboration with the industrial partner AVL List GmbH. The model was used to evaluate the performance of heavy-duty fuel cell electric vehicles in realistic driving scenarios for long-haul transportation and to develop optimal model-based control strategies. Figure 2.1 depicts the powertrain architecture of the vehicle under investigation in this work. The electric motor and fuel cell systems are connected to a DC bus through power converters, whereas the battery system is directly linked. The cooling systems of the battery, fuel cell, and motor are depicted together for compactness.

The vehicle modeling approach can generally be forward-facing or backward-facing [29]. The latter assumes that the vehicle always meets its desired performance to follow the speed profile strictly. Speed, acceleration, and road slope are used to calculate the power required to drive the vehicle without checking against the actual powertrain capabilities. On the other hand, the forward approach includes a driver model, which generates a power request by comparing actual and desired speeds. In this case, if the powertrain cannot provide the requested power, the vehicle slows down and starts to deviate from the desired speed. This thesis adopts the forward-facing modeling approach to simulate the vehicle performance and the backward facing one to develop the optimal control strategies [58].

The simulation model is developed in MATLAB/Simulink, adopting a fixed-step solver with a sample time of 200 ms. The implementation is shown in Figure 2.2, providing an

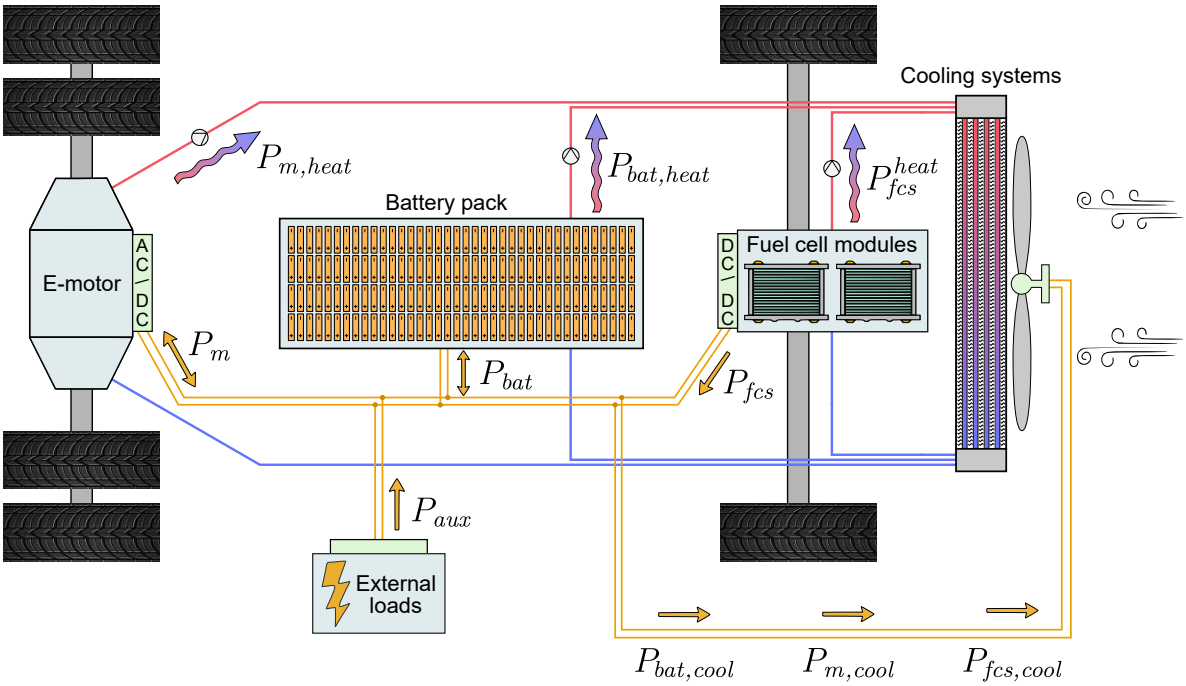

Figure 2.1: Powertrain architecture in fuel cell electric vehicles.

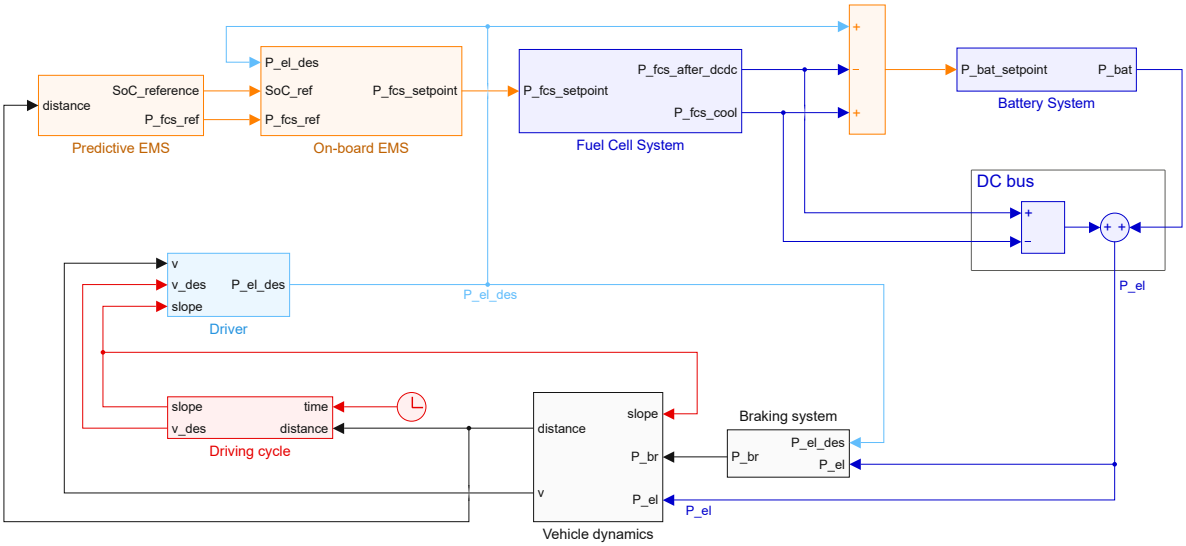

Figure 2.2: Implementation of fuel cell electric vehicle model in MATLAB/Simulink.

overview of the model structure and connections between the main component blocks. However, several signals are hidden and exchanged between subsystems for better readability. Following the forward-facing modeling approach, a driver model defines the desired electric load $P_{el,des}$ that the fuel cell and battery systems have to provide so that the vehicle can follow the specific driving cycle. In the driver model, a PI controller defines the load based on the deviation between the actual vehicle speed v and the desired one v_{des} following a classical approach from the literature [73]. Additionally, the road slope θ is used to create a feed-forward term to improve the tracking of the desired speed [61]. Eventually, the desired electric load is expressed as:

$$P_{el,des} = f(v, v_{des}, \theta) \ , \tag{2.1}$$

already including the electric losses associated with battery and motor cooling, and the remaining auxiliary loads shown in Figure 2.1. On the contrary, the actual load provided on the DC bus by the fuel cell and battery systems is:

$$P_{el} = P_{fcs} \ \eta_{dc,dc} + P_{bat} - P_{fcs,cool} \ , \tag{2.2}$$

where P_{fcs} is the net FCS power, $\eta_{dc,dc}$ is the DC/DC converter efficiency, P_{bat} the battery power, and $P_{fcs,cool}$ the electric losses associated with fuel cell cooling. The vehicle slows down if the powertrain does not provide sufficient power.

2.1.1 Vehicle dynamics

Figure 2.3 depicts the longitudinal motion dynamics of road vehicles. Three main resistant forces oppose the vehicle motion: rolling friction, gravity due to road slope, and aerodynamic drag. These resistant forces are calculated based on the vehicle speed and road slope as follows:

$$F_{roll} = m_v \ g \ c_r(v) \cos\theta \tag{2.3a}$$
$$F_{slope} = m_v \ g \ \sin\theta \tag{2.3b}$$
$$F_{drag} = v^2 A_v \ c_x \ \rho_{air}/2 \tag{2.3c}$$

where g is the gravitational acceleration and the remaining parameters of the vehicle dynamics model are listed in Table 2.1. In particular, it is assumed that the rolling friction coefficient $c_r(v)$ in (2.3a) changes linearly as a function of the vehicle speed. The total resistant force acting on the vehicle is:

$$F_{res} = F_{roll} + F_{slope} + F_{drag} \ . \tag{2.4}$$

The vehicle acceleration, $\dot{v}$, is calculated depending on the provided power at the wheels, P_w, as:

$$\dot{v} = \frac{P_w/v - F_{res}}{m_v} \ . \tag{2.5}$$

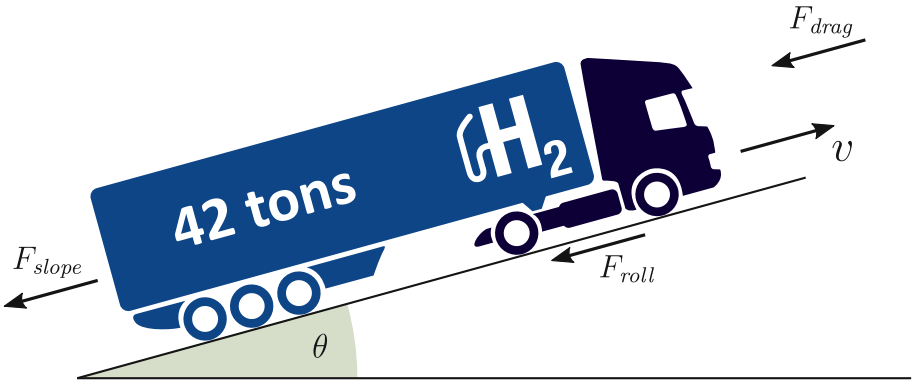

Figure 2.3: Scheme of longitudinal vehicle dynamics.

Table 2.1: Parameters of vehicle dynamics model.

Parameter	**Symbol**	**Value**
Vehicle mass	m_v	22–42 t
Rolling friction coefficient at 0 km/h	c_r	0.0055
Rolling friction coefficient at 100 km/h	c_r	0.0081
Vehicle frontal area	A_v	9.6 m^2
Drag coefficient	c_x	0.58
Air density	ρ_{air}	1.20 kg/m^3
Auxiliary loads	P_{aux}	11.5 kW
Total efficiency	η_T	0.87

The power at the wheels is calculated depending on the electric power (2.2) as:

$$P_m = P_{el} - P_{aux} \tag{2.6a}$$

$$P_w = P_m \, \eta_T^{\mathrm{sgn}(P_m)} - P_{br} \, , \tag{2.6b}$$

where P_m is the electric motor power, P_{aux} the auxiliary loads, and P_{br} the braking system power. All the auxiliary loads external to the powertrain (e.g. cabin conditioning, power-steering pump, battery cooling, cargo refrigeration) are assumed to be constant and equal to the value in Table 2.1. In deceleration, a system of mechanical brakes absorbs the negative loads that cannot be regenerated with the electric motor due to the battery charging power constraint. Lastly, the total efficiency η_T from the motor to wheels includes all the losses due to drivetrain components, inverters, and electric motors.

2.1.2 Fuel cell system

Fuel cells are electrochemical devices that convert hydrogen into electricity through chemical reactions. Fuel cells are connected in series to form stacks and increase the voltage and output power. Generally, a fuel cell system includes one or more stacks and auxiliary components (e.g. air compressors, humidifiers, circulating pumps) that perform necessary tasks for fuel cell operation.

The operation of fuel cell systems depends on many variables. The most important are current, temperature, relative humidity, and partial pressure of the reactants. Detailed modeling of stacks and auxiliary components is required to capture the complex dynamics of fuel cell systems. In addition, fuel cell efficiency and degradation strongly depend on low-level control strategies. References to dynamic models with different detail levels are available in [74]–[78].

However, due to the high computational cost, dynamic models are not suitable for optimization-based energy management strategies for real-time control. Thus, this work considers a simplified quasi-static model, a standard approach for system-level studies in the literature [28]. Here, the net fuel cell power, P_{fcs}, is intended as:

$$P_{fcs} = P_{fcs,\mathrm{H_2}} - P_{fcs,heat} - P_{fcs,BoP} \ , \tag{2.7}$$

where $P_{fcs,\mathrm{H_2}}$ is the hydrogen chemical power, $P_{fcs,heat}$ the electrochemical losses, and $P_{fcs,BoP}$ the losses due to the balance-of-plant (BoP) components (i.e. compressors, humidifiers, pumps, valves, sensors). Following the quasi-static modeling approach, the terms in (2.7) are expressed as a function of the net fuel cell power. The hydrogen chemical power is defined as:

$$P_{fcs,\mathrm{H_2}} = P_{fcs,\mathrm{H_2}}(P_{fcs}) = \dot{m}_{\mathrm{H_2}}(P_{fcs})\ \mathrm{LHV}_{\mathrm{H_2}} \ , \tag{2.8}$$

where $\dot{m}_{\mathrm{H_2}}$ is the hydrogen consumption rate, and $\mathrm{LHV}_{\mathrm{H_2}}$ the hydrogen lower heating value (i.e. 120 MJ/kg). The losses due to electrochemical conversion and BoP components are:

$$P_{fcs,heat} = P_{fcs,heat}(P_{fcs}) \ , \tag{2.9a}$$
$$P_{fcs,BoP} = P_{fcs,BoP}(P_{fcs}) \ . \tag{2.9b}$$

Eventually, the overall efficiency of the fuel cell system is defined as the ratio between the net power and the ideal power contained in the consumed hydrogen:

$$\eta_{fcs} = \frac{P_{fcs}}{P_{fcs,\mathrm{H_2}}} \ . \tag{2.10}$$

Therefore, combining (2.8) and (2.10), the hydrogen consumption rate is written as:

$$\dot{m}_{\mathrm{H_2}} = \frac{P_{fcs}}{\eta_{fcs}\ \mathrm{LHV}_{\mathrm{H_2}}} \ . \tag{2.11}$$

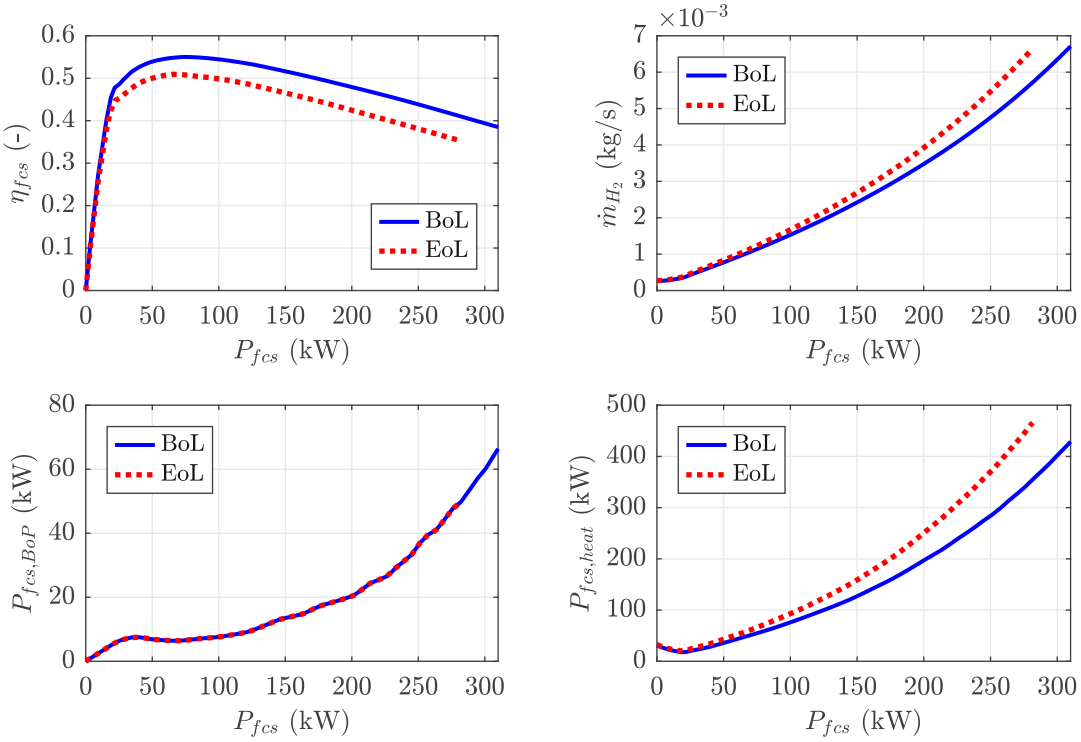

Figure 2.4: Begin and end-of-life characteristic curves of the overall fuel cell system efficiency, hydrogen consumption rate, BoP losses, and electrochemical losses as functions of the net system power.

The fuel cell system considered in this work has a nominal net power: $P_{fcs,nom} = 310$ kW. The peak system efficiency is 55% at 74 kW, whereas the efficiency at nominal power is 39%. Figure 2.4 depicts the characteristic curves of the overall fuel cell system efficiency, hydrogen consumption rate, BoP losses, and electrochemical losses as functions of the net system power. These characteristics were derived from a complex grey box developed by AVL, which was then tuned to fit experimental data.

The characteristics in Figure 2.4 are reported at begin-of-life (BoL) and end-of-life (EoL) conditions. It is important to note that at EoL, the fuel cell system can provide a maximum net power of only 281 kW, which is approximately 91% of the BoL value. Moreover, fuel consumption drastically increases because of the higher electrochemical losses. Eventually, the peak efficiency at EoL is 51%. The fuel cell degradation mechanisms are detailed in Section 2.1.4.

For clarity, the nominal fuel cell system power is considered constant, whereas the maximum power changes depending on the state of degradation. The fuel cell model is

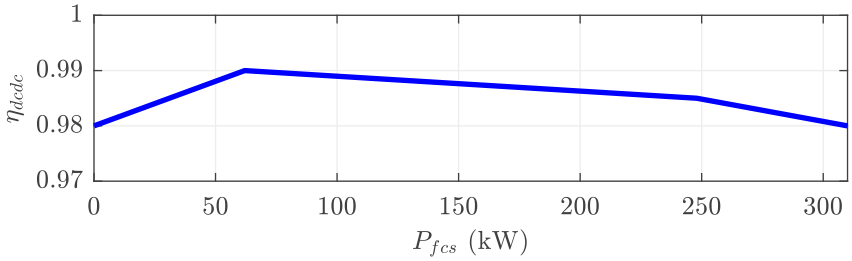

Figure 2.5: Characteristic curve of the DC/DC converter efficiency.

implemented with the following power constraints:

$$0 \leq P_{fcs} \leq P_{fcs,max} \tag{2.12a}$$

$$|\dot{P}_{fcs}| \leq 0.10\ P_{fcs,max} \tag{2.12b}$$

where $P_{fcs,max}$ is the maximum net power, and the rate of change is limited to the 10% of the maximum power per second.

The fuel cell system is connected to the DC bus via a power converter to reach the same voltage level as the battery system. Even though the electrical losses are low, this work considers the converter efficiency in (2.2) as a function of the fuel cell net power:

$$\eta_{dc,dc} = \eta_{dc,dc}(P_{fcs})\ . \tag{2.13}$$

Figure 2.5 depicts the characteristic curve of the converter efficiency.

Fuel cell thermal management is a challenging aspect for automotive applications. Usually, liquid cooling is implemented by adopting a similar structure to conventional vehicles, where a radiator removes the heat from the coolant to ambient air. However, fuel cell radiators must have a larger frontal area because of the lower operating temperatures of fuel cells (i.e. 80°C) compared with internal combustion engines [79]. In the system under investigation, a large fan is mounted on the radiator to improve the cooling with forced convection. A quasi-static modeling approach is also adopted for a simplified representation of the power consumption of the fuel cell cooling system, $P_{fcs,cool}$, which is required to power the radiator fan. In particular, a tridimensional static map is considered to express the consumption as:

$$P_{fcs,cool} = P_{fcs,cool}(v, T_{amb}, P_{fcs,heat}) \tag{2.14}$$

depending on the vehicle speed, ambient temperature T_{amb}, and fuel cell heat generation. Figure 2.6 depicts the characteristic maps of the fuel cell cooling system.

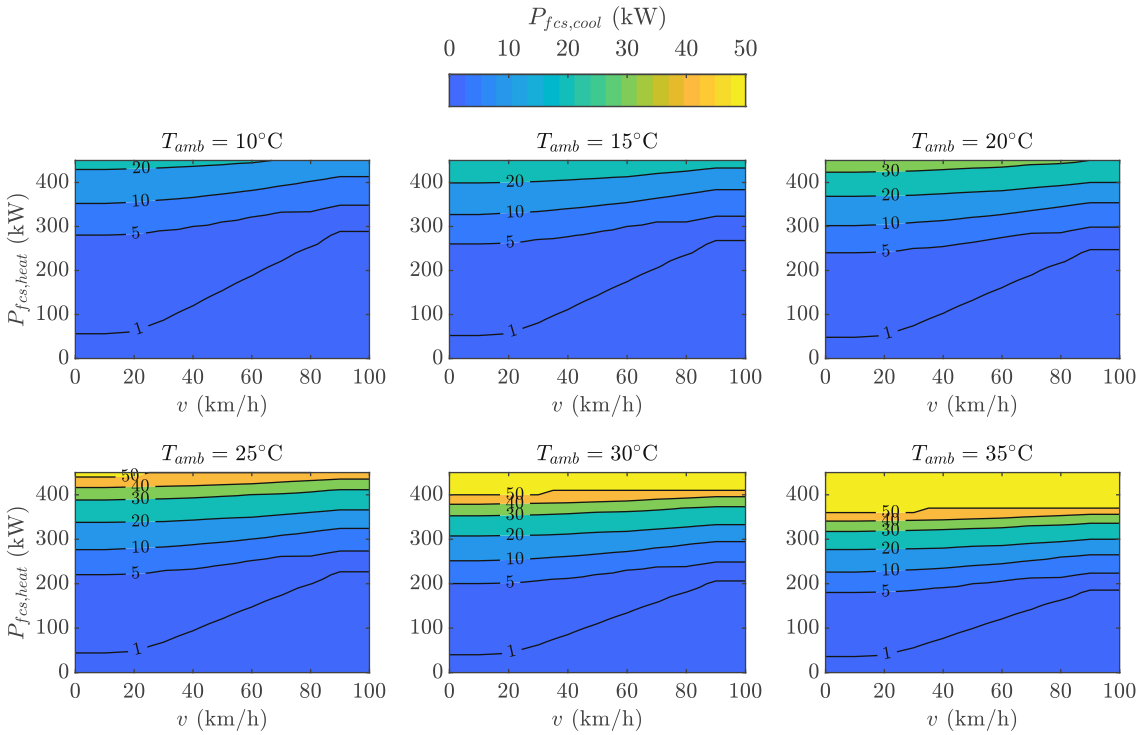

Figure 2.6: Characteristic maps of the fuel cell cooling system as a function of vehicle speed, ambient temperature, and fuel cell heat generation.

2.1.3 Battery system

The equivalent circuit depicted in Figure 2.7a is adopted for battery modeling. The open circuit voltage source, V_{oc}, is connected in series with the internal resistance, R_{int}. The battery power is expressed as:

$$P_{bat} = V_{bat}\, I_{bat} = (V_{oc} - R_{int}\, I_{bat})\ , \tag{2.15}$$

where the battery voltage, V_{bat}, is calculated using Kirchhoff's law. The battery current and power are assumed positive during discharge. The current is expressed as a function of the battery power by inverting (2.15):

$$I_{bat} = (V_{oc} - \sqrt{V_{oc}^2 - 4\, P_{bat}\, R_{int}})/(2R_{int})\ . \tag{2.16}$$

The battery SoC is defined as the ratio between actual and maximum charge as:

$$\mathrm{SoC} = \frac{Q_{bat}}{Q_{bat,max}}\ , \tag{2.17}$$

and its rate of change as:

$$\frac{d}{dt}\,\mathrm{SoC} = -\frac{I_{bat}}{Q_{bat,max}}\ . \tag{2.18}$$

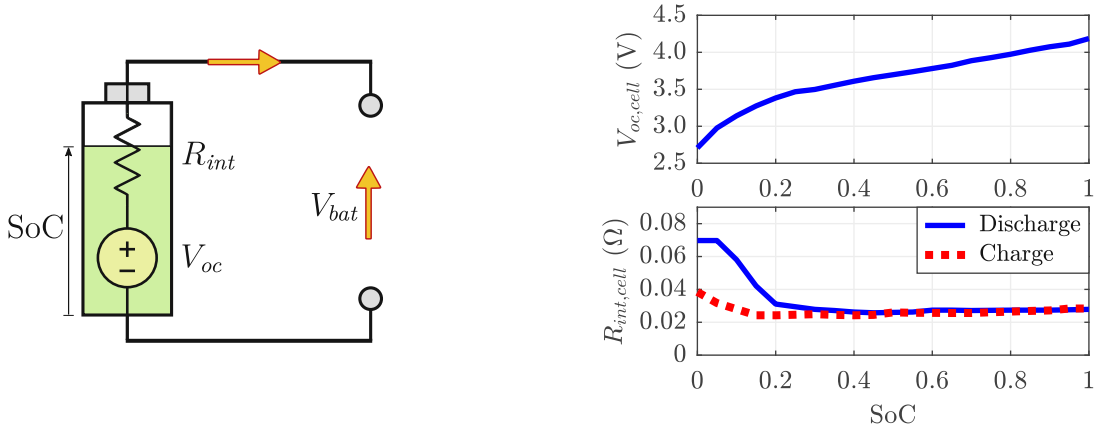

(a) Equivalent circuit model.

(b) Cell characteristic curves of open circuit voltage and internal resistance.

Figure 2.7: Battery scheme and parameters.

The heat generation in the battery system due to ohmic losses is calculated as:

$$P_{ohm} = R_{int}\, I_{bat}^2 \ . \tag{2.19}$$

The open-circuit voltage, internal resistance, nominal charge, and maximum capacity of the battery cell are scaled to the battery pack as in (2.20), where N_p is the number of parallel branches, each of which has N_s cells connected in series.

$$V_{oc} = V_{oc,cell}\ N_s \tag{2.20a}$$
$$R_{int} = R_{int,cell}\ N_s/N_p \tag{2.20b}$$
$$Q_{bat,max} = Q_{max,cell}\ N_p \tag{2.20c}$$

Based on experimental data, the battery cell open-circuit voltage and internal resistance depend on the SoC as depicted in Figure 2.7b. The impact of the cell temperature is neglected. The nominal energy of the battery system is calculated as:

$$E_{bat,nom} = V_{nom,cell}\ Q_{nom,cell}\ N_p\ N_s \ , \tag{2.21}$$

where $Q_{nom,cell}$ is the nominal cell capacity, and $V_{nom,cell}$ the nominal cell voltage. For clarity, the nominal cell capacity is considered constant, whereas the maximum cell capacity $Q_{max,cell}$ changes depending on the state of degradation.

The battery power is constrained to meet the cell voltage and C-rate limits indicated in Table 2.2, which are essential to avoid accelerated battery degradation.

Table 2.2: Parameters of battery system.

Parameter	Symbol	Value
Nominal cell capacity	$Q_{nom,cell}$	2.7 Ah
Nominal cell voltage	$V_{nom,cell}$	3.65 V
Number of parallel branches	N_p	32
Number of cells in series	N_s	317
Maximum cell voltage	max $V_{oc,cell}$	4.2
Minimum cell voltage	min $V_{oc,cell}$	2.6
Maximum C-rate	max C-rate	8
Minimum C-rate	min C-rate	-2.5

2.1.4 Component degradation models

Fuel cell degradation

Frequent start-up/shut-down cycles, transient loading, low-power and high-power operations accelerate fuel cell degradation. Therefore, in automotive applications, lifetime expectations are typically shorter than stationary ones (e.g. 5000 h vs. 40000 h [80]). In a review of experimental techniques to measure degradation, Zhao and Li [81] identify average voltage degradation rates of 1 μV/h in stationary operation and 100 μV/h in transient operation.

Table 2.3 summarizes the principal degradation phenomena reported in [80]–[83]. In particular, dynamic/transient loading induce temperature/humidity changes, potential cycling, and reactant starvation. Temperature/humidity changes induce cracks, delamination, ionomer redistribution, and pinholes in the membrane electrode assembly. Potential cycling accelerates the degradation of platinum particles on carbon supports due to dissolution, migration, agglomeration, and Ostwald ripening [84]. Local hydrogen starvation causes critical potentials in the cathode that corrode the carbon support. Global hydrogen starvation induces abnormal reactions in the anode that corrode the carbon support. Air starvation lowers the cathode potential, inducing abnormal reactions and the formation of hydrogen. Thus, hydrogen and oxygen are directly combined in highly exothermic reactions generating hot spots. Carbon corrosion and catalyst degradation determine permanent loss of electrochemically active area, higher charge, and mass transfer resistances.

Moving air/hydrogen boundaries are established during start-up/shut-down cycles. In particular, during starts, fuel cells experience the inevitable transition between air-filled and hydrogen-filled anodes. The opposite transition occurs during a shutdown. In air-filled areas, the anode potential decreases, causing a higher difference with the cathode. Abnormal reactions corrode the cathode carbon support and produce protons,

Table 2.3: Summary of the main fuel cell degradation phenomena.

Cause		Effect
Temperature/humidity change	$\xrightarrow{\text{dl}}$	Mechanical degradation
Reactant starvation	$\xrightarrow{\text{dl}}$	Carbon corrosion
Potential cycling	$\xrightarrow{\text{dl}}$	Catalyst degradation
Air/hydrogen boundary	$\xrightarrow{\text{ss}}$	Carbon corrosion
Sub-zero temperatures	$\xrightarrow{\text{ss}}$	Mechanical degradation
Reactant crossover	$\xrightarrow{\text{lp}}$	Chemical degradation
High temperatures	$\xrightarrow{\text{hp}}$	Membrane degradation

Abbreviations: dynamic loading (dl); start/shutdown (ss); low power (lp); high power (hp).

which then move to the anode, generating the so-called reverse current. In freezing environments, start-up/shut-down cycles cause severe structural damage within the membrane electrode assembly due to frost-heave and water volume expansion during freezing.

Low-power operations determine chemical degradation of the membrane due to intensified reactant crossover and high potentials. Indeed, direct reactions cause hotspots in the cathode and generate free radicals in the anode, which chemically attack the membrane. Higher partial pressures due to limited reactions promote gas crossover. Low water generation leads to membrane dehydration, opening pores for gas permeation. Moreover, oxygen crossover is promoted by a lack of intense proton and water fluxes to the cathode. Details about water transport phenomena and membrane nanostructure can be found in [85].

High-power operations cause flooding in the cathode due to excessive water generation. However, on the anode side, the membrane is dehydrated due to high proton currents, which hinder water's back-flow. Therefore, without proper water and thermal management, the high-power operation can cause mechanical and chemical degradation of the membrane due to dehydration and high temperatures.

Due to the complexity of the phenomena involved, physical modeling of fuel cell degradation is challenging. However, Pei et al. [83] developed a simple empirical model that evaluates the voltage degradation of fuel cells in automotive applications. This quick evaluation method derives from accelerated aging tests and offers adequate precision for a system-level analysis. For this reason, the method has been widely adopted in the literature on energy management strategies. The fuel cell voltage degradation, ΔV_{fcs},

Table 2.4: Fuel cell degradation rates.

Parameter	Symbol	Value
Degradation rate due to start-up/shut-down cycles	δ_{ss}	0.00196 %/start
Degradation rate due to low-power operation	δ_{lp}	0.00126 %/h
Degradation rate due to high-power operation	δ_{hp}	0.00147 %/h
Degradation rate due to dynamic loading	δ_{dl}	0.0000593 %/cycle

is calculated as:

$$\Delta V_{fcs} = \Delta V_{fcs,ss} + \Delta V_{fcs,lp} + \Delta V_{fcs,hp} + \Delta V_{fcs,dl} \tag{2.22a}$$

$$\Delta V_{fcs,ss} = \delta_{ss}\ N_{starts} \tag{2.22b}$$

$$\Delta V_{fcs,lp} = \delta_{lp}\ t_{lp} \tag{2.22c}$$

$$\Delta V_{fcs,hp} = \delta_{hp}\ t_{hp} \tag{2.22d}$$

$$\Delta V_{fcs,dl} = \delta_{dl} \int \frac{|\dot{P}_{fcs}|}{2\ P_{fcs,nom}}\, dt \tag{2.22e}$$

considering start-up/shut-down cycles, dynamic loading, low-power and high-power operations. Here, N_{starts} is the number of start-up/shut-down cycles, t_{lp} the time operating at low-power, and t_{hp} the time operating at high-power. It is assumed that the fuel cell system can idle at zero net power to avoid shut-down cycles (consequently, there is only one start-up/shut-down cycle per driving cycle). Moreover, the thresholds for low and high-power operations are 10% and 80% of the fuel cell nominal power. The degradation rates are indicated in Table 2.4 from [83].

The fuel cell voltage degradation, ΔV_{fcs}, is expressed in percentage from the nominal value. It is assumed that when the degradation is 10%, the fuel cell has reached EoL conditions (i.e. $\Delta V_{fcs,EoL} = 10\%$). Therefore, it is convenient to define the state of fuel cell degradation as:

$$\mathrm{SoD}_{fcs} = \frac{\Delta V_{fcs}}{\Delta V_{fcs,EoL}}\ . \tag{2.23}$$

According to this definition, at BoL the state of degradation is 0, whereas at EoL is 1.

Battery degradation

The maximum energy that lithium-ion (Li-ion) batteries can store decreases as they are used because of various irreversible degradation mechanisms affecting the different cell components: electrodes, electrolyte, separator, and current collectors. Battery degradation modeling is exceptionally challenging because of the different causes, rates, and inter-dependencies of the degradation mechanisms [86, 87].

Proper battery management is essential to mitigate degradation through charge control, thermal management, and cell balancing. Indeed, the principal factors affecting

degradation are battery temperature, C-rates, depth-of-discharge (DoD), and SoC. For example, the cell temperature influences some of the leading battery degradation mechanisms, such as solid electrolyte interface growth, lithium plating, and active material dissolution. In particular, higher temperatures determine faster (unwanted) chemical reactions and, thus, accelerated degradation.

As a result of the degradation, the battery capacity fades. Consequently, the battery can store less energy as it ages. In automotive applications, the battery is considered at EoL conditions when the capacity reaches 80% of the nominal value [88]. Here, the capacity fade is defined as the difference between the nominal and current maximum capacity:

$$\Delta Q_{bat} = Q_{bat,nom} - Q_{bat,max} \ , \tag{2.24}$$

and the EoL condition is: $\Delta Q_{bat,EoL} = 20\% Q_{bat,nom}$. Therefore, the battery state of degradation can be defined as:

$$\mathrm{SoD}_{bat} = \frac{\Delta Q_{bat}}{\Delta Q_{bat,EoL}} \ . \tag{2.25}$$

Reiners et al. [86] shows that different degradation models respond very differently to varying operating conditions. Moreover, the degradation mechanisms depend highly on the cell chemistry, making battery degradation modeling hard to generalize.

Due to the high complexity of electrochemical degradation models, this thesis adopts a simplified modeling approach, which is more suitable for a system-level study. In particular, the model relies on experimental data that express the number of charging/discharging cycles C_{EoL} until EoL at different depths of discharge, which highly affect the degradation. On the other hand, it is assumed that the battery thermal management system can maintain the temperature around the optimal operating value for low degradation. Under this assumption, the impact of temperature on the capacity fade is neglected.

Figure 2.8 compares experimental data reported in the literature [89]–[91]. The characteristic curve of the number of cycles was acquired by repeatedly discharging the battery to a specified DoD level and recharging it to the maximum capacity until the capacity fade reached 20%. The works from 2016 and 2018 have similar degradation rates, whereas the one from 2010 is significantly higher, probably due to technological advancement. The figure also shows the results in terms of equivalent full cycles EFC_{EoL} until EoL, which are calculated as:

$$\mathrm{EFC}_{EoL} = \mathrm{DoD} \cdot \mathrm{C}_{EoL} \ , \tag{2.26}$$

indicating that the maximum current throughput is achieved at a DoD of 0.3 for [90] and 0.4 for [89].

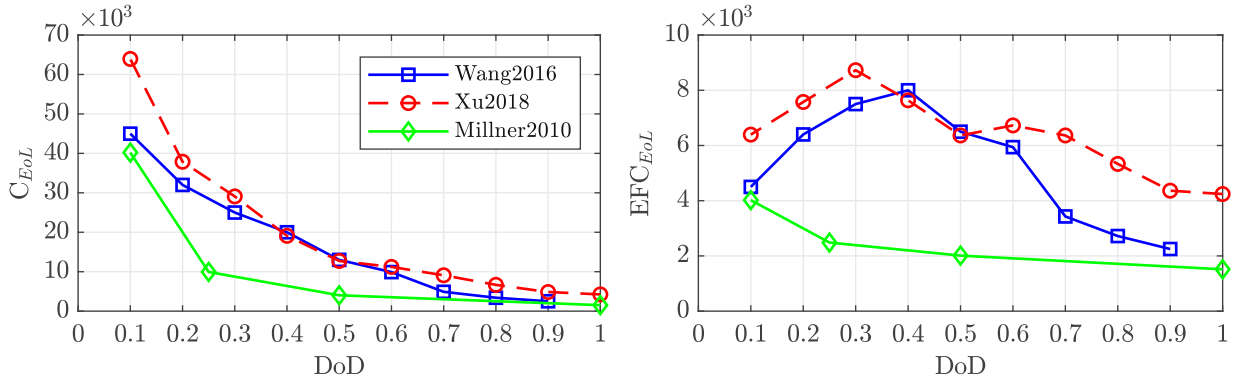

Figure 2.8: Comparison of experimental data for battery charging/discharging cycles until EoL conditions.

Eventually, the state of battery degradation is calculated as:

$$\mathrm{SoD}_{bat} = \frac{\mathrm{EFC}}{\mathrm{EFC}_{EoL}} \,, \tag{2.27}$$

where the equivalent full cycles are calculated as:

$$\mathrm{EFC} = \frac{\int |I_{bat}| \; dt}{2 \; Q_{bat,max}} \,. \tag{2.28}$$

Replacing (2.26) and (2.28) in (2.27), the state of battery degradation can be expressed as:

$$\mathrm{SoD}_{bat} = \int \delta_{bat} \; |I_{bat}| \; dt \,, \tag{2.29}$$

with the battery degradation rate δ_{bat} defined as:

$$\delta_{bat} = \delta_{bat}(\mathrm{SoC}) = \frac{1}{2 \; Q_{bat,max} \; \mathrm{EFC}_{EoL}(\mathrm{SoC})} \,. \tag{2.30}$$

Considering the definition of depth-of-discharge: $\mathrm{DoD} = 1 - \mathrm{SoC}$, the battery degradation rate is represented as a function of the state of charge in Figure 2.9, adopting the experimental data of [89], and $Q_{bat,max} = 86.4$ Ah as in Table 2.2.

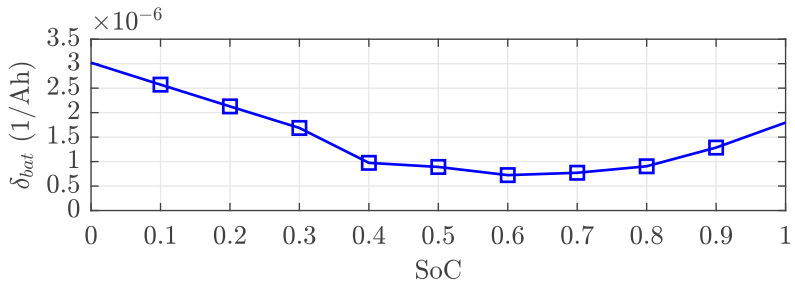

Figure 2.9: Battery degradation rate as a function of the SoC.

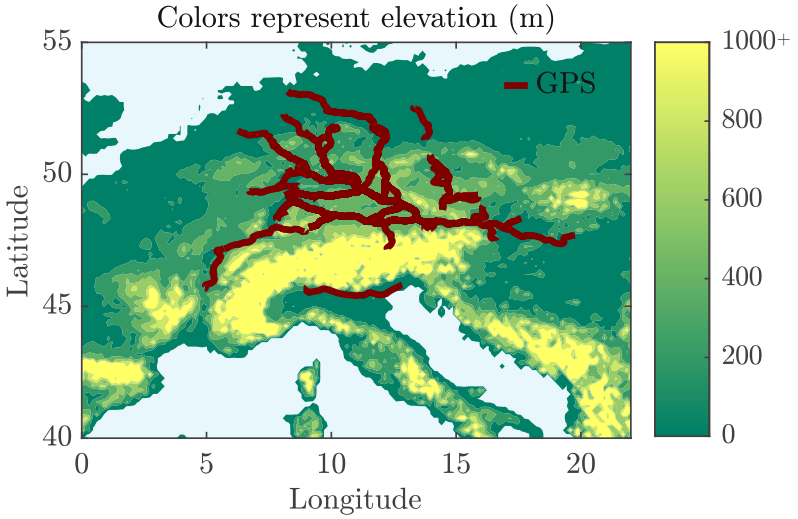

Figure 2.10: Geographic distribution of GPS data against the elevation map of Central Europe.

2.2 Real-world driving cycles

The control strategies developed in this thesis are validated in realistic driving scenarios of heavy-duty vehicles for road freight transportation. In particular, the simulations consider real-world driving cycles of long-haul trucks operating in Central Europe, a challenging region due to many hills and mountains. The driving cycles derive from GPS data collected by a fleet of conventional diesel trucks. Figure 2.10 shows the geographic distribution of the GPS data, clearly indicating that most data were recorded on hilly or mountain routes.

The real-world driving cycles are based on latitude, longitude, speed, and elevation measurements with 1 s sampling time. The data was recorded with a resolution of 1 m for the elevation and 1 km/h for the speed. Moreover, there are frequent gaps in the data because of signal losses, and low speeds (below 5 km/h) were not recorded. Therefore, the measurements were processed to represent the driving cycles better. In particular, the latitude and longitude were projected on an XY-plane using the map projection ETRS89 Lambert Azimuthal Equal-Area (center: 52°N 10°E). After filling the gaps by linear interpolation, the speed was calculated from the X and Y position components. Lastly, to remove measurement noise and smooth the signals, a centered moving average filter was used for the speed (with a 20 s time-span) and the elevation (with a 100 m distance-span) profiles.

Figure 2.11 shows the recorded data for a driving cycle example. In particular, Figure 2.11a shows the latitude and longitude of the entire route and a zoomed section during the initial 900 seconds of driving. Moreover, Figure 2.11b depicts the speed and elevation signals for the same segment, showing the difference between the processed

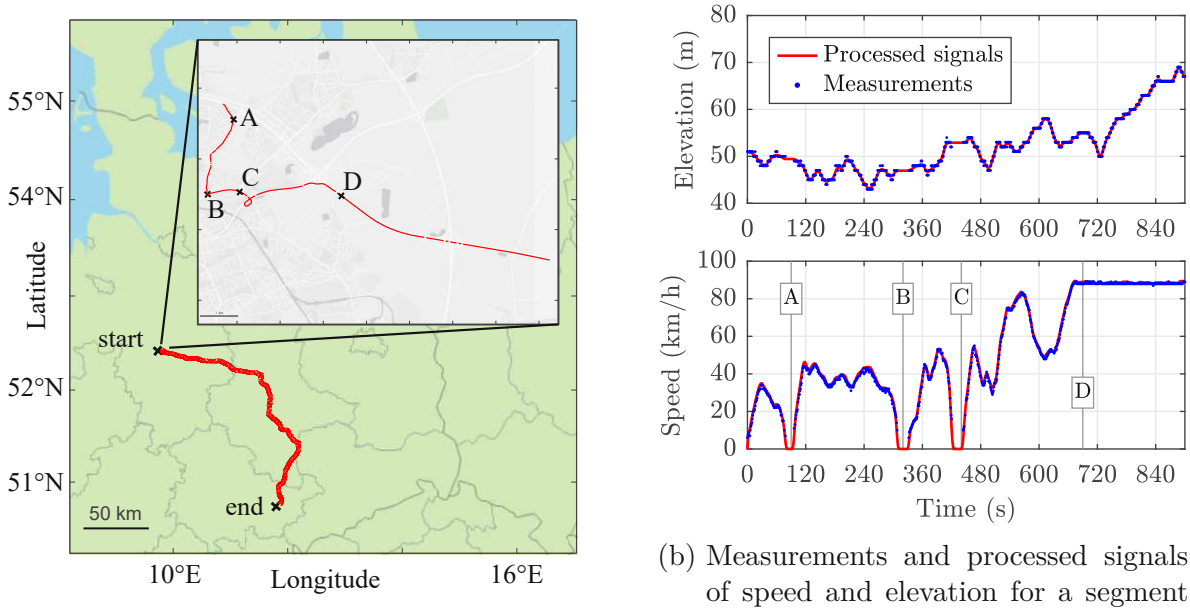

(a) Latitude and longitude measurements.

(b) Measurements and processed signals of speed and elevation for a segment of the driving cycle.

Figure 2.11: Recorded data of a real-world driving cycle.

signals and the measurements. Points A and B correspond to stops due to intersections, whereas C refers to a stop before entering the motorway. Point D corresponds to the start of the constant-speed motorway cruising.

The vehicle weight was not recorded as part of the driving cycle data. However, a method was developed to estimate the maximum weight possible for the simulation of each driving cycle. In particular, the maximum weight is such that the wheel power profile exceeds the 400 kW threshold for 0.5% of the driving time.

Figure 2.12 shows three selected driving cycles frequently considered in this work to demonstrate the benefits of predictive energy management strategies. These real-world driving cycles correspond to flat, hilly, and mountain routes, as noticeable from the elevation profiles.

- Figure 2.12a shows a driving cycle on a flat route. The vehicle is mostly driving on a motorway at a constant speed. Moreover, the speed profile is smooth because the driving cycle was recorded at night. The slowdowns are due to the road curvature and traffic of slower vehicles. The maximum elevation change of the route is 73 meters, which is small enough to consider it flat.

- Figure 2.12b shows a driving cycle on a hilly route. The speed profile indicates that the cycle starts and ends in an urban area, but most of the drive is on a motorway. At minute 125, the vehicle stops for refueling and then goes back to

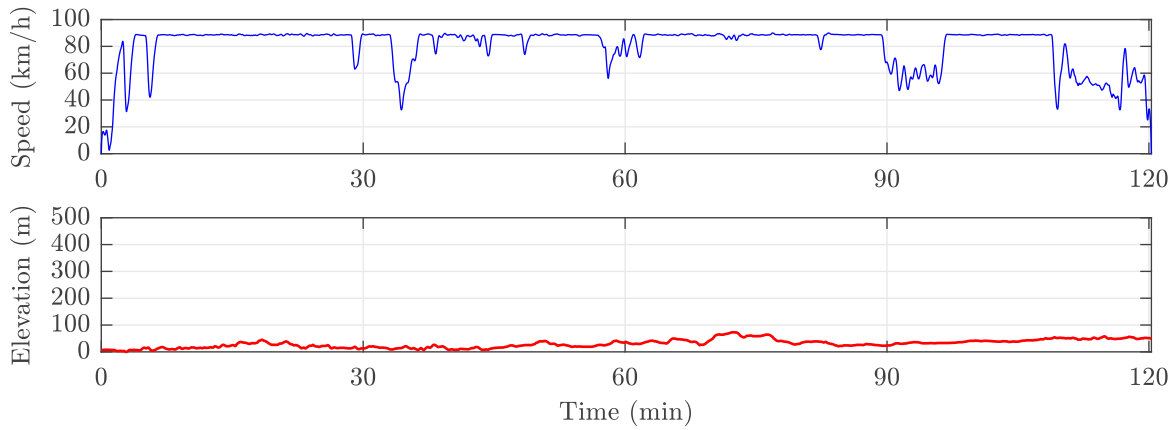

(a) Flat route.

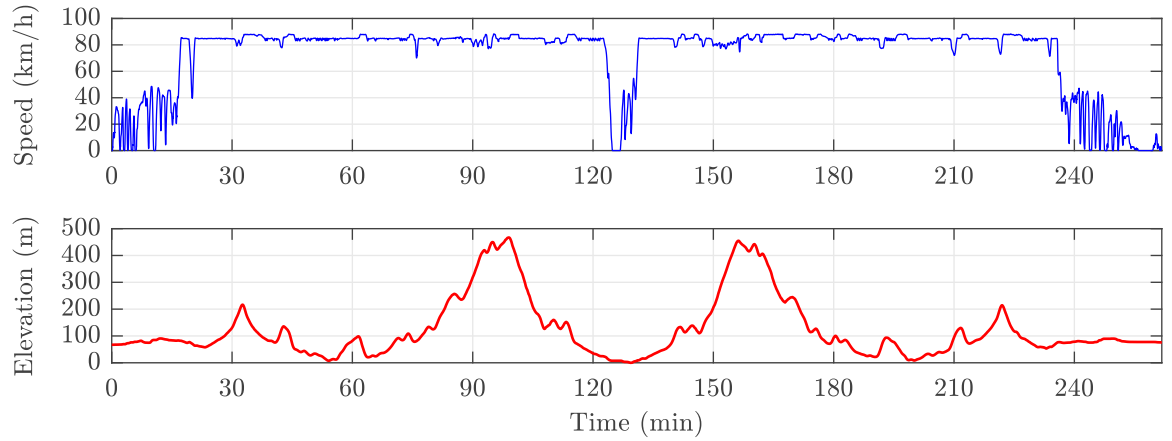

(b) Hilly route.

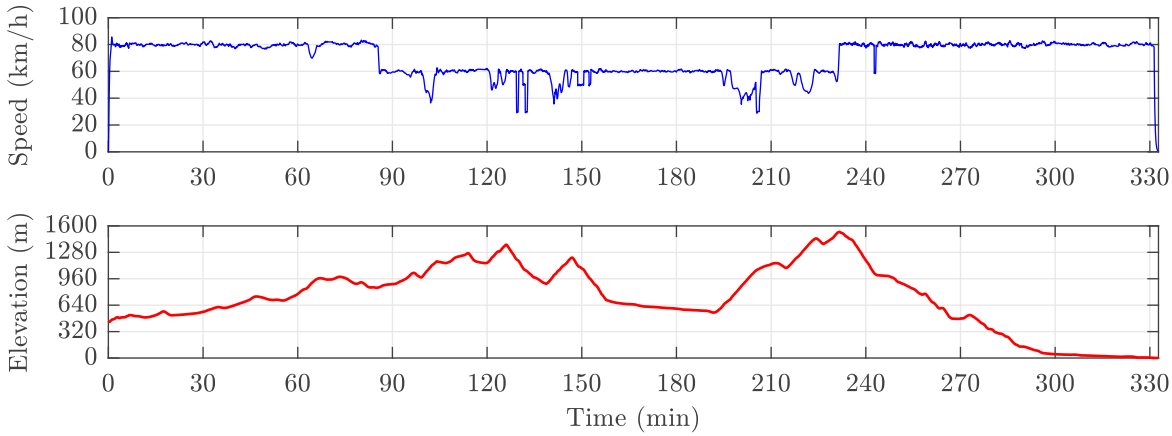

(c) Mountain route.

Figure 2.12: Real-world driving cycles in different route topographies.

the starting point. The route connects Graz and Vienna (in Austria) and the maximum elevation change is 465 meters.

- Figure 2.12c shows a driving cycle on a mountain motorway route through the Brenner Pass in the Italian and Austrian alps. The vehicle cruises at two different speed levels: 80 km/h in the initial and final sections and 60 km/h in between. The maximum elevation change is 1530 meters, making this driving cycle extremely challenging for long-haul transportation.

The three real-world driving cycles described above are part of a larger pool (containing 300 in total) used in this work for the robust validation of the proposed energy management strategies. Visualizing the speed and elevation profiles of all the driving cycles would be too cumbersome. Nevertheless, Figure 2.13 shows some driving metrics that help characterize the real-world driving cycles. The metrics are vehicle mass, trip duration, distance, average speed, relative positive acceleration (RPA), total climb, maximum elevation change, average electric load, and total electric load. Analyzing these metrics reveals how diverse the driving cycle pool is.

- The vehicle mass is calculated as mentioned above and ranges between 22 and 42 tons. Each value corresponds to the maximum payload that the truck can carry on the specific route following the recorded driving cycle.
- The trip duration, distance, and average speed have a straightforward meaning.
- High RPAs indicate that the cycle includes long sub-urban/urban roads, heavy traffic, or frequent turns. On the other hand, low RPAs indicate a stable motorway cruising with low or absent traffic.
- A high total climb distinguishes long steep roads or frequent ups and downs. The maximum elevation change indicates flat, hilly, or mountain roads.
- The electric load is calculated as explained in Section 2.1.1. The average load ranges between 80 kW and 160 kW, indicating how demanding the driving cycle is. The total electric energy demanded during the driving cycle ranges between 200 kWh and 700 kWh.

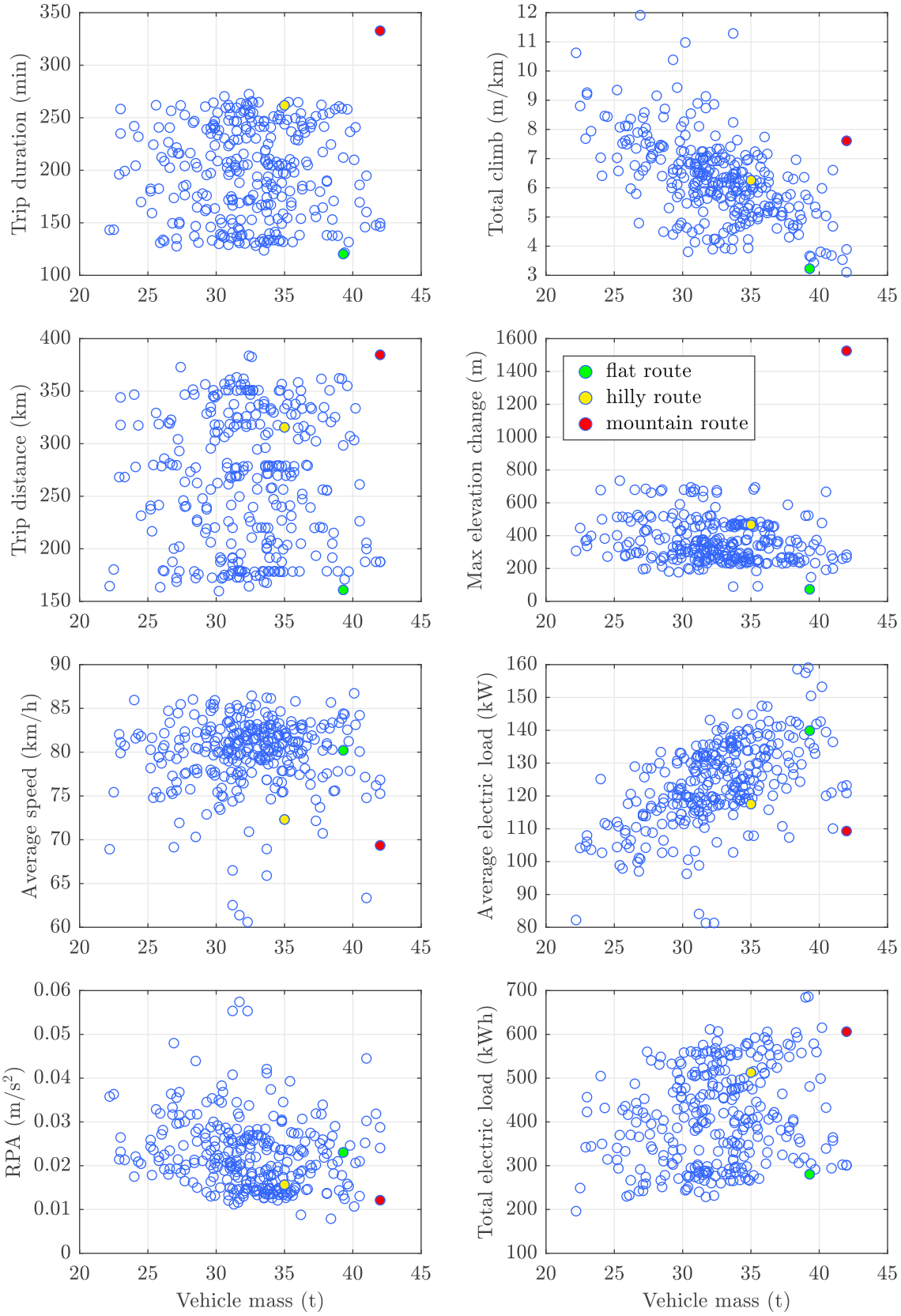

Figure 2.13: Speed and elevation metrics of the selected real-world driving cycles.

2.3 Optimal control theory

This section summarizes the most relevant methods from optimal control theory for developing energy management strategies. Solving an optimal control problem generally means finding the control law that minimizes an objective function while meeting a set of constraints. For example, in energy management strategies, the goal could be to find the optimal power-split law that minimizes the overall fuel mass and meets the constraints related to the maximum, minimum, and final value of the battery state of charge.

2.3.1 General formulation of optimal control problems

The following notation is adopted for the general formulation of the optimal control problem: x for the state variables, u for the input variables, and z for the disturbance variables. The optimization considers 0 as initial time and t_{fin} as final time. Eventually, the optimal control problem is formulated as in (2.31), and solving it means finding the optimal control law $u(t)$ that minimizes the objective function C.

$$\min_{u(t)} C = \int_0^{t_{fin}} L(x(t), u(t), z(t))\, dt \tag{2.31a}$$

with:

$$\dot{x} = f(x(t), u(t), z(t)) \tag{2.31b}$$

subject to:

$$x(0) = x_{in} \tag{2.31c}$$

$$x(t_{fin}) = x_{fin} \tag{2.31d}$$

$$x_{min}(t) \leq x(t) \leq x_{max}(t) \tag{2.31e}$$

$$u(0) = u_{in} \tag{2.31f}$$

$$u(t_{fin}) = u_{fin} \tag{2.31g}$$

$$u_{min}(t) \leq u(t) \leq u_{max}(t) \tag{2.31h}$$

Here, $L(\cdot)$ is the stage cost function, whereas $f(\cdot)$ expresses the state dynamics. The constraints for the state and input variables are imposed on the initial, final, minimum, and maximum values. The objective function can sometimes contain penalty functions and terminal costs to implement soft constraints.

Three methods from the optimal control theory are investigated in this thesis. Dynamic programming (DP) can find the optimal solution to any problem by adopting a combinatorial approach, given that all the disturbances are known and the computational power is sufficient. Pontryagin's minimum principle (PMP) is a set of necessary but not sufficient conditions for optimality. Model predictive control (MPC) optimizes the control law over a finite time horizon using a model of the system to predict its future

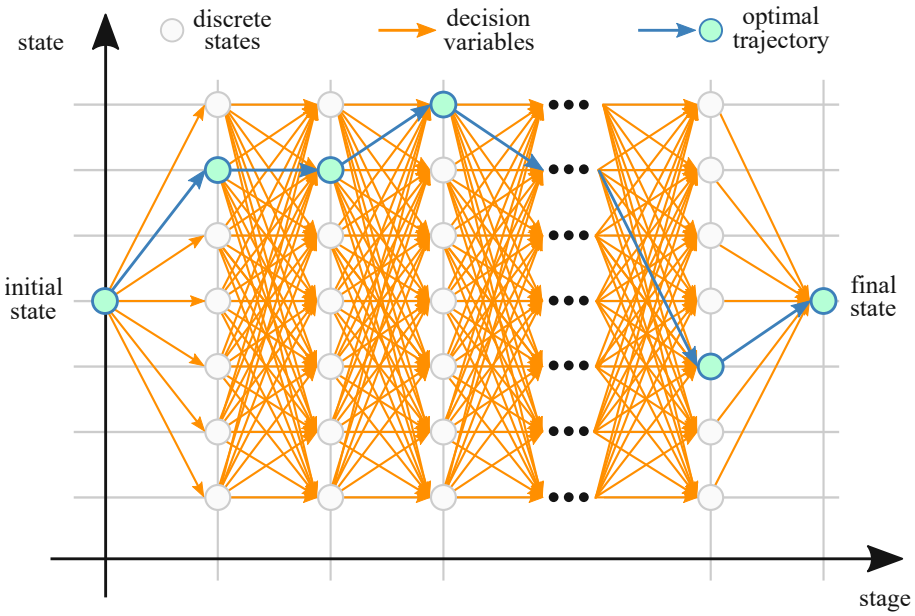

Figure 2.14: Representation of dynamic programming principle.

outputs. Eventually, dynamic programming is the method selected for developing the predictive energy management strategy at the core of this thesis because PMP and MPC generally yield sub-optimal solutions to the optimal energy management problem. Therefore, dynamic programming is detailed below, whereas PMP and MPC are detailed in the Appendix A.

2.3.2 Dynamic programming

Richard Bellman introduced dynamic programming in 1957 as a solution for multi-stage decision problems in which time plays a significant role, and the order of operations may be crucial [92]. Dynamic programming is one of the most common techniques to solve optimal control problems because the solution is guaranteed to be globally optimal and because of its capability to handle multiple complex constraints. The optimization principle of dynamic programming is sketched in Figure 2.14. In particular, the optimization considers all the possible trajectories to go from an initial state to a final one. Eventually, the optimal trajectory is the one that minimizes the objective function over the entire timespan.

The practical implementation of a DP algorithm requires discretization of the time, state, and input variables. Therefore, the optimal control problem in (2.31) is rewritten in discrete form as in (2.32). For simplicity, the notation refers to a system with single state, single input, and single disturbance. Regarding the discretization, $k \in \{1, \dots N\}$ indicates the k-th time stage.

$$\min_{\{u_1,\dots u_N\}} C = \sum_{k=1}^{N} \left[L(x_k, u_k, z_k) + \phi(x_k, u_k, z_k)\right] \tag{2.32a}$$

with:

$$x_{k+1} = F(x_k, u_k, z_k) \tag{2.32b}$$

subject to:

$$x_1 = x_{in} \tag{2.32c}$$
$$x_N = x_{fin} \tag{2.32d}$$
$$x_{min} \leq x_k \leq x_{max} \tag{2.32e}$$
$$u_1 = u_{in} \tag{2.32f}$$
$$u_N = u_{fin} \tag{2.32g}$$
$$u_{min} \leq u_k \leq u_{max} \tag{2.32h}$$

Here, the penalty function $\phi(\cdot)$ was introduced to include soft constraints on the state and input variables. Moreover, the maximum and minimum constraint thresholds for the state and input variables are assumed to be constant. The function $F(\cdot)$ expresses the discrete dynamics of the system.

The implementation of dynamic programming relies on the so-called *Bellman's principle of optimality* [93]:

> "An optimal policy has the property that whatever the initial state and initial decision are, the remaining decisions must constitute an optimal policy with regard to the state resulting from the first decision."

Based on this principle, the DP algorithm calculates the optimal control policy U^* and the optimal cost-to-go J at every stage k proceeding backward in time. A representation of the algorithm is shown in Figure 2.15. The following notation is adopted: $x_i \in \{x_{min}, \dots x_{max}\}$ is the i-th element of the discrete state variable space. Similarly, $u_j \in \{u_{min}, \dots u_{max}\}$ indicates j-th element of the discrete input variable space. In the discretized time-state space, $J_k(x_i)$ denotes the optimal cost-to-go in the node at stage k and state x_i. Following the backward optimization procedure, the optimal cost-to-go is:

$$J_k(x_i) = \min_{u_j} \left[J_{k+1}(F(x_i, u_j, z_k)) + L(x_i, u_j, z_k) + \phi(x_i, u_j, z_k)\right] . \tag{2.33}$$

For the same node, the optimal control policy $U_k^*(x_i)$ is calculated as:

$$U_k^*(x_i) = \arg\min_{u_j} \left[J_{k+1}(F(x_i, u_j, z_k)) + L(x_i, u_j, z_k) + \phi(x_i, u_j, z_k)\right] . \tag{2.34}$$

The so-called grid mismatch is an implementation issue originating from the fact that $F(x_i, u_j, z_k)$ is likely not included in the discrete grid of the state variable. This issue is shown by the red points in Figure 2.15. Since these points are not part of the grid,

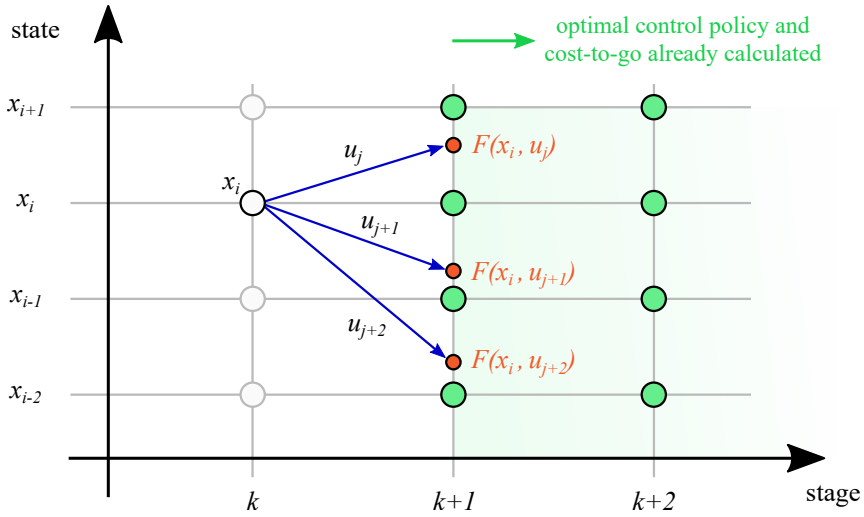

Figure 2.15: Scheme for the DP algorithm, including the discretized time-state space and input variable.

the corresponding cost-to-go is not known. In this thesis, a linear interpolation of the cost-to-go is used to overcome the grid mismatch, as suggested in [94].

One of the main drawbacks of DP is that it requires the apriori knowledge of all disturbances. However, future disturbances are usually unknown in most applications, making dynamic programming unsuitable for real-time control. Due to its non-causal nature, dynamic programming has been mostly used to create an optimal performance benchmark for the design of causal real-time controllers.

The dynamic programming solution is optimal up to the error introduced by the discretization of the distance, state, and input variables. In general, the denser the discretization grids, the better the solution. However, another disadvantage of dynamic programming is its significant complexity [28]. In general, the computational burden of DP scales linearly with the number of stages N and exponentially with the number of states n and input variables m:

$$\mathcal{O}(N \cdot p^n \cdot q^m) \ , \tag{2.35}$$

where p and q are the number of elements in the discrete state and input grids. The exponential increase in computational time due to the higher number of state and input variables is often referred to as the *curse of dimensionality*.

Chapter 3

Predictive energy management strategy

This chapter first offers an overview of energy management strategies, analyzing the benefits and drawbacks of typical methods from literature. Then, it focuses on the design of a predictive energy management strategy that can yield optimal results for fuel consumption and SoC control even in high-demanding driving cycles.

This chapter incorporates the findings of the author's publications [57, 58, 60, 61, 65].

3.1 Overview on energy management strategies

The energy management strategy distributes the load demand between the power sources of hybrid vehicles. Since the EMS defines how the powertrain components operate, this control function significantly impacts their efficiency and degradation. The literature on energy management strategies for fuel cell electric vehicles is vast [34]–[69]. Since a one-solution-fits-all energy management strategy does not exist, several studies have been conducted considering different methods, targets, and powertrain configurations. In Chapter 1, it has already been mentioned that there is a fundamental research gap in energy management strategies for long-haul fuel cell electric trucks. Moreover, the strategies developed for light-duty vehicles cannot be directly transferred to long-haul trucks because they are usually less effective due to the significant impact of the vehicle weight on the electric load demands.

Energy management strategies are usually categorized as *online* if they can be employed for on-board vehicle control. On the other hand, *offline* strategies are unsuitable for on-board control because they require complete and apriori knowledge of the driving cycle, which is impossible in road vehicles. Nevertheless, offline strategies can provide performance benchmarks for designing online strategies, which is why they have been widely used in the literature. Dynamic programming and Pontryagin's minimum principle are by far the most used methods for offline energy management strategies.

Dynamic programming can find the global optimum solution to any control problem.

However, its fundamental drawback is that it requires high computational time and memory, and complete and apriori knowledge of the disturbances. For these reasons, dynamic programming has been typically used as a benchmark to design online energy management strategies.

Pontryagin's minimum principle finds the extremal solutions of optimal control problems, which generally are sub-optimal. Nonetheless, the literature has shown that for hybrid electric vehicles, PMP has similar performance to DP for fuel consumption optimization but has the advantage of being computationally faster [95]. However, PMP has the fundamental limitation of being unable to deal with state constraints intrinsically. This issue can be critical for energy management strategies if the battery is undersized compared with the electric load demands. Moreover, if the objective function of the optimization includes more targets than simply fuel consumption, it is not valid anymore that the extremal solution found with PMP is close to the optimal one found with DP.

Opposite to offline energy management strategies, the online ones can be implemented for on-board vehicle control because they do not require apriori knowledge of the entire driving cycle. In general, online strategies are either *heuristic* (designed using engineering experience and relying on sets of rules) or *optimal* (based on the minimization of an objective function). The most popular method for online energy management is the equivalent consumption minimization strategy (ECMS), which can be seen as a simplified implementation of Pontryagin's minimum principle.

Further details on energy management strategies for fuel cell electric vehicles can be found in the review works [30]–[32]. Moreover, the author has already addressed the most relevant aspects of literature works in the publications [57, 58, 60], focusing on the most relevant aspects of energy management of fuel cell electric trucks. One of the outcomes of these publications is that using long-term elevation forecasts in predictive energy management strategies is significantly beneficial for fuel consumption in challenging driving cycles. Moreover, predictive energy management strategies are the only way to prevent the worst-case scenario in which the vehicle must slow down or even stop because the battery is fully discharged and the fuel cell cannot sustain the load demand on its own.

In the literature, health-conscious energy management strategies have been developed for light-duty fuel cell vehicles in [40]–[44], but no study has focused on trucks yet. In this chapter, the optimal energy management problem considers fuel consumption and battery SoC control as targets. However, the strategy presented here is extended in the following chapter to include fuel cell and battery degradation within the optimization targets.

In this thesis, the energy management strategy performs the power-split between the fuel cell and battery systems based on the electric power request of the driver. In this thesis, the EMS defines the power setpoints for the fuel cell system, P^*_{fcs}, and for the battery system, P^*_{bat}. Eventually, the fuel cell and battery systems follow these setpoints under the constraints described in (2.12) and Table 2.2. Assuming that the driver demand must always be met, the EMS defines the battery setpoint as:

$$P^*_{bat} = P_{el,des} - P_{fcs}\ \eta_{dc,dc} + P_{fcs,cool}\ , \tag{3.1}$$

based on the current load demand and fuel cell power. Thus, the battery always operates as a buffer between the fuel cell and the electric loads. This means that the EMS only has one degree of freedom for the power-split: defining the fuel cell setpoint.

The objective function for optimal energy management is the fuel consumption over the driving cycle. For a fair comparison of different strategies, this work always considers the equivalent battery consumption to calculate the overall fuel consumption as:

$$C = \int_0^{t_{fin}} \dot{m}_{\mathrm{H_2}}(t)\ dt + \frac{(\mathrm{SoC}_{in} - \mathrm{SoC}_{fin})\ E_{bat,max}}{\tilde{\eta}_{fcs}\ \mathrm{LHV}_{\mathrm{H_2}}}\ , \tag{3.2}$$

where $\tilde{\eta}_{fcs}$ is the average efficiency of the fuel cell system during the driving cycle, SoC_{in} is the initial state of charge, and SoC_{fin} the final one. The second term in the equation above is the equivalent battery consumption associated with the SoC change over the driving cycle.

Controlling the state of charge is important to ensure that the battery always has enough charge to sustain the driving requirements (e.g. fast accelerations or route changes) but is never fully charged to perform regenerative braking consistently. Moreover, overcharging and fully discharging accelerate battery degradation (see Figure 2.9). Therefore, the SoC is constrained between maximum and minimum values as follows:

$$\mathrm{SoC}_{min} \leq \mathrm{SoC}(t) \leq \mathrm{SoC}_{max}\ . \tag{3.3}$$

The results below are obtained considering the vehicle model described in Chapter 2 and a battery system with a nominal energy capacity of 70 kWh. Moreover, the fuel cell and battery systems are always assumed in begin-of-life conditions since the objective function of the optimal energy management problem does not include fuel cell and battery degradation. Lastly, the ambient temperature, which impacts the energy consumption due to fuel cell cooling, is assumed at 20°C.

Preliminary findings and investigations on energy management strategies are described in Appendix B as a supplement to this chapter. Appendix B.1 studies offline energy management strategies based on dynamic programming and Pontryagin's minimum principle. The results show that the strategies are practically equivalent when the driving requirements are low. However, for more demanding driving cycles, PMP does not

yield global optimality as DP and cannot deal with the SoC constraints. Appendix B.2 compares online energy management strategies that can be practically implemented for on-board control. The first is based on simple heuristics, whereas the second is a model predictive control strategy with short-term load forecasts. The simulation results indicate that both strategies yield similar fuel consumption, even though their complexity is entirely different. However, the comparison with dynamic programming shows that both strategies are close to optimality for low-demanding driving cycles, but the results are significantly worse for more challenging ones. These findings also indicate that predictive energy management strategies with short-term horizons cannot yield optimal results.

3.2 Design of a dual-stage predictive energy management strategy

This thesis proposes a predictive energy management strategy with the dual-stage control structure depicted in Figure 3.1. In the first stage, the energy management strategy is optimized at the beginning of the driving cycle based on the speed and elevation forecasts of the navigation system. The optimization results are stored as predictive references for the entire route, which the on-board energy management strategy uses in the second control stage.

The main advantage of using the dual-stage control structure is that it allows predictive energy management with long horizons while fulfilling real-time computational requirements. Indeed, in the first stage, the fuel cell power profile is optimized in one shot over the entire route: i.e. the predictive horizon corresponds to the full driving cycle length.

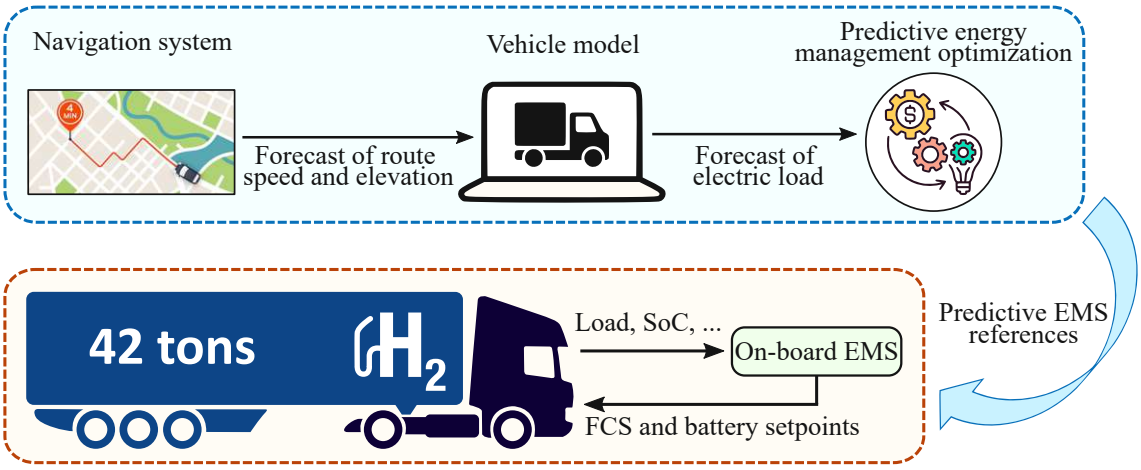

Figure 3.1: Dual-stage structure of the predictive energy management strategy.

The one-shot optimization can be performed in a relatively low computational time at the beginning of the driving cycle and does not have to be repeated (if the route does not change). This approach results in a significantly lower computational complexity than the receding horizon optimization approach at the base of MPC strategies.

Another advantage of the proposed structure is that it allows the implementation of dynamic programming as an online energy management strategy with low computation complexity even though, in the literature, it is usually only used for offline ones.

The author's works [60] and [61] already described the dual-stage structure, where the optimal control problem is formulated so that it can be solved using quadratic programming. Then, in the recent work [65], the predictive energy management strategy has been improved in two main aspects:

- The optimal control problem in the first stage is solved using dynamic programming to obtain the optimal solution. This improvement is significant because, with quadratic programming, the system needs to be represented with a simplified linear model, resulting in a sub-optimal solution.
- The second improvement regards the on-board energy management strategy: initially, it only used the predictive SoC reference. Then, also the predictive reference of the fuel cell power was included in the on-board strategy, resulting in a significantly better SoC control.

3.2.1 Dynamic programming optimization in the first stage

In the first stage, the speed and elevation forecasts coming from the navigation system are converted into the electric load forecast for the entire route, using the longitudinal dynamics with a backward-facing modeling approach (see Section 2.1.1). The speed, elevation, and electric load forecasts are assumed as position-based (or distance-based) profiles because, in real applications, it is impossible to predict the vehicle speed before the driving cycle starts with absolute precision. Therefore, it is unrealistic to express the forecasts as time-based since time depends on speed. For example, at the beginning of the driving cycle, one can say that the vehicle will be at the highest elevation after a specific amount of kilometers. On the contrary, it is impossible to precisely say how much time it will take to reach that point because it depends on the driver's behavior, traffic conditions, and several other factors.

The speed forecast can be realized with different levels of accuracy. For example, it could derive from a sophisticated forecasting system considering current and usual traffic speed, road curvature, and weather. However, the speed forecast can also be simply obtained from the speed limits over the route or even assuming a constant speed value.

In general, the implementation of dynamic programming requires discretization of the time, state, and input variables (see Section 2.3.2). However, unlike other approaches

in the literature, dynamic programming is implemented for an optimal control problem formulated over the traveled distance s instead of time. The distance grid is created with uniform spacing, Δs. The time interval to travel the distance Δs changes depending on the vehicle speed. Thus, the time interval for the k-th element is calculated as:

$$\Delta t_k = \Delta s / v_k \ . \tag{3.4}$$

The optimal control problem in Section 2.3 is adapted below for the energy management of fuel cell electric vehicles. In this case, there is one state variable (i.e. the battery SoC), one input variable (i.e. the fuel cell power), and one disturbance variable (i.e. the electric load). The objective function of the optimization is the fuel consumption expressed in (3.2). The SoC control is guaranteed by imposing constraints on the initial, final, minimum, and maximum values. Therefore, the optimal control problem (2.32) is rewritten as:

$$\min_{\{P_{fcs,1},\dots P_{fcs,N}\}} \sum_{k=1}^{N} \dot{m}_{\mathrm{H_2}}(P_{fcs,k})\ \Delta t_k + \phi_k \tag{3.5a}$$

subject to:

$$\mathrm{SoC}_1 = \mathrm{SoC}_{in} \tag{3.5b}$$

$$\mathrm{SoC}_N = \mathrm{SoC}_{fin} \tag{3.5c}$$

$$\mathrm{SoC}_{min} \leq \mathrm{SoC}_k \leq \mathrm{SoC}_{max} \tag{3.5d}$$

$$0 \leq P_{fcs,k} \leq P_{fcs,max} \tag{3.5e}$$

with the discrete system dynamics expressed as:

$$\mathrm{SoC}_{k+1} = \mathrm{SoC}_k - \Delta t_k \ \frac{V_{oc,k} - \sqrt{V_{oc,k}^2 - 4\, P_{bat,k}^{*}\, R_{int,k}}}{2\ R_{int,k}\ Q_{bat,max}} \ . \tag{3.6}$$

with the battery power expressed as in (3.1), depending on the fuel cell power and the electric load. The open circuit voltage and internal resistance have the stage subscript k because they change with the SoC. The additive penalty function ϕ_k allows to implement soft constraints on the state of charge. The function is defined as:

$$\phi_k = \begin{cases} \phi^* & \text{if} \quad \mathrm{SoC}_k > \mathrm{SoC}_{max,soft} \\ \phi^* & \text{if} \quad \mathrm{SoC}_k < \mathrm{SoC}_{min,soft} \\ 0 & \text{otherwise} \end{cases} \tag{3.7}$$

where $\phi^* = 0.67$, that is a constant value 100 times higher than the maximum hydrogen consumption from Figure 2.4. The values for the soft constraints, $\mathrm{SoC}_{min,soft}$ and $\mathrm{SoC}_{max,soft}$, are 0.20 and 0.95, unless otherwise indicated.

The solution to the optimal control problem found with dynamic programming is optimal up to the error introduced by the discretization of the distance, state, and input

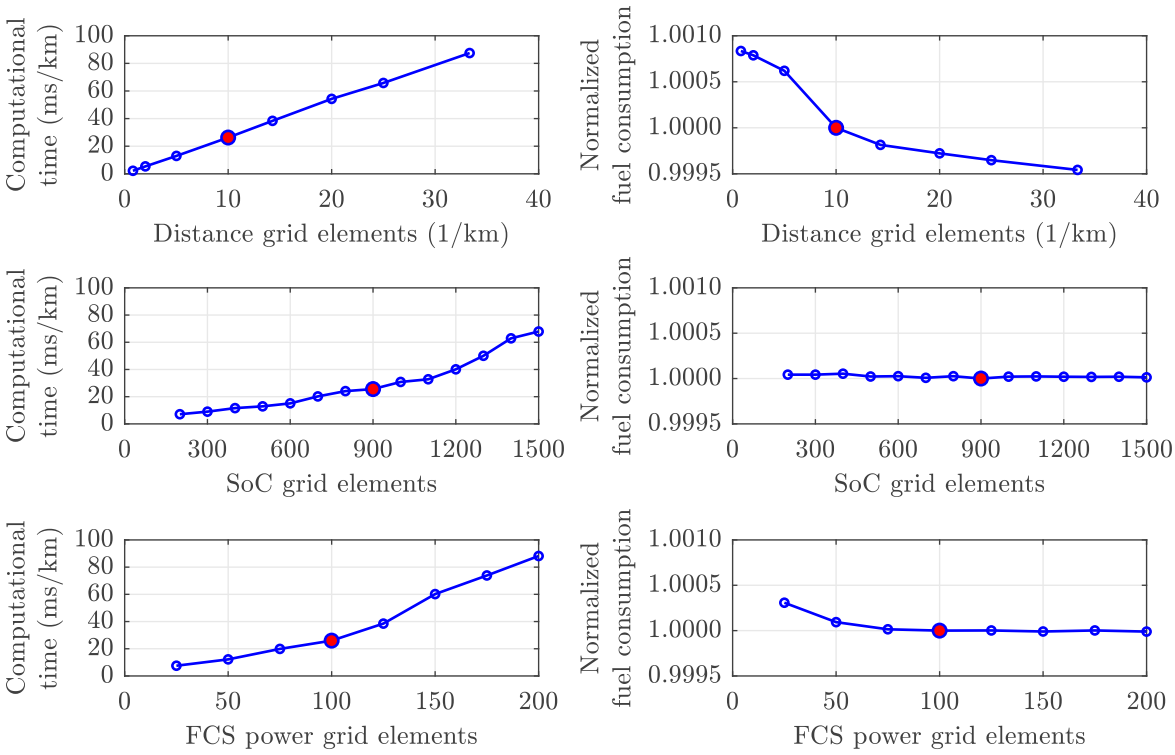

Figure 3.2: Impact of discretization grids on computational time and fuel consumption.

variables. In general, more elements in the discretization grids result in more accurate solutions but at the cost of higher computational time. After studying the impact of the discretization grids on computational time and fuel consumption in Figure 3.2, it is assumed that the distance grid spacing is 100 meters, the number of elements in the SoC grid is 900, and 100 in the fuel cell power grid. Eventually, the computational time required for the optimization is 25 ms/km, which is well within the real-time control requirements. Indeed, assuming that the vehicle travels at 80 km/h, it would take 45 seconds to drive 1 kilometer. Therefore, the real-time computing factor would be: $45/0.025 = 1800$.

Figure 3.2 shows the results of the complexity analysis obtained by changing the discretization of one of the grids while keeping the others at the mentioned values (corresponding to the red markers). The computational time increases linearly with the distance grid elements but quadratically with the SoC and fuel cell power elements. On the other hand, the impact on fuel consumption is negligible, and even broader grids can yield excellent results. Eventually, the real-time computing factor could be increased with a negligible impact on the optimization results. The computational times Figure 3.2 refer to simulations performed using MATLAB R2022a on a computer with 3.60 GHz of base CPU speed and 32 Gb of RAM.

The results of the dynamic programming optimization are stored as position-based predictive references for the battery state of charge and fuel cell power over the entire route: SoC_{ref} and $P_{fcs,ref}$. These references are used in the second stage by the on-board energy management strategy.

3.2.2 On-board rule-based strategy in the second stage

The second control stage of the predictive energy management strategy is essential to compensate for the modeling and forecasting uncertainties that the predictive reference optimization cannot consider. Several approaches with different complexity levels could be adopted for on-board energy management, relying on the predictive references optimized in the first stage. This thesis adopts a simple heuristic control approach that has minimal computational time. In particular, the on-board energy management strategy is rule-based and similar to the one described in Appendix B.2.1.

The fuel cell power setpoint is defined considering the deviation of the electric load and SoC from the predictive references:

$$P^*_{fcs} = P_{fcs,ref} + r_1 \left(P_{el,des} - P_{fcs,ref}\right) + r_2 \left(\mathrm{SoC}_{ref} - \mathrm{SoC}\right) . \tag{3.8}$$

Additionally, the fuel cell power setpoint is subject to the following constraints:

$$|\dot{P}^*_{fcs}| \leq r_3 , \tag{3.9a}$$

$$r_4 \leq P^*_{fcs} \leq P_{fcs,max} . \tag{3.9b}$$

The parameter r_3 is the rate of change limit for the fuel cell power setpoint, whereas r_4 is the idle fuel cell power defined by the energy management strategy. In this chapter, it is set to zero. However, to avoid fuel cell degradation due to low-power operation, it can be set to 10% of the nominal power (see Section 2.1.4).

Another constraint ensures that the battery can absorb the available regenerative braking power entirely by reducing the fuel cell power:

$$P^*_{fcs} \geq P_{el,des} - P_{bat,ch} \text{ , active if: } r_5 = 1. \tag{3.10}$$

The maximum battery charging power, $P_{bat,ch}$, derives from the C-rate and voltage limits indicated in Table 2.2 and changes over time depending on the SoC. The constraint is active only if the parameter r_5 is 1. However, deactivating the constraint can result in significant mitigation of the fuel cell degradation due to dynamic loading.

Here, the parameter r_1 is set to zero, so the energy management strategy strictly follows the predictive fuel cell power reference generated in the first stage. On the other hand, r_2 is set to 400 kW to ensure that the strategy compensates for the SoC deviations caused by the forecasting and modeling uncertainties. Lastly, the parameter r_3 is set to 9 kW/s, r_4 to 0, and r_5 to 1.

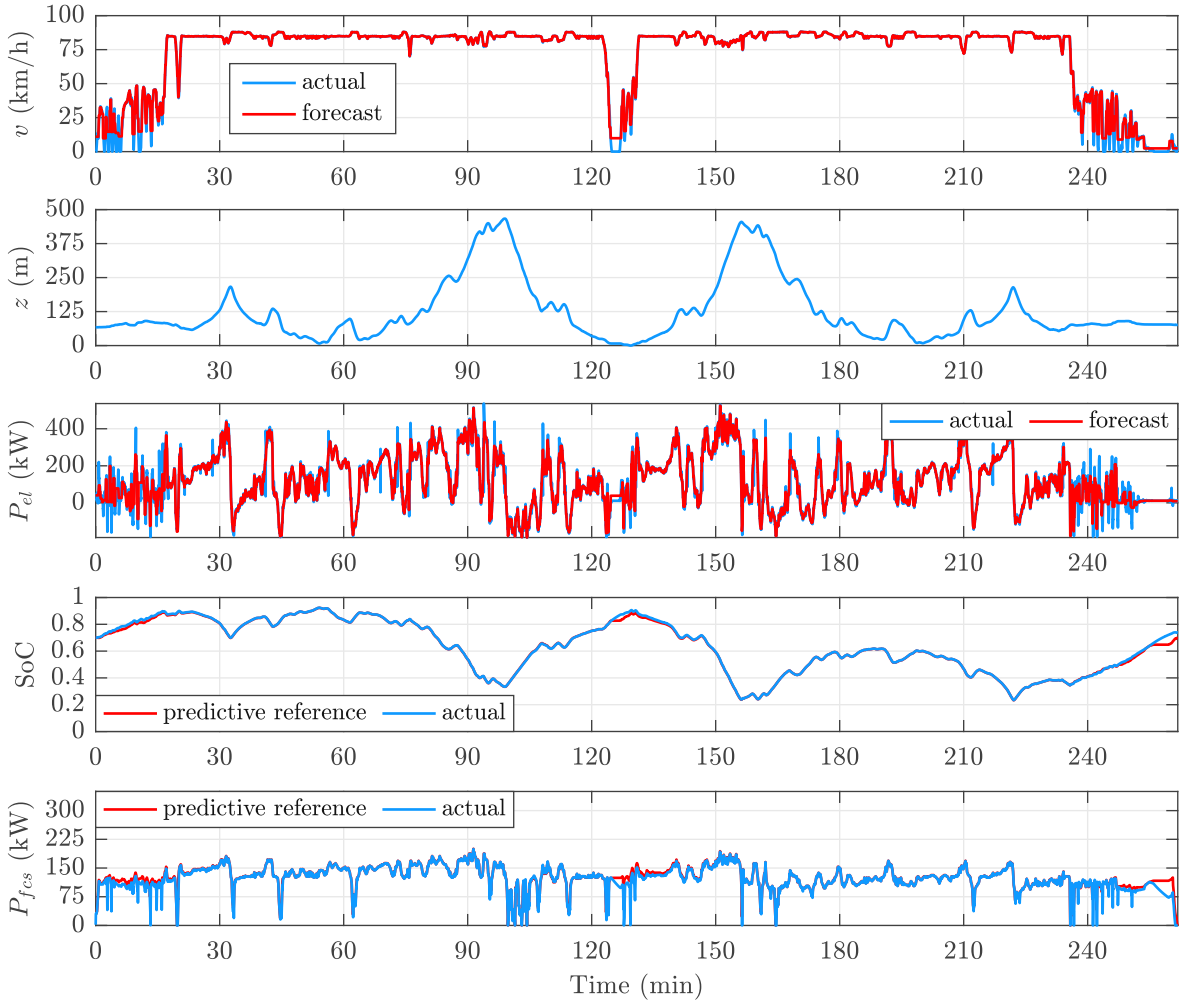

Figure 3.3: Simulation results of the dual-stage predictive energy management strategy assuming accurate speed forecast.

3.2.3 Robust validation in realistic driving scenarios

Figure 3.3 shows the simulation results of the dual-stage predictive energy management strategy for the driving cycle on the hilly route, assuming that the speed forecast is highly accurate. However, the forecast does not correspond precisely to the actual speed of the driving cycle due to the distance grid discretization. The deviation is particularly noticeable at low speeds and during stops. Consequently, the electric load forecast also does not precisely match the actual one, even though it is quite accurate. Thanks to this accurate load forecast, the predictive references for the SoC and fuel cell power are strictly followed, demonstrating the goodness of the optimization in the first stage. Indeed, deviations from the predictive references are only visible during the low-speed sections of the driving cycle, even if limited.

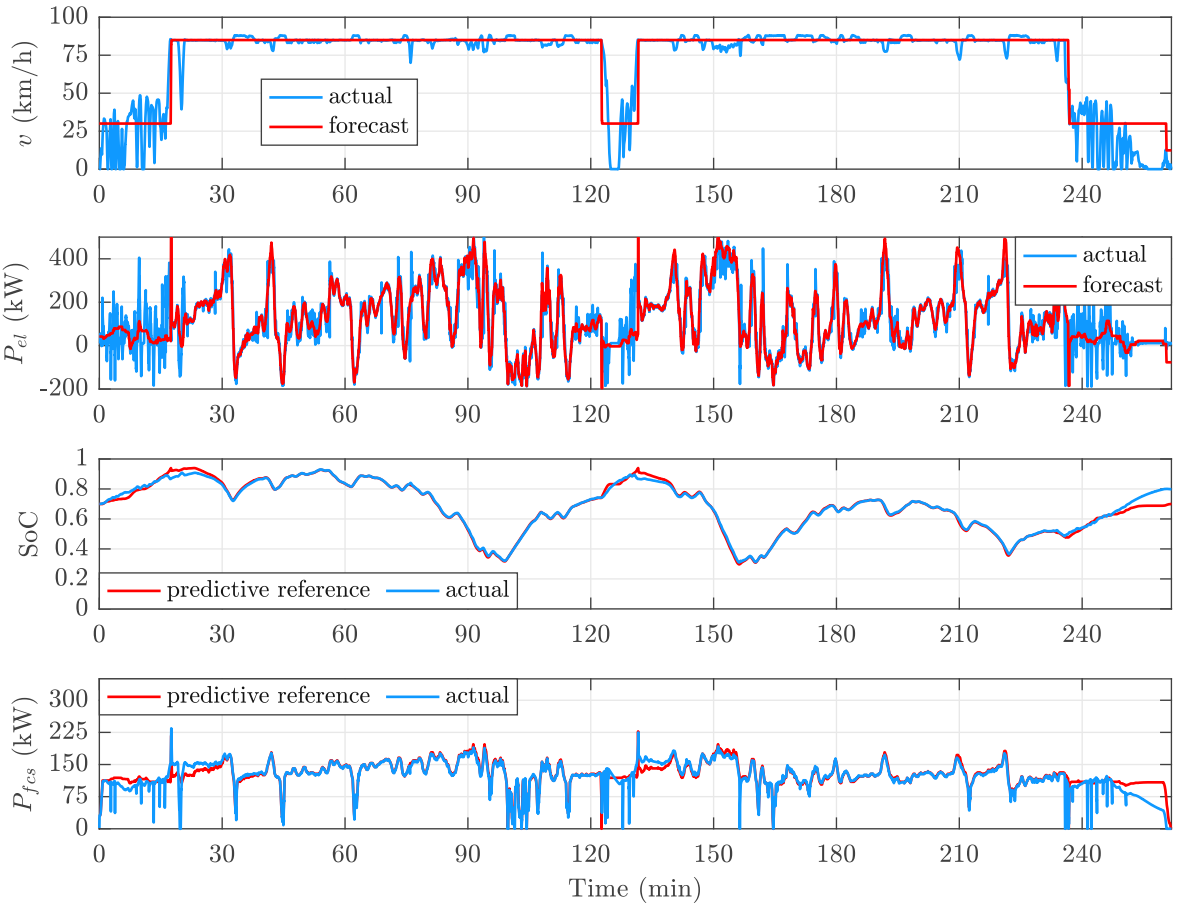

Figure 3.4: Simulation results assuming an uncertain speed forecast.

Figure 3.4 shows the simulation results of the predictive strategy considering an uncertain speed forecast derived from the speed limits. Nevertheless, the electric load forecast retains good accuracy because the road slope has the dominant impact on it. The predictive references are strictly followed during the motorway cruising sections of the driving cycle. Slight deviations are evident during the urban sections of the driving cycles. However, the on-board energy management strategies can compensate for the deviations and swiftly return close to the references.

One of the main advantages of the predictive energy management strategy is that it results in excellent SoC control while retaining optimal fuel consumption. For example, the soft constraints in the penalty function (3.7) are set to 0.60 and 0.80 to demonstrate the high degree of SoC control. Figure 3.5 shows the simulation results of the predictive energy management strategy (P-EMS) with tight SoC constraints and uncertain speed forecast. Remarkably, the P-EMS can keep the SoC bounded in such a narrow operating range even if the driving cycle is challenging due to the elevation profile. The figure also compares the results against the optimal dynamic programming solution. Notably,

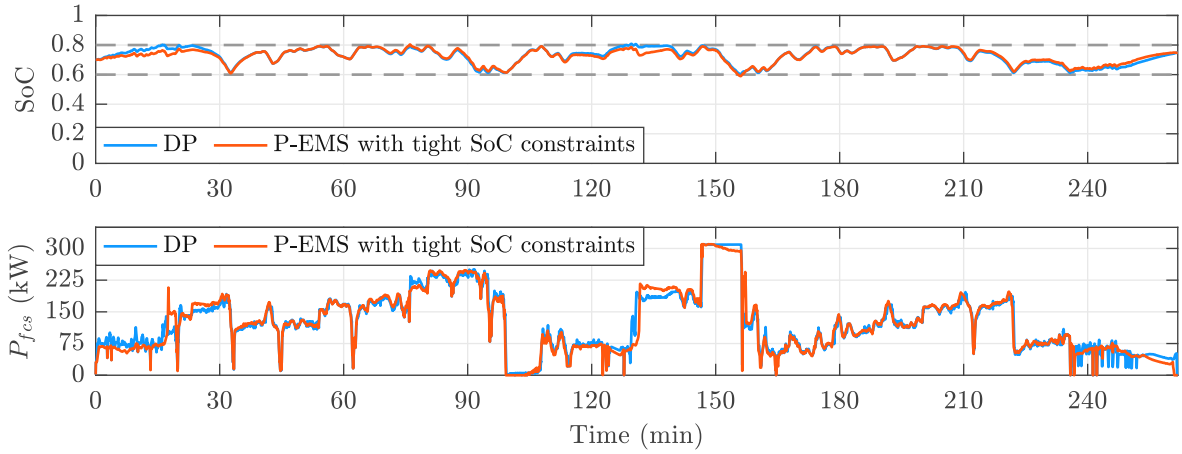

Figure 3.5: Simulation results considering tight SoC constraints in the predictive reference optimization and comparison with dynamic programming.

the SoC and fuel cell power profiles are similar, meaning that the predictive strategy is still close to optimality even with an uncertain speed forecast. This is because the route elevation is dominant in determining the electric load because of the heavy vehicle mass.

Table 3.1 summarizes the simulation results in terms of fuel consumption and final, minimum, and maximum SoC values. The fuel consumption comparison with DP is fair because the final SoC is the same. The comparison in the first row shows that when the P-EMS considers an accurate speed forecast, the results are practically optimal and identical to DP. At the same time, when the speed forecast is uncertain, the results are still relatively close to optimality since the deviation from the DP solution is 0.27% and 0.43%. For the same driving cycle, the fuel consumption of the strategies described

Table 3.1: Performance comparison between the P-EMS and DP on the hilly route driving cycle.

EMS	Fuel consumption		SoC		
	(kg/ 100 km)	deviation (%)	final	min	max
DP	9.666	-	0.74	0.24	0.92
P-EMS (accurate speed forecast)	9.672	0.06	0.74	0.23	0.92
DP	9.680	-	0.80	0.25	0.92
P-EMS (uncertain speed forecast)	9.706	0.27	0.80	0.31	0.93
DP	10.327	-	0.75	0.60	0.81
P-EMS (uncertain speed + tight SoC range)	10.371	0.43	0.75	0.59	0.80

in Appendix B.2 are 4.59% and 4.82% worse than the dynamic programming results (see Table B.2). Therefore, the predictive EMS significantly improves the performances thanks to the long-term load forecasts that included in the optimization of the predictive references.

Another important finding is that the fuel consumption increases by approximately 7% to keep the battery SoC within the tight operating range. The main reason is that the fuel cell needs to operate at maximum power between minutes 147 and 156, resulting in significantly higher hydrogen consumption (see Figure 2.4). A generalization of this finding is that restricting the operating range or reducing the battery size results in less degree of freedom for the fuel consumption optimization.

Lastly, the predictive energy management strategy was validated on the 300 real-world driving cycles described in Section 2.2 to confirm its robustness. The simulations considered the driving cycles in sequence, meaning that the final SoC at the end of a cycle becomes the initial one for the next cycle. This approach enables a fair comparison of the fuel consumption of different energy management strategies, regardless of the SoC change in the individual cycles.

Eventually, the performance of the energy management strategy is evaluated over a total distance of 80.000 km to demonstrate its goodness from a global point of view rather than for specific driving cycles. For simplicity, it is assumed that the speed forecast is highly accurate, i.e. the error is only due to the distance grid discretization.

Table 3.2 compares four energy management strategies. In particular, the predictive energy management strategy is considered with normal and tight SoC constraints. The third is the rule-based strategy described in Appendix B.2.1, whereas the last is a version with a more aggressive tuning ($r_1 = 0.5$ and $r_2 = 1500$ kW). The average fuel consumption is reported in tonne-kilometer (tkm): the product of vehicle mass and traveled distance, which is a standard metric in road freight transportation [3].

Table 3.2: Performance comparison of energy management strategies over the sequence of 300 real-world driving cycles.

	Fuel consumption			FCS	FCS energy	Battery ohmic
	(kg)	(kg/100 tkm)	change (%)	efficiency	(MWh)	losses (MWh)
P-EMS	7421	0.287	-	0.522	129.05	3.33
P-EMS (tight)	7457	0.288	0.35	0.519	128.93	3.17
RB	7489	0.290	1.05	0.515	128.61	2.71
RB (aggressive)	8005	0.309	7.67	0.482	128.74	1.38

A standard measure of freight activity is the tonne-kilometer (tkm) [3]. The predictive energy management strategy with normal SoC operating range has a fuel consumption of 0.287 kg/100 tkm, whereas the one with the tight SoC range has 0.35% higher consumption. This result differs significantly from the one in Table 3.1 because that one refers to a driving cycle that is extremely challenging from an energy management point of view. This outcome indicates that most driving cycles from the considered pool can be performed while keeping the SoC in a tight operating range with a negligible impact on fuel consumption. Interestingly, the ohmic losses of the battery system represent 2.6% of the total energy produced by the fuel cell system.

In this context, the rule-based strategy is representative of non-predictive energy management strategies. The rule-based strategy performs surprisingly well on average, as the fuel consumption is only 1.05% higher than the P-EMS. The reason is again that most of the driving cycles are not as challenging as the one shown in Figure 3.3. However, if the RB strategy is not properly tuned, the performance deteriorate quite significantly. For example, the strategy with the more aggressive tuning has 7.67% higher fuel consumption than the P-EMS. On the other hand, this tuning keeps the SoC in a tighter operating range than the other strategy.

3.3 Summary

The strategies proposed by the author in this thesis represent pioneering investigations on predictive energy management of fuel cell electric trucks. These works significantly contribute to advancing the scarce literature on energy management strategies for fuel cell electric trucks.

This section summarizes the main findings of this chapter:

- The predictive energy management strategy proposed in this thesis yields optimal fuel consumption and SoC control even in driving cycles that are extremely challenging from an energy management point of view. On the contrary, online strategies that do not consider long-term load forecasts perform significantly worse.
- The dual-stage control structure enables the implementation of an online energy management strategy based on dynamic programming, resulting in a highly efficient and novel approach for the literature.
- The computational complexity of the predictive EMS meets the requirements for real-time control. Moreover, the real-time computing factor of the predictive EMS could be improved (if necessary) without compromising the goodness of the solution.

- The speed forecast has a marginal impact on the performance of the predictive energy management strategy because the elevation plays the dominant role in forecasting the electric load of the vehicle.
- The predictive energy management strategy has excellent SoC control thanks to long-term load forecasts. Remarkably, it is possible to keep the SoC in a very narrow operating range, retaining optimal fuel consumption.
- The actual battery capacity significantly impacts the performance of fuel cell electric trucks in challenging driving cycles. Indeed, restricting the SoC operating range is highly detrimental to fuel consumption. On the contrary, larger battery sizes result in more degree of freedom for optimizing the energy management targets.
- The robust validation of the predictive energy management strategy considering 300 real-world driving cycles shows that the average fuel consumption is 0.287 kg/100 tkm. In comparison, the rule-based EMS, which is non-predictive, results in a 1.05% higher fuel consumption. This outcome indicates that the non-predictive EMS can perform relatively well because, on average, the driving cycles are not as challenging as the one on the hilly route.

This chapter designed a predictive energy management strategy with a dual-stage control structure based on dynamic programming. This energy management strategy yields excellent fuel consumption and SoC control, assuming that the fuel cell and battery state-of-health are known. In the next chapter, this strategy is extended to include fuel cell and battery degradation in the optimal control problem. In this way, the energy management strategy can adapt to the current state-of-health of the components and mitigate their degradation.

Chapter 4

Health-conscious energy management strategy

This chapter focuses on energy management strategies that consider fuel cell and battery degradation as additional optimization targets to extend the vehicle lifetime. Initially, it shows the energy management impact on degradation by calibrating the on-board strategy, as investigated in the author's publications [63, 65]. Then, it proposes a novel health-conscious dynamic programming energy management for optimizing the predictive references. Lastly, it analyzes the battery size impact on the control targets and the performance deterioration due to progressive powertrain degradation.

4.1 Overview on health-conscious energy management

The energy management strategy plays a critical role in ensuring that the powertrain components meet the lifetime requirements of long-haul transportation. Therefore, this chapter focuses on the design of a strategy that includes the fuel cell and battery degradation as additional energy management targets.

However, these targets are contrasting. Thus, a suitable trade-off between them should be found considering techno-economic criteria. Here, the energy management strategy is designed to obtain a balanced degradation between the components, assuming that the individual replacement of either component is unfavorable cost-wise. Therefore, the overall state of degradation of the powertrain SoD_{pt} corresponds to the one from the more degraded component:

$$\mathrm{SoD}_{pt} = \max(\,\mathrm{SoD}_{fcs}\,,\,\mathrm{SoD}_{bat}\,)\,. \tag{4.1}$$

The energy management strategy performances are analyzed considering the change in SoD over the individual driving cycle, which practically indicates the average degradation rate. In particular, following the definition of the fuel cell state of degradation

(2.23), the change in SoD_{fcs} is expressed as:

$$\Delta \mathrm{SoD}_{fcs} = \Delta V_{fcs}^{dc} / \Delta V_{fcs,EoL} \ , \tag{4.2}$$

where ΔV_{fcs}^{dc} is the voltage degradation over an individual driving cycle. Similarly, the change in battery state of degradation (2.29) is expressed as:

$$\Delta \mathrm{SoD}_{bat} = \int_{dc} \delta_{bat} \ |I_{bat}| \ dt \ . \tag{4.3}$$

In order to obtain a robust energy management design, this chapter considers the mountain-route driving cycle (see Figure 2.12c) for performance evaluation since it is the most challenging one from an energy management point of view. The SoC control is not always analyzed in detail, but all the results below have SoC within 0.25 and 0.90 to avoid battery overcharging or critical discharges. For simplicity, it is assumed that fuel cell and battery systems are always in begin-of-life conditions. Moreover, the vehicle mass is set to 42 tons and the ambient temperature to 35°C to create a worst-case scenario regarding the electric load request. Lastly, the battery system has a nominal energy capacity of 100 kWh unless otherwise indicated.

4.2 Calibration of on-board energy management strategy

The parameters of the on-board energy management strategy in (3.8), (3.9), and (3.10) significantly impact fuel consumption, fuel cell degradation, and battery degradation. Properly calibrating these parameters can greatly improve the energy management strategy performances.

Using a design of experiment (DoE) strategy is a practical way to calibrate the control parameters systematically. Here, the on-board strategy calibration results are analyzed to study the energy management impact on degradation and its trade-off with fuel consumption. This preliminary investigation considers predictive references for the EMS optimized for fuel consumption, following the approach described in Section 3.2.1.

Latin hypercube sampling [96] is used to generate 2000 combinations of the four parameters: r_1, r_2, r_4, and r_5. The parameter r_3 is kept constant because it has a negligible influence. The variation ranges of the parameters are indicated in Table 4.1. The square brackets indicate that the parameters variate continuously in the range, whereas the curly ones indicate the set of possible values. For example, r_5 can only be 0 or 1.

Table 4.1: Variation range of the on-board strategy parameters for the Latin hypercube sampling.

r_1	r_2	r_4	r_5
[0, 1]	[100 kW, 2000 kW]	{0, 31 kW}	{0, 1}

Figure 4.1 shows the calibration results in terms of average degradation and fuel consumption rates. The first tile indicates that fuel cell and battery degradation are inversely proportional: reducing one increases the other. In other words, simultaneously minimizing the degradation of both components is impossible, and an appropriate trade-off must be found to minimize the overall powertrain degradation. In particular, it is essential to ensure balanced degradation of the fuel cell and battery systems. The figure highlights the results corresponding to the minimum fuel consumption and powertrain degradation, which lies close to the balanced degradation line.

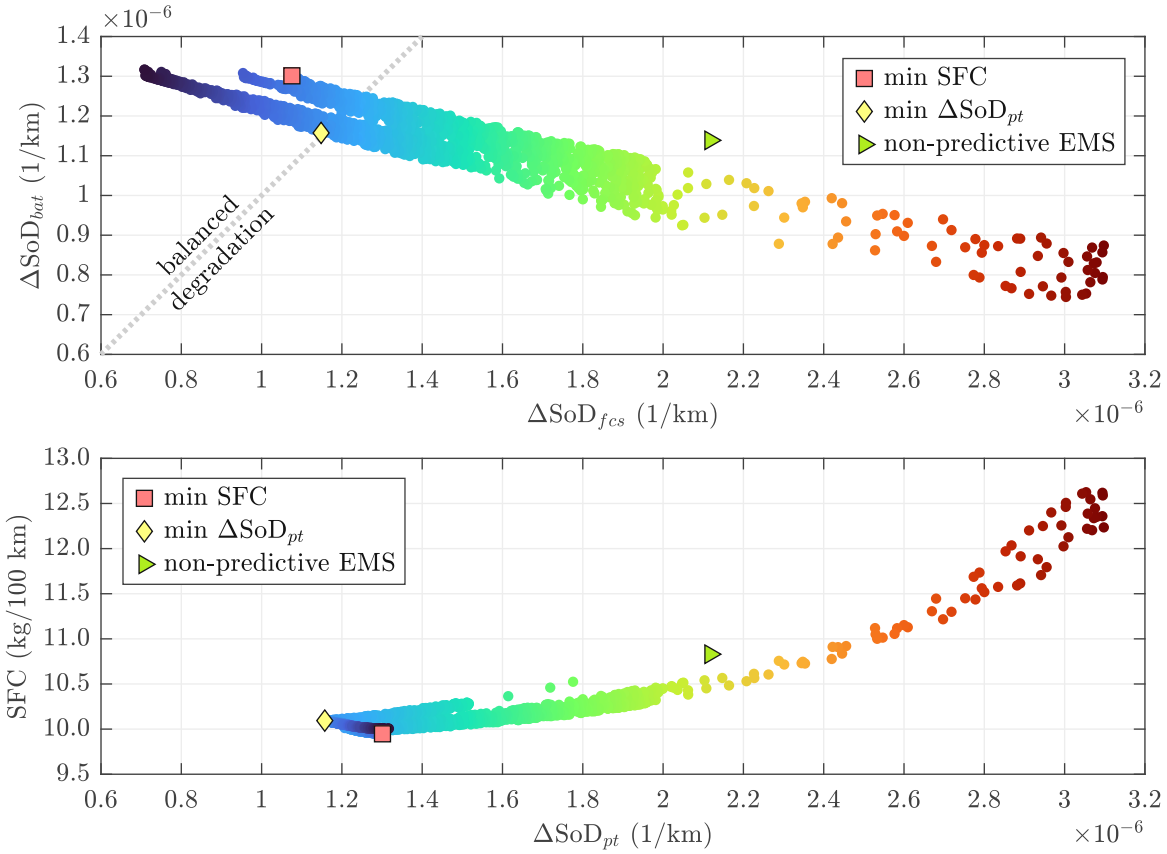

Figure 4.1: Results of the on-board strategy calibration for the trade-off between fuel cell and battery degradation, and between fuel consumption and overall powertrain degradation.

Table 4.2: Results of the on-board strategy calibration.

	SFC	ΔSoD_{pt}	ΔSoD_{bat}	ΔSoD_{fcs}	SoC			EMS parameters			
	(kg/100 km)		(10^{-6}/km)		final	min	max	r_1	r_2 (kW)	r_4 (kW)	r_5
min SFC	9.95	1.30	1.30	1.08	0.69	0.26	0.89	0	600	0	1
min ΔSoD_{pt}	10.09	1.16	1.16	1.15	0.70	0.28	0.90	0.14	549	31	1
non-predictive EMS	10.83	2.12	1.14	2.12	0.65	0.24	0.89	0.20	400	0	1

The second tile of Figure 4.1 shows the trade-off between fuel consumption and powertrain degradation rate. Here, the meaningful region is the Pareto front between the minimum fuel consumption and ΔSoD_{pt} points. Eventually, the degradation rate can be reduced by 11% with a fuel consumption increase of only 1.4%. The extreme case of low battery degradation (dark red markers) can only be achieved with a significant increase in hydrogen consumption and fuel cell degradation. The minimum fuel cell degradation (dark blue markers) results in relatively low consumption but higher battery degradation compared to the minimum ΔSoD_{pt} point.

Lastly, the non-predictive EMS considered in Chapter 3 is also reported in Figure 4.1, showing a significantly higher fuel cell degradation than the predictive one. Moreover, the fuel consumption is 8.8% higher than the minimum value, whereas the powertrain degradation rate is 83% higher. The much higher fuel consumption was expected because, as mentioned, the driving cycle under investigation is the most challenging one.

Table 4.2 reports the fuel consumption, indicated with SFC, and degradation rates of the most relevant cases from Figure 4.1, along with the final, minimum, and maximum SoC values and the corresponding EMS parameters.

4.3 Health-conscious dynamic programming optimization

The previous section has shown that the energy management strategy significantly impacts the trade-off between fuel consumption and degradation rates. However, a fundamental limitation was that the predictive references were optimized only considering the fuel consumption. This section overcomes the mentioned limitation and proposes an innovative formulation for the multi-objective optimization of fuel consumption and degradation using dynamic programming.

The difference compared to the dynamic programming formulation detailed in Section 3.2.1 is the objective function of the optimization, which is now expressed as:

$$\min_{\{P_{fcs,1},\dots P_{fcs,N}\}} \sum_{k=1}^{N} L_k + \phi_k \ . \tag{4.4}$$

The stage cost of the objective function consists of three terms: fuel consumption, fuel cell, and battery degradation rates. Since simultaneously minimizing all terms is impossible, the stage cost is expressed as the weighted sum:

$$L_k = (1-\alpha)\ L_{fuel,\,k} + \alpha\,[\beta L_{bat,\,k} + (1-\beta) L_{fcs,\,k}]\,w\ , \tag{4.5}$$

where α and β are the weighting parameters that can shift the optimization towards the individual targets. For example, setting $\alpha = 0$ results in fuel consumption optimization. When $\alpha = 1$, the optimization target is the battery degradation rate if $\beta = 1$, or the fuel cell degradation rate if $\beta = 0$. The parameter w is a scaling factor equal to 10^5.

The fuel consumption term is expressed as in (3.5), considering the hydrogen consumption rate as a function of the fuel cell power:

$$L_{fuel,\,k} = \dot{m}_{\mathrm{H_2}}(P_{fcs,k})\ \Delta t_k\ . \tag{4.6}$$

The battery degradation term is expressed as the argument of the integral in (2.29):

$$L_{bat,\,k} = \delta_{bat,k}\ |I_{bat,k}|\ \Delta t_k\ , \tag{4.7}$$

where $\delta_{bat,k}$ is the battery degradation rate and depends on the SoC as in (2.30). The current is expressed as a function of the battery power (3.1):

$$I_{bat,k} = \frac{V_{oc,k} - \sqrt{V_{oc,k}^2 - 4\,P^*_{bat,k}\,R_{int,k}}}{2\ R_{int,k}}\ . \tag{4.8}$$

The fuel cell degradation term includes the four causes mentioned in (2.22): start-up/shut-down cycles, dynamic loading, low-power and high-power operations. Eventually, it is expressed as:

$$L_{fcs,\,k} = \frac{\delta_{ss}}{N} + \delta_{lp}\ \Delta t_k^{lp} + \delta_{hp}\ \Delta t_k^{hp} + \delta_{dl}\ \frac{|\Delta P_{fcs,\,k}|}{2\,P_{fcs,nom}}\ . \tag{4.9}$$

Since there is always one start-up/shut-down cycle, the first degradation term is distributed along the entire driving cycle by diving by the number of stages, N. The low-power degradation is present when the fuel cell operated below 10% of the nominal power. Therefore, the operating time at low-power is expressed as:

$$\Delta t_k^{lp} = \begin{cases} \Delta t_k & \text{if} \quad P_{fcs,\,k} < 10\% \text{ of } P_{fcs,nom}\ , \\ 0 & \text{otherwise.} \end{cases} \tag{4.10}$$

Similarly, the operating time at high-power is expressed as:

$$\Delta t_k^{hp} = \begin{cases} \Delta t_k & \text{if} \quad P_{fcs,\,k} > 80\% \text{ of } P_{fcs,nom}\ , \\ 0 & \text{otherwise.} \end{cases} \tag{4.11}$$

The change in fuel cell power is expressed as:

$$\Delta P_{fcs,\,k} = P_{fcs,\,k+1} - P_{fcs,\,k} \tag{4.12}$$

It should be noted that, when in the stage k, the optimal control policy U^* at $k+1$ is already defined over the entire SoC grid (see Figure 2.15). Therefore, remembering that SoC_{k+1} is as in (3.6), the fuel cell power in the next stage is expressed as:

$$P_{fcs,\,k+1} = U^*_{k+1}(\mathrm{SoC}_{k+1}) \ . \tag{4.13}$$

It should be mentioned that including the degradation terms in the objective function of dynamic programming increases the computational time for the optimization. In particular, keeping the same discretization grids selected in Section 3.2.1, the computational time is now 40 ms/km, i.e. 60% higher than without degradation. The main reason for this increase is the interpolation required to overcome the grid mismatch occurring in the implementation of (4.13) (see Figure 2.15).

Changing the weights α and β allows exploring different trade-offs between the three targets: fuel consumption, fuel cell, and battery degradation. The parameters of the on-board strategy are kept constant as: $r_1 = 0$, $r_2 = 600$ kW, $r_3 = 9$ kW/s, and $r_4 = 0$ kW. On the other hand, the parameter r_5 is always considered in both of its possible values. This parameter defines whether or not the constraint (3.10) is active, significantly impacting the fuel cell degradation due to dynamic loading. Indeed, if the constraint is not active (i.e. $r_5 = 0$), the EMS will not lower the fuel cell power during regenerative braking. Consequently, the fuel cell will be less fluctuating, but the fuel consumption will be higher because part of the regenerative braking energy will not be absorbed.

The initial performance analysis of the health-conscious energy management considers the extreme cases for optimizing the predictive references. Figure 4.2 shows the simulation results corresponding to minimum fuel cell degradation for the driving cycle on the mountain route. First, it should be noted that there is an extremely close tracking of the predictive references. The SoC is kept within 0.25 and 0.90 thanks to the additive penalty function (3.7) implementing the soft constraints. The fuel cell does not operate at low or high power to avoid the corresponding degradation. Moreover, the fuel cell operation is remarkably stationary and almost looks like four different power levels. Eventually, the major contribution to the fuel cell voltage degradation is due to the inevitable start-up/shut-down cycle, which causes 93% of the total degradation.

Figure 4.3 shows the simulation results corresponding to minimum fuel consumption for the same driving cycle. The SoC profile is similar to the previous case, whereas the fuel cell power profile is quite different, as it is not as stationary as before. Here, the fuel consumption is improved not because of higher FCS efficiency but because the battery absorbs more regenerative braking energy. On the contrary, the fuel cell degradation is higher due to the low-power and transient operation, which cause 19%

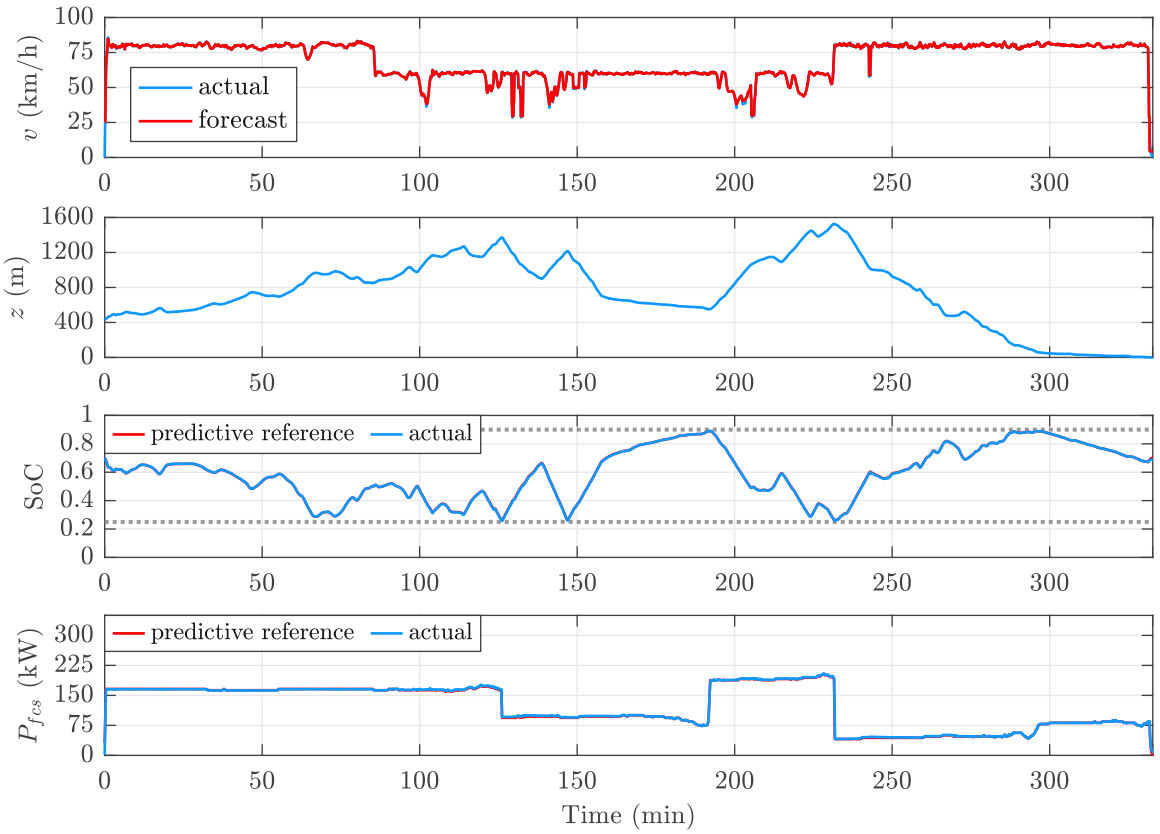

Figure 4.2: Simulation results of the health-conscious EMS with predictive references optimized for minimum fuel cell degradation ($\alpha = 1$, $\beta = 0$, and $r_5 = 0$).

and 34% of the total degradation, respectively. The remaining degradation is due to the start-up/shut-down cycle since the fuel cell never operates at high power.

Lastly, Figure 4.4 shows the simulation results corresponding to minimum battery degradation. In this case, the SoC is kept in a narrower operating range to avoid accelerated degradation rates (see Figure 2.9). The SoC profile is flat in many sections because the battery is not operating, whereas the fuel cell is working in power-following mode. From the FCS power profile, a much higher fuel consumption is expected compared to the previous cases due to the frequent operation at maximum power, where the efficiency is low.

Table 4.3 compares the fuel consumption and component degradation for the three cases analyzed above. There is a huge difference in fuel consumption between the minimum degradation cases: for the fuel cell, the consumption is 3.8% higher than the minimum, whereas 31.5% higher for the battery. On the other hand, the fuel cell degradation is almost two times higher for the minimum consumption case and almost five times

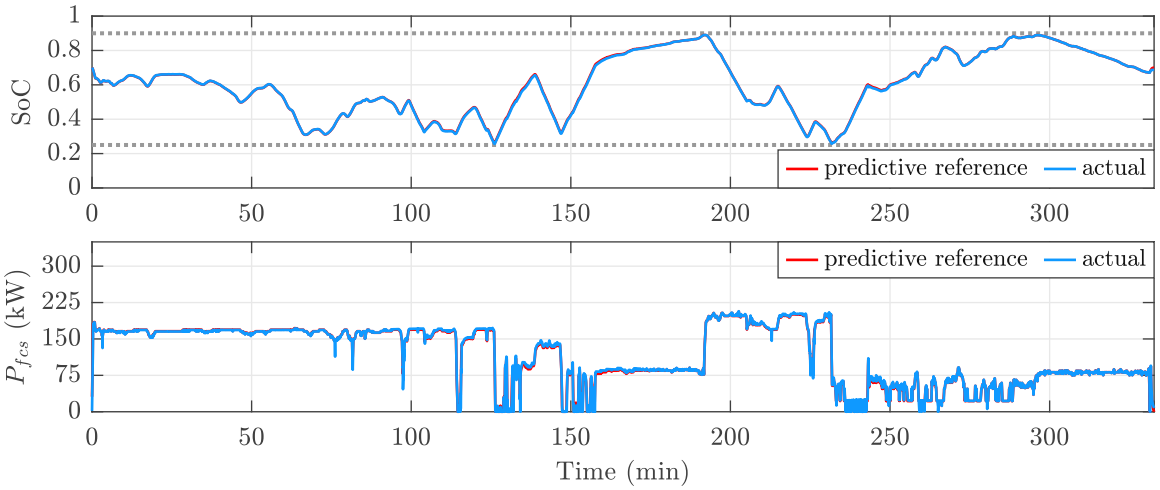

Figure 4.3: Simulation results with predictive references optimized for minimum fuel consumption ($\alpha = 0$ and $r_5 = 1$).

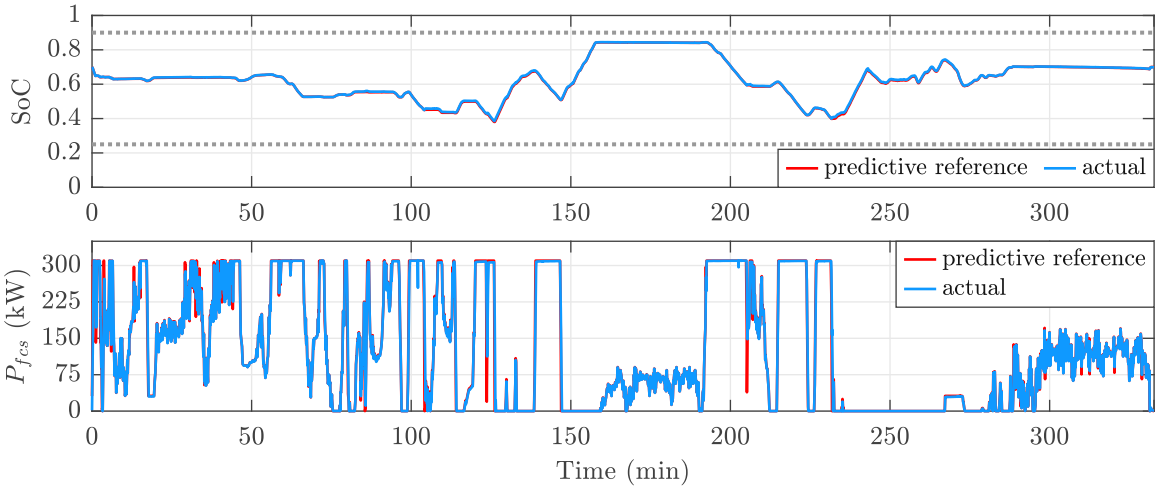

Figure 4.4: Simulation results with predictive references optimized for minimum battery degradation ($\alpha = 1$, $\beta = 1$, and $r_5 = 1$).

Table 4.3: Performance comparison between the extreme optimization cases of the health-conscious energy management strategy.

α	β	r_5	SFC (kg/100 km)	ΔSoD_{fcs} (10^{-6}/km)	ΔSoD_{bat} (10^{-6}/km)	SoC		
						final	min	max
1	0	0	10.33	0.55	1.41	0.69	0.26	0.89
0	-	1	9.95	1.08	1.30	0.69	0.26	0.89
1	1	1	13.08	2.49	0.63	0.70	0.39	0.84

higher for the other case. Lastly, the battery degradation is similar for the first two cases and more than two times higher than the minimum.

Since the problem under investigation is the multi-objective optimization of conflicting targets, no individual solution exists that simultaneously optimizes each objective individually. When improving an individual objective is impossible without degrading at least one of the other objectives, the problem is also called Pareto optimality. In particular, a solution is called nondominated or Pareto optimal if there is no other solution that is equally good or better than it with respect to all the objectives. The set of nondominated solutions is called the Pareto front [97, 98].

The weighting choice to analyze the extreme optimization cases is straightforward, as it is shown in Table 4.3. However, finding the weights that yield an appropriate trade-off between all the targets is not as simple. For this reason, Latin hypercube sampling was used again to create 600 combinations of α and β and systematically explore the trade-offs between fuel consumption and component degradation. The results of this study are reported in Figure 4.5.

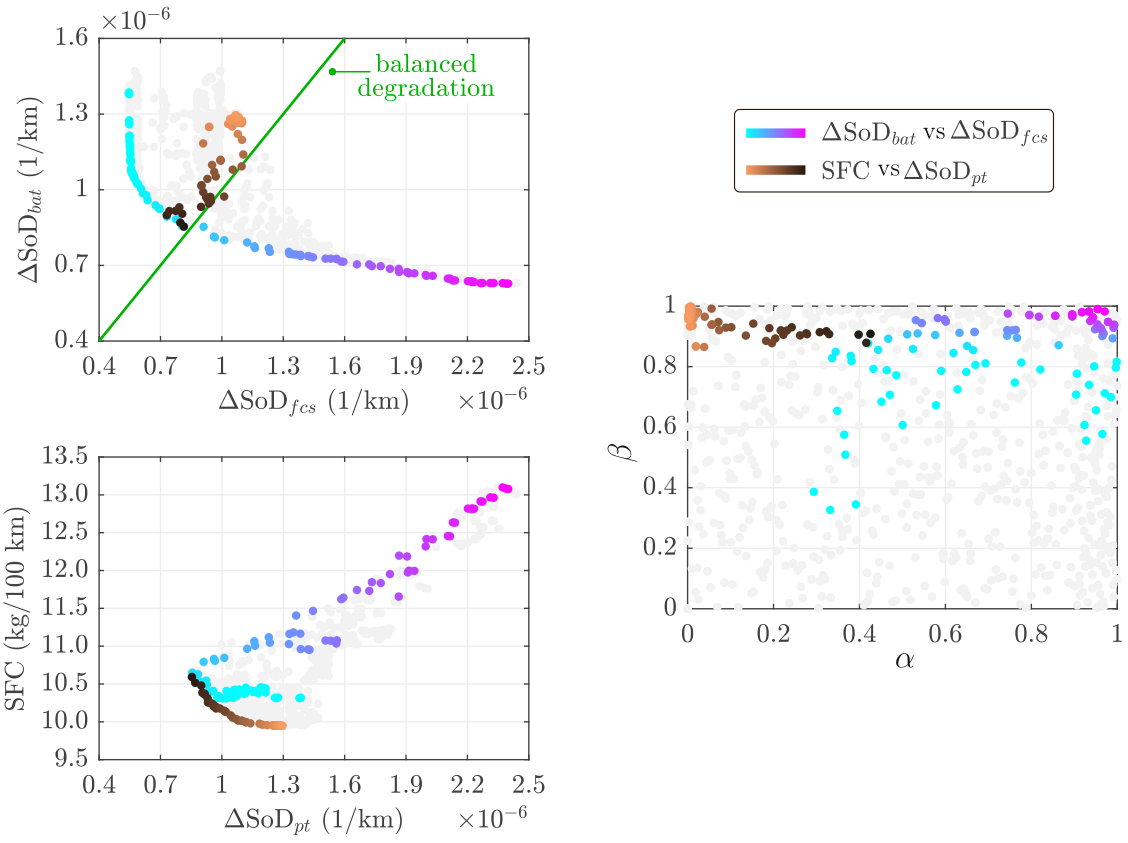

Figure 4.5: Pareto fronts between battery and fuel cell degradation rates, and between fuel consumption and powertrain degradation rate.

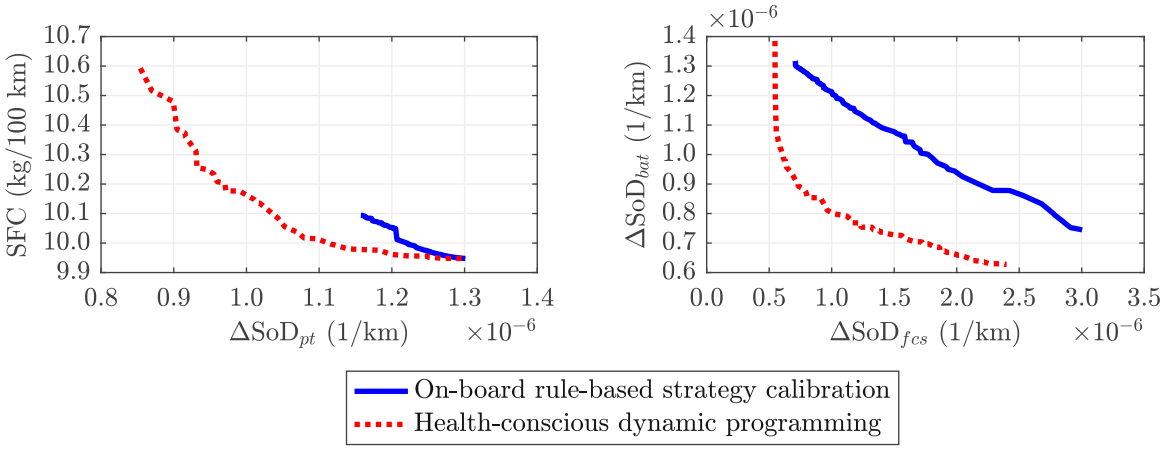

Figure 4.6: Comparison of Pareto fronts between fuel consumption and powertrain degradation (SFC vs SoD$_{pt}$), and fuel cell and battery degradation (SoD$_{fcs}$ vs SoD$_{bat}$).

For better visualization, the figure highlights the results along two Pareto fronts: the first between battery and fuel cell degradation; and the second between fuel consumption and powertrain degradation. First, the figure shows the Pareto front between battery and fuel cell degradation. The flat edges of this front suggest that the health-conscious energy management strategy can find solutions that optimize the individual degradation rates. Moreover, it is evident that battery degradation has a higher impact on fuel consumption and overall powertrain degradation (4.1) because reducing it has a highly detrimental impact on fuel cell degradation. The second Pareto front is between fuel consumption and powertrain degradation. Almost all solutions are on the left side of the balanced degradation line, meaning that optimizing the fuel cell degradation has a lower impact on fuel consumption. The figure also shows the weights α and β corresponding to each Pareto optimal solution.

The fact that both Pareto fronts are intensely populated along their extension clearly indicates that the health-conscious dynamic programming has a high degree of flexibility in shifting the trade-off between the optimization targets. The goodness of the proposed optimization approach is demonstrated by comparing the Pareto fronts against the results of the on-board strategy calibration shown in Section 4.2. Figure 4.6 shows that the novel optimization is considerably superior to the other solution. First, the overall powertrain degradation rate can be reduced by 35% compared to the minimum fuel consumption results, whereas only by 11% with the other case. Moreover, the health-conscious dynamic programming yields lower fuel consumption for the same powertrain degradation. Therefore, it can be concluded that simply calibrating the on-board strategy results in dominated solutions, whereas the health-conscious dynamic programming finds Pareto optimal solutions. This difference is even more evident in the trade-offs between battery and fuel cell degradation.

4.4 Impact of battery sizing on fuel consumption and degradation

Powertrain component sizing problem is a compelling topic in the research related to fuel cell electric vehicles. In the literature, it is widely acknowledged that component sizing must be coupled with optimal EMS design because the power-split criteria change depending on the powertrain configuration [99, 100]. Jain et al. [101] use a genetic algorithm to optimize the parameters related to component sizing and load-follower charge sustaining EMS. Tazelaar et al. [102] use different energy management strategies for the optimal powertrain design showing that the minimum component size requirements are highly affected by the control strategy choice. Hu et al. [103] use convex programming for the combined optimization of energy management and component sizing, examining the influence of driving cycles on the optimization results. Xu et al. [100] investigate the optimal component sizing problem to find the best trade-off between consumption and degradation indicators, adopting an EMS based on dynamic programming. As follow-up work, Hu et al. [104] derive simplified EMSs from DP, showing that the hydrogen consumption is near-optimal if the battery capacity is large enough. Wu et al. [105] use convex programming for the combined optimization of energy management and component sizing of a plug-in fuel cell city bus, showing how the economic assumptions on the hydrogen price affect the energy management strategy. Fletcher et al. [106] use stochastic dynamic programming as EMS within their component sizing investigation, showing the impact of fuel cell size on the individual causes of fuel cell voltage degradation. Feng et al. [107] define an optimal component sizing problem to minimize the lifecycle cost of a fuel cell mining truck, using simplified degradation models to estimate the component lifetime and, based on that, the total cost of ownership. Xu et al. [54, 55] investigate the joint component sizing and energy management for fuel cell electric trucks proposing to decompose the problem into two sub-problems that are solved by sequential convex programming. Fewer works investigate the component sizing problem through techno-economic assessments, neglecting the role of energy management strategies [108]–[110].

This section studies the vehicle performance with different battery capacities to examine the impact of battery sizing on fuel consumption and component degradation. The health-conscious energy management strategy described in Section 4.3 is used to find the optimal trade-off between these targets. The battery pack size can be easily changed in the model through the overall number of cells (see Section 2.1.3). On the contrary, the fuel cell system model is not changed.

The first aspect to consider for a proper investigation is that a larger battery size results in higher vehicle weight. Therefore, in this section, the vehicle weight is expressed as:

$$m_v = m_{v_0} + \mu_{bat}\, E_{bat,nom}\ , \tag{4.14}$$

assuming the base vehicle weight m_{v_0} as 42 tons, and the specific battery weight μ_{bat} as 6.35 kg/kWh [111, 112].

A larger battery generally means a higher degree of freedom for the power-split optimization, and the health-conscious dynamic programming can take full advantage of this. However, the weights of the multi-objective optimization function can significantly change because the optimal power-split criteria can differ depending on the battery size. For this reason, the DoE approach described to obtain the results in Figure 4.5 was adopted again to explore the Pareto optimal solutions systematically. The results of this study are shown in Figure 4.7 for battery sizes ranging from 60 kWh to 250 kWh. Smaller batteries are not considered because the SoC cannot be kept within the desired operating range, i.e. 0.25–0.90.

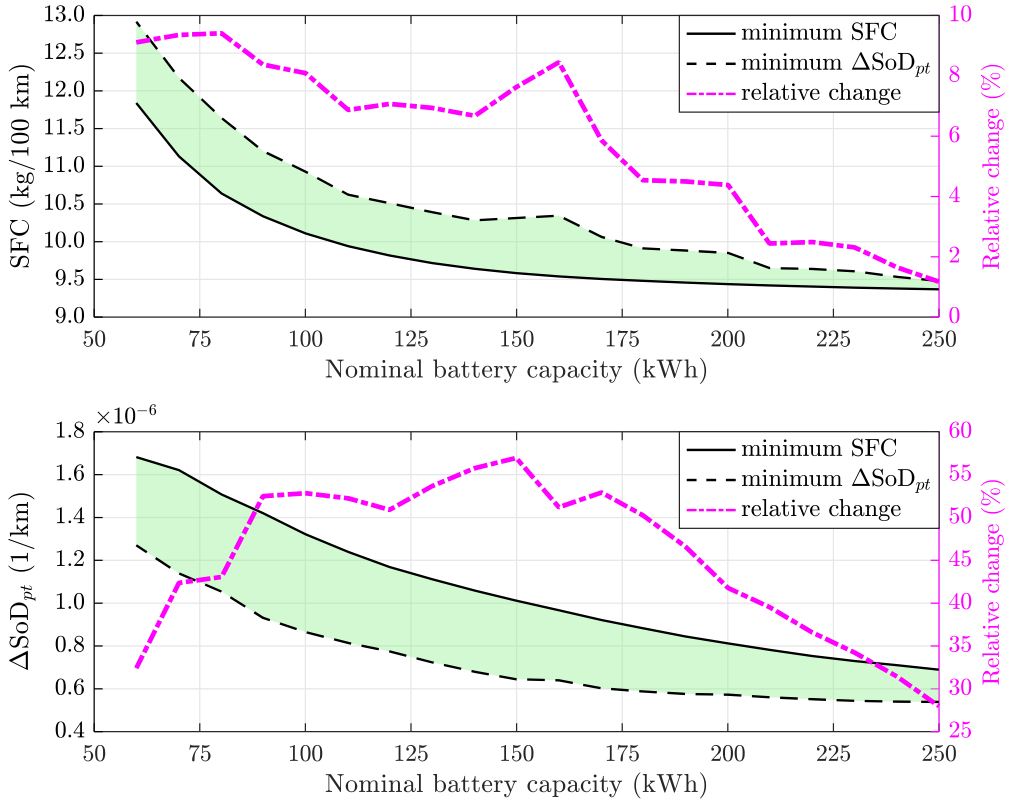

Figure 4.7: Impact of battery sizing on fuel consumption and powertrain degradation rate using the health-conscious EMS.

The first tile of the figure shows the fuel consumption for the weights that yield its minimum value, but also for those that yield the minimum powertrain degradation rate. Moreover, the right-side y-axis shows the relative change between the extreme values for each battery size. The first interesting finding is that the minimum fuel cell consumption with the smallest battery size is 26.4% higher than the one with the largest battery (11.84 vs. 9.37 kg/100 km). However, most of the improvement is already obtained with a battery size of 150 kWh. Another interesting finding is that the relative change between the solutions with minimum fuel consumption and

minimum powertrain degradation decreases significantly with the battery size due to the higher degree of freedom for the optimization. In particular, if the battery size is 250 kWh, the powertrain degradation rate can be minimized with only a 1.2% higher fuel consumption than the minimum.

The second tile of Figure 4.7 shows the powertrain degradation rate. Here, it is remarkable that, for the smallest battery, the minimum powertrain degradation rate is 2.36 times higher than for the largest battery. What is also surprising is that the relative change between the solutions with minimum fuel consumption and minimum powertrain degradation is significant even for large batteries.

Figure 4.7 demonstrates that larger batteries result in lower fuel consumption and powertrain degradation. However, it does not provide information on the goodness of the health-conscious EMS compared with other strategies. Indeed, with larger batteries, it is generally easier to perform the power-split task. To investigate this aspect, the performances of the health-conscious predictive EMS are compared with those of the rule-based strategy described in Appendix B.2.1, which is non-predictive and based on simple heuristics (i.e. not optimal). The parameters of the rule-based strategy were varied as detailed in Section 4.2 to explore the trade-off between the optimization targets.

For this comparison, an additional performance indicator is considered to define the best trade-off between fuel consumption and powertrain degradation. This indicator is the total cost of ownership of the fuel cell electric powertrain. Generally, the total cost of ownership (TCO) assesses the long-term value of assets, considering the fixed and operating costs over their lifespan. For commercial vehicles, a detailed TCO analysis includes direct and indirect costs of purchase, fuel, maintenance, insurance, downtime, repairs, fees, and taxes. However, this study only considers the purchase cost of the fuel cell and battery systems and the hydrogen cost, assuming that the impact of energy management and components sizing on the other costs is negligible.

Here, total cost of ownership of the powertrain, TCO_{pt}, is expressed as:

$$\mathrm{TCO}_{pt} = c_{\mathrm{H}_2}\ \mathrm{SFC} + (c_{bat}\ E_{bat,nom} + c_{fcs}\ P_{fcs,nom})\,\Delta\mathrm{SoD}_{pt}\ , \tag{4.15}$$

where c_{H_2} is the hydrogen price, c_{bat} the battery system price, and c_{fcs} the fuel cell system price. It is assumed that the current market prices are 6 \$/kg for hydrogen [113], 40 \$/kW for fuel cell systems [114], and 160 \$/kWh for battery systems [115]. The minimum TCO solution will always lie on the Pareto front between fuel consumption and powertrain degradation, and the market prices determine where the best trade-off solution is located along the front. From the formulation, it should be clear that it is a simple estimate of the actual TCO because the fuel consumption and degradation rates are projected, assuming that the vehicle always repeats the same driving cycle. Moreover, the effect of the degradation itself on the fuel consumption and degradation

rates is not considered because they are calculated when the vehicle is in begin-of-life conditions and then projected to estimate the TCO as in (4.15).

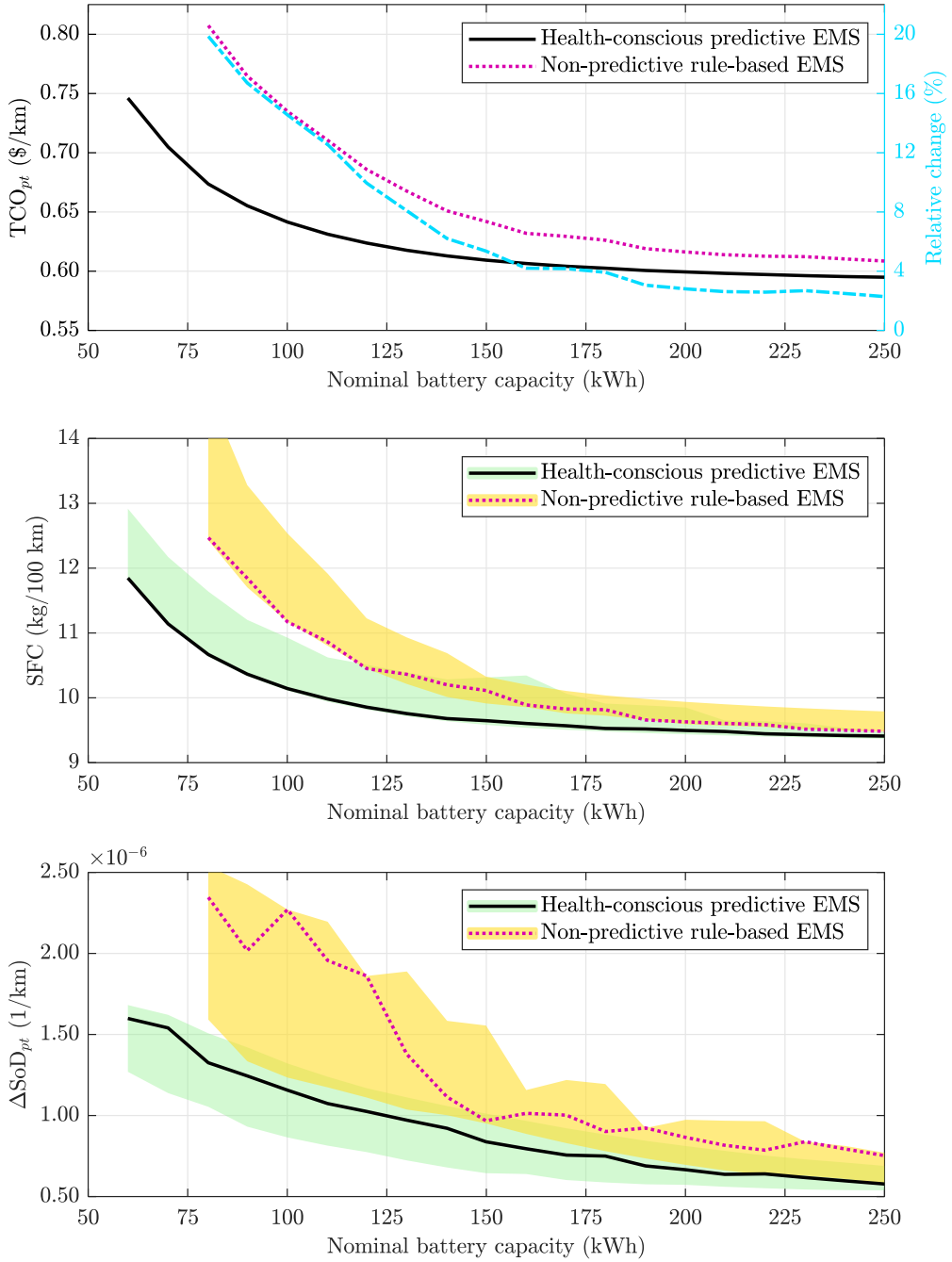

Figure 4.8: Performance comparison between the health-conscious predictive EMS and the non-predictive rule-based EMS.

Figure 4.8 shows the performance comparison between the health-conscious predictive

EMS and the non-predictive rule-based EMS, showing the minimum TCO obtained during the calibration of each strategy. Eventually, the powertrain TCO is considerably lower with the proposed health-conscious EMS, especially for configurations with small batteries. For example, if the nominal battery capacity is 100 kWh, the expected TCO is 15% higher for the rule-based EMS. Moreover, using the rule-based EMS, the minimum battery capacity required to keep the SoC in the desired operating range is higher than the other strategy and equal to 80 kWh. The figure also shows the minimum and maximum values obtained with each strategy for fuel consumption and powertrain degradation. Interestingly, the solution that yields the minimum TCO results in fuel consumption that is extremely close to its minimum value, meaning that fuel consumption has a dominant role over the TCO under assumptions made for the market prices.

4.5 Performance deterioration due to progressive component degradation

A limiting assumption of the investigations conducted in the previous sections is that the fuel cell and battery systems are always assumed in begin-of-life conditions. However, this section overcomes this limitation, offering a detailed analysis of how the progressive component degradation deteriorates the performances of fuel cell electric trucks.

The degradation models are described in Section 2.1.4. For the fuel cell system, the state of degradation (SoD) affects its hydrogen consumption, heat generation, and maximum power (see Figure 2.4). On the other hand, the battery degradation affects its maximum capacity as indicated in (2.24). For example, if at begin-of-life the maximum battery capacity is 100 kWh, at end-of-life, it is 80 kWh.

Table 4.4 shows the effect of the battery and fuel cell SoDs on fuel consumption, battery degradation rate, and fuel cell degradation rate. The simulation results refer to the health-conscious EMS (with $\alpha = 0$) and the driving cycle on the mountain route for two different ambient temperatures. Four extreme degradation cases are considered in the table, i.e. with the components in begin-of-life or end-of-life conditions.

The performance deterioration from BoL to EoL conditions is significant. In particular, the fuel consumption increases by 24%, the battery degradation rate by 15%, and the fuel cell degradation rate by 29%. Remarkably, the performance deterioration due to EoL conditions is much higher at an ambient temperature of 35°C than at 10°C. On the contrary, the performances are comparable at BoL conditions. This difference is expected because heat generation at EoL conditions is significantly higher, and the energy consumption of the fuel cell cooling system can reach up to 50 kW (see Figure 2.6).

Table 4.4: Effect of SoD and ambient temperature on performance indicators.

SoD_{bat}	SoD_{fcs}	$T_{ambient}$ (°C)	SFC (kg/100 km)	change	ΔSoD_{bat} (10^{-6}/km)	change	ΔSoD_{fcs} (10^{-6}/km)	change
0	0	35	9.95	-	1.30	-	1.08	-
1	0	35	10.40	+5%	1.52	+17%	1.21	+12%
0	1	35	11.28	+13%	1.30	-	1.12	+4%
1	1	35	12.30	+24%	1.50	+15%	1.39	+29%
0	0	10	9.88	-	1.27	-	1.10	-
1	0	10	10.26	+4%	1.46	+15%	1.22	+11%
0	1	10	10.99	+11%	1.29	+2%	1.12	+2%
1	1	10	11.48	+16%	1.47	+16%	1.23	+12%

The results reported in Table 4.4 consider the extreme degradation cases for the battery and fuel cell systems. However, they do not consider how the actual degradation progresses during the vehicle lifetime. Of course, the energy management strategy significantly impacts the overall performance. Therefore, four Pareto optimal solutions were selected from the investigation conducted in Figure 4.5 to study the performance deterioration due to the progressive component degradation. Table 4.5 lists the selected solutions with the fuel consumption and degradation rates at begin-of-life conditions. The first solution has the minimum SFC; the second has a much lower fuel cell degradation rate with a negligible impact on fuel consumption; the third has the minimum powertrain degradation rate; whereas, the fourth has the minimum expected powertrain total cost of ownership.

First, the performance deterioration due to the progressive component degradation is analyzed, assuming that the vehicle always drives the cycle on the mountain route. It is important to note that the predictive energy management references are optimized

Table 4.5: Selected solutions of the health-conscious EMS to study the performance deterioration due to progressive component degradation.

α	β	r_5	SFC (kg/100 km)	$\Delta SoD_{pt/bat}$ (10^{-6}/km)	ΔSoD_{fcs} (10^{-6}/km)	TCO_{pt} (\$/km)
0	-	1	9.95	1.30	1.07	0.634
0.01	0.66	0	9.97	1.29	0.78	0.635
0.43	0.91	0	10.59	0.85	0.81	0.660
0.04	0.96	1	9.98	1.14	1.10	0.631

Table 4.6: Performance comparison considering progressive component degradation for the driving cycle on the mountain route.

α	β	Mileage (10^6 km)	SoD_{bat}	SoD_{fcs}	SFC* (kg/100 km)	ΔSoD^*_{bat} (10^{-6}/km)	ΔSoD^*_{fcs} (10^{-6}/km)	TCO^*_{pt} ($/km)
0	-	0.71	1.00	0.83	10.75	1.41	1.17	0.685
0.01	0.66	0.72	1.00	0.62	10.60	1.39	0.86	0.676
0.43	0.91	1.02	1.00	0.96	11.52	0.98	0.94	0.719
0.04	0.96	0.80	1.00	0.95	10.88	1.25	1.19	0.688

in each driving cycle considering the current state of degradation for the fuel cell and battery systems. Consequently, this study requires quite a significant computational time, i.e. approximately 15 hours to simulate one million kilometers. For this reason, only a few selected energy management strategies are considered for the analysis.

The results of this study are reported in Table 4.6 and Figure 4.9. The table indicates the total vehicle mileage, the final battery and fuel cell states of degradation. Moreover, the table reports the average fuel consumption, degradation rates, and the final powertrain TCO. On the other hand, the figure shows how the performance indicators deteriorate as the vehicle mileage and degradation increase.

Comparing the results from Tables 4.5 and 4.6, it is evident that, due to the performance deterioration, the fuel consumption, degradation rates, and TCO are underestimated if the components are always considered at BoL conditions. The first remarkable finding comes from the comparison of the first two solutions. Indeed, the average fuel consumption is 1.4% higher when $\alpha = 0$, which might be counter-intuitive because the objective function weighting corresponds to the minimum fuel consumption over the individual driving cycle. However, this outcome is reasonable because the fuel cell degrades faster for the first solution, resulting in lower fuel cell efficiency for the following driving cycles. Indeed, Figure 4.9 shows that SFC is initially lower for the first solution, but it rapidly becomes higher as the fuel cell degradation progresses.

The third and fourth solutions have a much more balanced degradation between the powertrain components, resulting in a longer life than the other solutions. The third one results in the longest vehicle life, as expected. However, the average degradation rates are approximately 16% higher than expected from the results at the begin-of-life conditions. On the other hand, the fourth solution does not result in the minimum TCO but in a 1.8% higher value than the second solution. This outcome indicates that using the simulation results at BoL conditions to calculate the TCO in (4.15) is insufficient to obtain an accurate estimation.

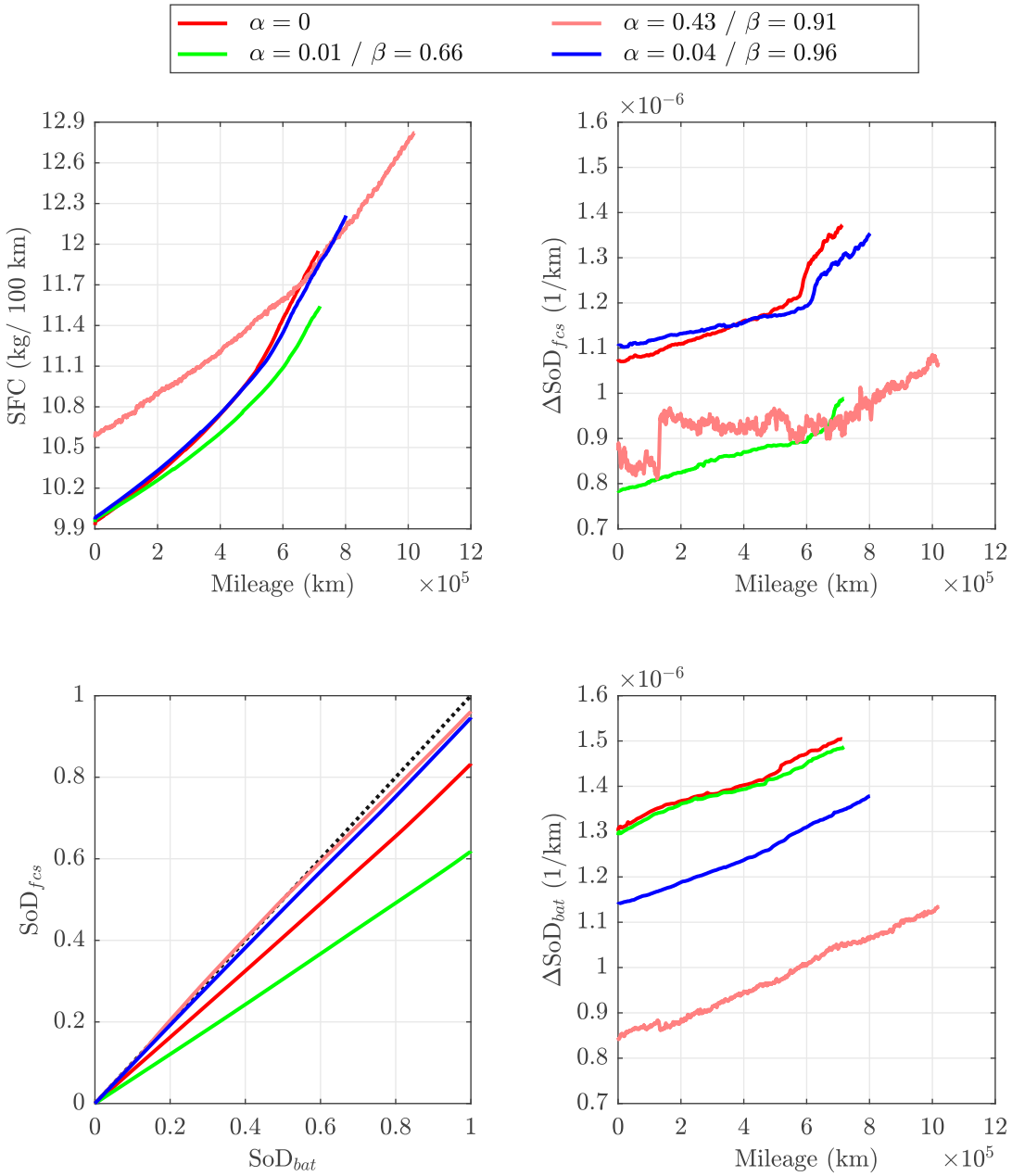

Figure 4.9: Performance deterioration due to the progressive component degradation for the driving cycle on the mountain route.

Table 4.7: Performance comparison considering progressive component degradation for the random sequence of driving cycles.

α	β	Mileage (10^6 km)	SoD_{bat}	SoD_{fcs}	SFC* (kg/100 km)	ΔSoD^*_{bat} (10^{-6}/km)	ΔSoD^*_{fcs} (10^{-6}/km)	TCO^*_{pt} ($/km)
0	-	0.89	0.77	1	9.59	0.87	1.12	0.607
0.01	0.50	1.09	0.99	1	9.63	0.91	0.92	0.604
0.50	0.85	1.17	0.96	1	9.84	0.82	0.85	0.615

Table 4.8: Performance comparison with focus on degradation metrics.

	Mileage (10^6 km)	Cycle length (km)	SoD_{bat}	EFC	SoD_{fcs}	fuel cell voltage degradation (%)				
						total	ss	dl	lp	hp
mountain route	0.71	385	1	5240	0.83	8.33	3.63	2.95	1.68	0.07
	0.72	385	1	5300	0.62	6.19	3.66	1.18	1.33	0.01
	1.02	385	1	6190	0.96	9.61	5.19	2.45	1.74	0.22
	0.80	385	1	5630	0.95	9.46	4.08	3.14	2.13	0.11
mixed cycles	0.89	264	0.77	5010	1	10	6.62	3.23	0.14	0
	1.09	265	0.99	6340	1	10	8.07	1.79	0.14	0
	1.17	265	0.96	6590	1	10	8.64	1.29	0.07	0

The performance deterioration due to the progressive component degradation is also studied considering a random sequence of the 300 real-world driving cycles detailed in Section 2.2. Moreover, the ambient temperature fluctuates between 5°C and 35°C with a sinusoidal shape and a period of 500 driving cycles to emulate a seasonal behavior. The results of this study are listed in Tables 4.7. The first solution considers $\alpha = 0$ to obtain the minimum fuel consumption on each cycle. The main difference compared with the results for the mountain route is that the fuel cell degradation rate is higher than the battery one. On the other hand, the final powertrain TCO is lower because the driving cycles are, on average, less demanding. The second solution results in balanced component degradation, yielding a 22.5% longer mileage with only a 0.4% increase in fuel consumption. This trade-off leads to a more profitable TCO. The third solution yields an even longer mileage but much higher fuel consumption.

Lastly, Table 4.8 analyzes all the simulation results with more focus on the degradation metrics. The equivalent cycles until the end-of-life of the battery system are generally lower for the driving cycle on the mountain route because the battery operates in a wider SoC range. The leading cause of fuel cell voltage degradation is the start-up/shut-down cycles. For the mixed driving cycles, the degradation due to start-up/shut-down

cycles is particularly dominant for two reasons: first, the average driving cycle length is shorter. Second, there is more freedom to optimize the power-split to reduce the degradation due to dynamic loading, low-power, and high-power operation because the driving cycles are, on average, less demanding.

4.6 Summary

This chapter focused on health-conscious energy management strategies, considering fuel cell and battery degradation rates as additional optimization targets. The study considered the most challenging driving cycle from an energy management point of view, with the worst-case scenario for the route topography, truckload, and ambient temperature.

At first, the powertrain lifetime was improved by calibrating the on-board strategy parameters, with a slight increase in fuel consumption. This result demonstrated that energy management strategies significantly impact fuel cell and battery degradation.

Then, the dual-stage predictive energy management strategy was improved to include the degradation rates directly in the optimal control targets. In particular, a health-conscious energy management strategy using dynamic programming is proposed for the multi-objective optimization of the predictive energy management references, considering fuel consumption, fuel cell degradation, and battery degradation.

The optimal power-split results corresponding to the optimization of the individual targets are analyzed in detail to demonstrate the goodness and flexibility of the health-conscious energy management strategy. In particular, the fuel cell and battery degradation rates can individually reach up to half the values obtained with the solution for minimum fuel consumption. However, since the energy management targets conflict with each other, no solution exists that simultaneously optimizes all the objectives.

A detailed analysis is presented for the Pareto fronts between battery and fuel cell degradation rates, and between fuel consumption and powertrain degradation. Comparing the results with those of the on-board strategy calibration demonstrates the absolute superiority of the proposed health-conscious EMS.

Under the assumption that the fuel cell and battery systems cannot be individually replaced, the optimization results show that it is essential to ensure a balanced degradation between them to maximize the powertrain lifetime. Remarkably, the health-conscious energy management strategy can reduce the overall powertrain degradation rate by up to 35% compared with the minimum fuel consumption results.

The component sizing study demonstrates that the battery size significantly impacts fuel consumption and degradation rates and that the health-conscious energy management strategy can take full advantage of the higher degree of freedom for the power-split optimization due to larger battery sizes. In particular, the minimum fuel consumption

can be reduced by 26% if the battery size goes from 60 kWh to 250 kWh, whereas the powertrain degradation rate by 58%.

The study shows how the total cost of ownership of the powertrain can be used to define the best trade-off among the Pareto optimal solutions for fuel consumption and powertrain degradation rate. Moreover, the comparison with a non-predictive and non-optimal energy management strategy demonstrates the absolute superiority of the proposed health-conscious EMS, especially for modest battery sizes. For example, if the nominal battery capacity is 100 kWh, the expected TCO is 15% higher for the non-predictive EMS, clearly indicating its inadequacy in finding a good trade-off between the energy management targets.

Lastly, this chapter establishes that the progressive component degradation considerably deteriorates the performances of fuel cell electric vehicles. Indeed, considering the powertrain components in begin-of-life conditions leads to severe underestimations of fuel consumption and degradation rates. A significant finding is that the energy management strategy should not be optimized for fuel consumption in each driving cycle if the goal is to minimize the consumption over the entire vehicle lifetime. On the other hand, the EMS should find a suitable trade-off between fuel consumption and fuel cell voltage degradation in each driving cycle.

Remarkably, for the simulation results considering the vast pool of driving cycles, the health-conscious energy management strategy leads to 22.5% longer mileage with only a 0.4% increase in fuel consumption. The results also show that the leading cause of fuel cell voltage degradation is the start-up/shut-down cycles, since all the other causes are mitigated by the health-conscious energy management strategy.

Chapter 5

Energy management strategies for holistic vehicle control

This chapter investigates the synergies between the energy management strategy and other control functions from a holistic standpoint. The chapter is divided into three sections:

- *The first one focuses on developing an adaptive energy management strategy that includes battery thermal management targets to mitigate its degradation, as published in the author's work [62].*
- *The second section describes a health-conscious activation strategy for vehicles with multi-module fuel cell systems to reduce the number of start-up/shut-down cycles to mitigate fuel cell degradation.*
- *The third one studies optimal eco-driving strategies for fuel cell electric trucks in mountain motorway routes. In particular, it proposes a speed planning and energy management co-optimization method based on dynamic programming, continuing the author's work [64].*

5.1 Adaptive energy management strategy for improved battery thermal management

Proper thermal management is essential to mitigate degradation and guarantee a sufficient lifetime for battery systems in electric vehicles. It is particularly crucial to maintain the battery temperature within a safe operating range, mainly focusing on avoiding temperature peaks that accelerate degradation or even cause thermal runaways.

The degradation mechanisms occurring in batteries vary depending on the cell chemistry. However, it is well known that the most relevant degradation mechanisms are accelerated by high temperatures, which determine faster unwanted chemical reactions.

In Lithium-ion batteries, for example, the cell temperature affects lithium plating, active material dissolution, and SEI growth [86]. Experimental tests from several works indicate that the battery capacity fade is significantly higher for temperatures between 40°C and 60°C [116]–[119].

Due to the considerable complexity of electrochemical mechanisms and the diversity of cells for automotive applications, it is especially challenging to generalize degradation models, especially those with a higher level of complexity. Therefore, simple empirical models are usually adopted in health-conscious energy management strategies [88]. However, most energy management strategies for fuel cell electric vehicles neglect the role of battery temperature on degradation [120]. Only a few works investigated the interaction between energy and thermal management in fuel cell electric vehicles [121, 122].

This section describes an energy management strategy to limit the battery usage in critical conditions and avoid temperature peaks, as published in the the author's work [62]. The strategy is adaptive because its parameters are adjusted depending on the battery temperature to modify the power-split criterion.

This section considers a battery system with a nominal capacity of 100 kWh, which is twice as large as the one in [62]. Therefore, the battery thermal management system (BTMS) is also slightly different. However, this aspect shows that the general concept of adaptive EMS is also valid for a different system and can be used to improve battery thermal management and avoid accelerated degradation even if the cooling system is not sufficiently powerful. In particular, it is assumed that the threshold for accelerated degradation is 40°C, whereas the desired operating temperature is 35°C.

The model adopted for the battery thermal management system is simple. Assuming that the battery temperature is uniform over the entire pack, the thermal dynamics are expressed as:

$$m_{bat}\, c_{p,bat}\, \dot{T}_{bat} = \dot{Q}_{bat,heat} - \dot{Q}_{bat,cool}\ , \tag{5.1}$$

where m_{bat} is the battery pack mass, $c_{p,bat}$ the specific heat capacity, and T_{bat} the temperature. The heat generation in the battery pack, $\dot{Q}_{bat,heat}$, corresponds to the ohmic losses calculated as in (2.19). The battery mass is 635 kg, considering the same specific weight as in (4.14). Since the characteristics in Figure 2.7b refer to a nickel manganese cobalt battery cell, the specific heat capacity can be assumed as 1000 J/kg/K [123], which is also in line with the values reported in [124].

A detailed cooling system model considers several variables to define the maximum available cooling power, such as the (battery, coolant, ambient) temperatures, and the (coolant and air) mass flows. However, this work assumes for simplicity that the cooling system can always absorb up to 6 kW of heat from the battery pack. This assumption is sufficient for a system-level analysis. The cooling power absorbed from the battery is indicated with $\dot{Q}_{bat,cool}$, and its setpoint is defined with a hysteresis control logic to keep

the battery temperature around 35°C. In particular, the cooling system turns on (at maximum power) when the temperature reaches 36°C and off at 34°C. It is important to note that this cooling system (on its own) is inadequate to keep the battery temperature below 40°C, which is why the adaptive EMS was developed to compensate for that.

The electric energy consumption due to the components of the cooling system is calculated as:

$$P_{bat,cool} = \frac{\dot{Q}_{bat,cool}}{\mathrm{COP}} \ , \tag{5.2}$$

assuming for simplicity that the coefficient of performance (COP) is constant and equal to 2. This battery cooling power consumption is an additional electric load in (2.2).

The adaptive EMS is implemented by defining the main parameters of the on-board strategy as a function of the battery temperature. In particular, the parameters that most affect the power-split and the battery usage are r_1 and r_2 in (3.8). Therefore, they are expressed as:

$$r_1 = r_1(T_{bat}) \ , \tag{5.3a}$$
$$r_2 = r_2(T_{bat}) \ . \tag{5.3b}$$

The parameter r_1 is the most influencing on the power-split. Indeed, if it is 0, the on-board strategy follows the predictive references generated by the health-conscious dynamic programming optimization. On the other hand, if r_1 is 1, the EMS operates the fuel cell in power-following mode. In this case, the battery operates only to provide the loads exceeding the fuel cell power limit, to regenerate braking energy, and to follow the predictive SoC reference (based on the value of r_2).

Following these considerations, the control parameter characteristics were designed as depicted in Figure 5.1 to limit the battery usage at critical temperatures. In particular, below 37°C, the on-board strategy is the same adopted in Section 4.3, which follows the optimal power-split defined by the predictive references. On the contrary, above the assumed accelerated degradation threshold of 40°C, the fuel cell operates in power-following mode to ensure minimal battery usage. This way, the heat generation is

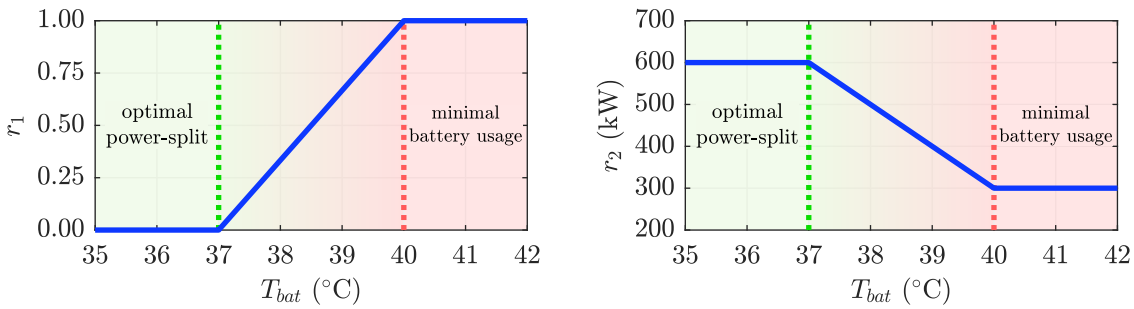

Figure 5.1: Characteristics of the adaptive parameters in the on-board energy management strategy as function of the battery temperature.

significantly reduced to enable a faster cooldown of the battery pack. The parameter r_2 is reduced to half its value to loosen the SoC reference following, decreasing the battery usage. Between 37°C and 40°C, there is a gradual transition between the two power-split criteria.

The transition from optimal power-split to minimal battery usage depicted in Figure 5 should not start at lower temperatures to avoid hindering the overall performance. Indeed, the power-following energy management strategies are significantly worse in fuel consumption and fuel cell degradation. However, the EMS must adapt quickly enough to prevent temperature peaks. Therefore, it is essential to suitably define the transition to find a proper trade-off between maximum battery temperature and the other targets.

The adaptive EMS is validated considering the driving cycle on the mountain route, which was already amply analyzed in Chapter 4. The predictive references are generated using the health-conscious energy management strategy, with $\alpha = 0.01$ and $\beta = 0.66$ in the multi-objective optimization function. In this case, the predictive references result in low fuel cell degradation with negligible impact on fuel consumption (see Table 4.5). Moreover, an uncertain speed forecast with lower accuracy is considered for the predictive references optimization to again demonstrate the robustness of the dual-stage predictive EMS to the forecasting uncertainties.

Figure 5.2 compares the simulation results of the adaptive EMS with the non-adaptive one, which is equivalent to the one in Section 4.3. Looking at the fuel cell power and SoC profiles, it is evident that the power-split is essentially the same, except between minutes 125 and 163. The difference is evident from the profile of parameter r_1. The battery temperature is the most relevant signal to analyze because it immediately shows the benefit of the adaptive EMS compared to the non-adaptive solution. Indeed, the first strategy keeps the battery temperature below 40°C, whereas the other one results in a maximum battery temperature of 47.5°C, so well above the accelerated degradation threshold. Remarkably, the adaptive EMS can significantly reduce the battery heat generation between minutes 136 and 150 by temporarily deviating from the optimal power-split.

Table 5.1 offers a performance comparison between the adaptive and non-adaptive energy management strategies. It is necessary to clarify that the actual effect of avoiding temperature peaks is not quantified by the battery degradation model considered in this work. However, the performance comparison is useful to evaluate the detrimental impact of deviating from the optimal power-split for fuel consumption and fuel cell voltage degradation. Eventually, the adaptive EMS results in a 0.6% higher fuel consumption, 4.1% lower battery degradation rate, and 12.5% higher fuel cell degradation rate. Here, the decrease in battery degradation is only due to the lower battery usage.

As mentioned, the actual benefit of the adaptive EMS on battery degradation is not directly quantified. However, the maximum battery temperature is 39.8°C (below the

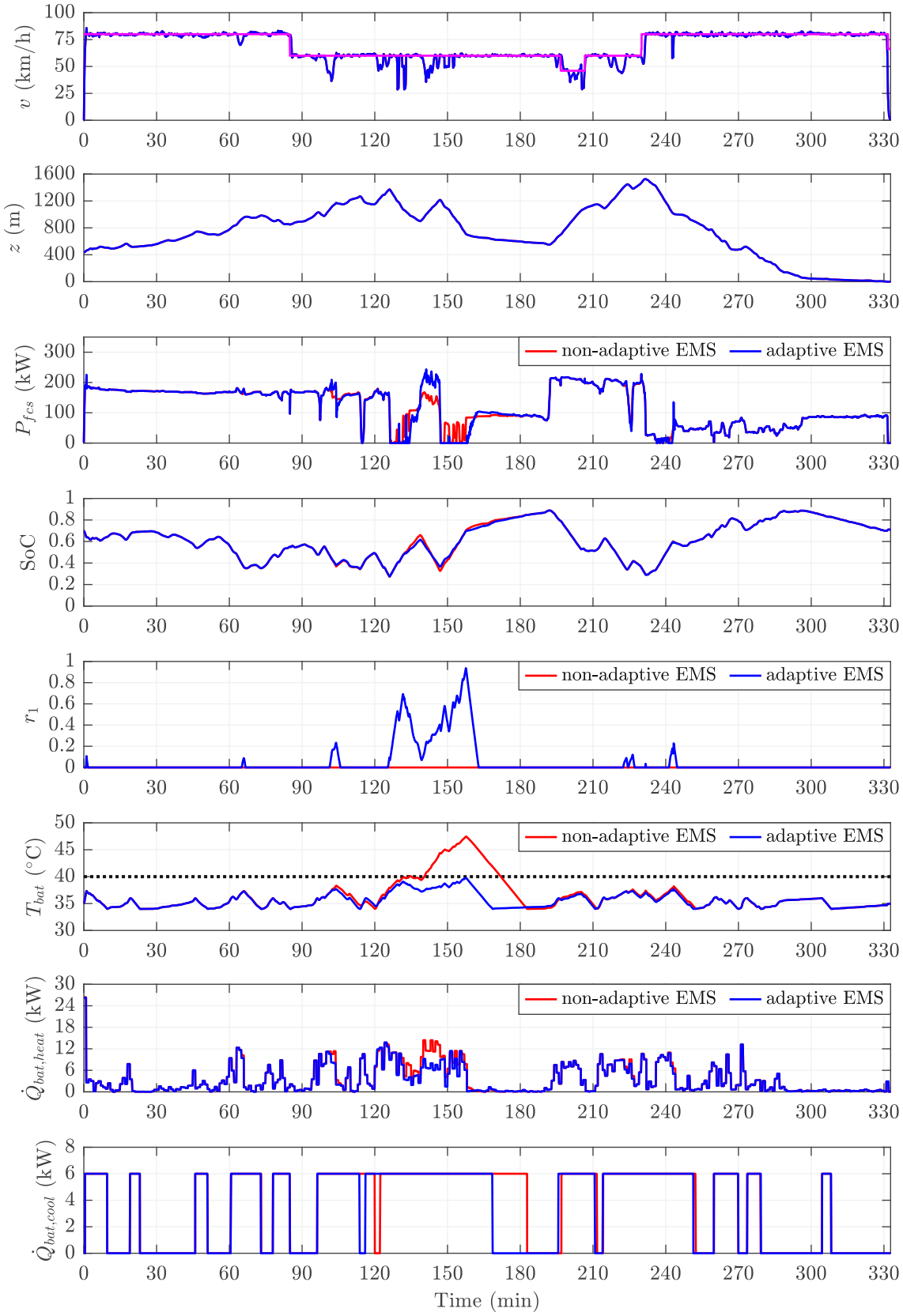

Figure 5.2: Comparison between the adaptive and non-adaptive strategies with focus on the battery thermal management results.

Table 5.1: Performance comparison between the adaptive and non-adaptive strategies.

EMS	SFC (kg/100 km)	ΔSoD_{bat} (10^{-6}/km)	ΔSoD_{fcs} (10^{-6}/km)	maximum T_{bat} (°C)	$t_{+40°C}$ (min)
non-adaptive	10.20	1.22	0.80	47.5	33
adaptive	10.26	1.17	0.90	39.8	0

accelerated degradation threshold) against the 47.5°C reached with the non-adaptive EMS. Moreover, the time operating above the accelerated degradation threshold (indicated with $t_{+40°C}$ in the table) is 33 minutes, which is 10% of the total driving cycle duration. Therefore, the adaptive EMS is expected to mitigate battery degradation significantly.

Comparing the results with those reported in Table 4.5 also demonstrates that the less accurate speed forecast has a minimal impact on the component degradation rates. Note that the fuel consumption is 2.3% higher due to the additional loads of the battery cooling system reported in (5.2).

In summary, this section proposed an adaptive energy management strategy that is conscious of the battery thermal management targets. The underlying idea is to exploit the interaction between energy and thermal management by limiting the battery usage in critical situations to decrease the heat generation in the system. In particular, the adaptive EMS can keep the temperature between an assigned accelerated degradation threshold by suitably designing the control parameter characteristics as a function of the battery temperature. Eventually, it is expected that the improvement in battery degradation is considerable enough to justify the higher fuel consumption and fuel cell degradation.

5.2 Predictive strategy for health-conscious activation of multi-module fuel cell systems

The results reported in Section 4.5 have shown that fuel cell degradation is severely affected by start-up/shut-down cycles, even under the assumption that only one occurs per driving cycle. Moreover, the driving scenarios studied so far always considered motorway routes, meaning that long distances are covered per cycle. However, in urban or rural driving cycles, it is expected that the degradation due to start-up/shut-down cycles is even more dominant because the driving cycles are usually shorter.

Therefore, this section proposes an innovative strategy to reduce fuel cell degradation caused by start-up/shut-down cycles. The base for this investigation is that the overall fuel cell system comprises several modules that can be operated independently, i.e. each module has its own BoP components and power converter. Such a system is called a *multi-module* fuel cell system. In practice, most fuel cell manufacturers have adopted a modular production philosophy that allows them to use the same modules for different applications. Therefore, truck manufacturers use multi-module systems in their heavy-duty commercial vehicles. In this section, the fuel cell system comprises two modules with nominal power of 155 kW, as implemented in project FC4HD [26].

The low-level control strategies on the individual fuel cell modules significantly impact the degradation caused by start-up/shut-down cycles. Suitable strategies can reduce the degradation due to each start-up/shut-down event. However, this study aims to reduce the degradation by entirely avoiding start-up/shut-down cycles in short and low-demanding driving scenarios. This way, there will be fewer start-up/shut-down cycles over the average life span of trucks.

Several studies were published recently on energy management strategies for multi-module or multi-stack fuel cell systems [125]–[135]. Some works focus on hybrid locomotives [125]–[127], and some focus on the power distribution between the fuel cell modules to improve the overall system efficiency [128, 129]. The activation strategies proposed in the literature for road vehicle applications are either rule-based [130]–[132] or optimization-based [133]–[135]. However, due to its high complexity, no work in the literature formulated the optimal control problem for multi-module energy management considering the number of active modules as a state variable, which would enable the optimization of the number of start-up/shut-down cycles. Moreover, dynamic programming was never adopted to find the global optimal solution to the energy management problem.

This thesis proposes a predictive strategy for the health-conscious activation of multi-module fuel cell systems. The underlying idea is to avoid activating one or both fuel cell modules in short and low-demanding driving cycles to reduce the overall degradation due to start-up/shut-down cycles. Moreover, if the average load demand is low, using only one fuel cell module can also improve fuel consumption. However, battery degra-

dation is neglected for simplicity. Thus, the optimization targets are fuel consumption and fuel cell degradation rate.

The dual-stage structure of the predictive energy management strategy is the same as in the previous chapters. However, a main difference concerns the optimization of the predictive EMS references in the first control stage. Regardless, the optimal control problem has a similar formulation to the one described in Section 4.3 because the overall targets and constraints are the same. Nevertheless, the formulation must be adapted to the multi-module fuel cell system so that the energy management strategy not only defines the power setpoints for the two fuel cell modules (FCMs) but also whether they are active or not.

An essential consideration for formulating the new optimal control problem is that if the FCMs have the same efficiency characteristics, equally distributing the power between them is the most efficient power-split, when they are both active. In particular, if the modules are in the same degradation state (or close to it), it is reasonable to consider that they have the same efficiency characteristics. Therefore, assuming an equal power-split between the FCMs, the overall fuel cell system power can be conveniently expressed as in (5.4), where P_{fcm} is the power of the individual module, and N_{fcm} the number of active modules.

$$P_{fcs} = P_{fcm}\ N_{fcm} \tag{5.4}$$

The optimal control problem can be formulated considering two state variables, i.e. SoC and N_{fcm}, and two input variables, i.e. P_{fcm} and ΔN_{fcm}. The latter indicates the change in active modules, which can assume the following integer values:

$$N_{fcm} \in \{0, 1, 2\}\ . \tag{5.5}$$

Therefore, the optimal control problem can be classified as a mixed integer program because it involves continuous and integer variables. Conveniently, dynamic programming is the ideal candidate to solve such an optimization problem because of the grid discretization for the state and input variables. Figure 5.3 offers a representation of the dynamic programming principle to solve the health-conscious activation problem for multi-module fuel cell systems. The principle would be equivalent to the one depicted in Figure 2.14 if the only possible state of N_{fcm} was 2 (i.e. both fuel cell modules were always active).

Eventually, the optimal control problem is expressed as follows:

$$\min_{\left\{\begin{bmatrix} P_{fcm,1} \\ \Delta N_{fcm,1} \end{bmatrix}, \dots, \begin{bmatrix} P_{fcm,N} \\ \Delta N_{fcm,N} \end{bmatrix}\right\}} \sum_{k=1}^{N} L_k + \phi_k \tag{5.6}$$

where L_k is the stage cost and ϕ_k the penalty function for the implementation of SoC soft constraints as in (3.7). The discrete battery dynamics are expressed as in (3.6),

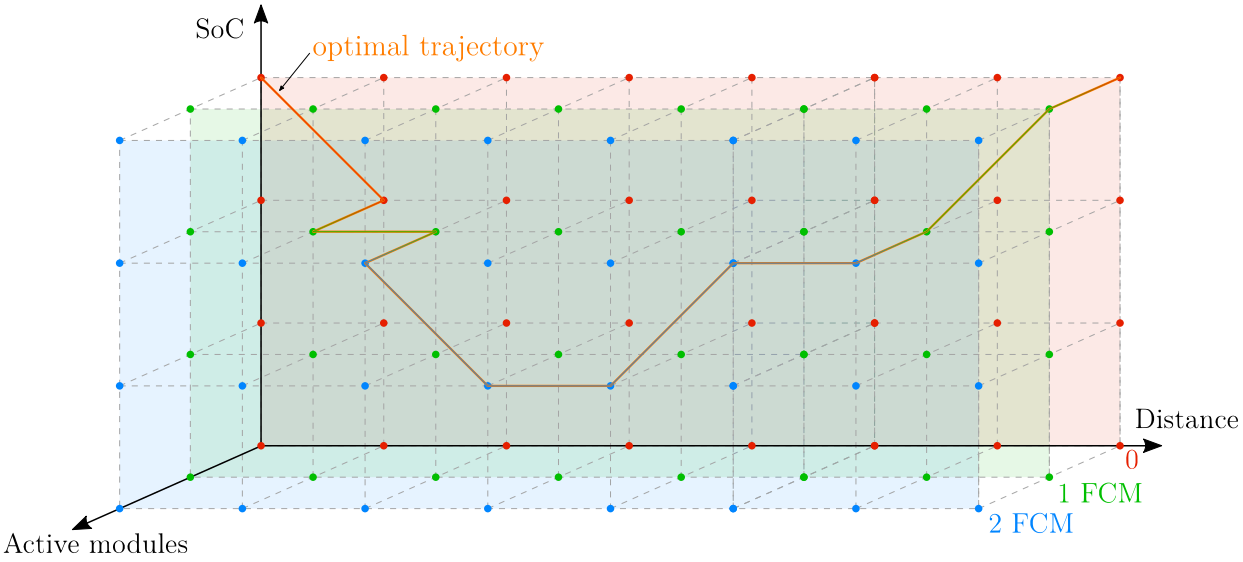

Figure 5.3: Representation of dynamic programming principle for optimal activation of multi-module fuel cell systems.

whereas the number of active modules changes as follows:

$$N_{fcm,\,k+1} = N_{fcm,\,k} + \Delta N_{fcm,\,k} \ . \tag{5.7}$$

The following constraints are imposed on the admissible values of the number of active modules:

$$N_{fcm,\,k} \in \{0, 1, 2\} \ , \tag{5.8a}$$
$$\Delta N_{fcm,\,k} \in \{-1, 0, 1\} \ . \tag{5.8b}$$

Moreover, it is enforced that the fuel cell modules are not active at the beginning and end of the driving cycle:

$$N_{fcm,\,1} = N_{fcm,\,N} = 0 \ . \tag{5.9}$$

The constraints on the initial, minimum, and maximum SoC values are defined as in (3.5). However, in this case, the final SoC is not subject to a hard constraint, so the optimization can favor the one-module or battery-only operations when possible. Here, a soft constraint on the final SoC is implemented considering the equivalent battery consumption in the final stage of the penalty function:

$$\phi_N = \alpha \frac{(\mathrm{SoC}^* - \mathrm{SoC}_{fin})\ E_{bat,max}}{\eta^*_{fcs}\ \mathrm{LHV}_{\mathrm{H_2}}} \ , \tag{5.10}$$

where η^*_{fcs} is the maximum fuel cell system efficiency and SoC^* is a reference value, set as 0.70. The equivalent battery consumption is multiplied by α, which expresses

the weighting between fuel consumption and degradation. Indeed, the multi-objective function of the optimization consists of only two terms: fuel consumption and fuel cell degradation rate. Thus, the stage cost is expressed as:

$$L_k = (1-\alpha)\ L_{fuel,\,k} + \alpha \frac{L_{fcm,\,k}}{2}\ w\ , \tag{5.11}$$

where α is the weighting parameter that can shift the optimization towards the individual targets, and w is a scaling factor equal to 10^5. The fuel consumption at the stage k is calculated similarly to (4.6) and expressed as:

$$L_{fuel,\,k} = N_{fcm,\,k}\ \dot{m}_{\mathrm{H_2}}^{fcm}(P_{fcm,k})\ \Delta t_k\ , \tag{5.12}$$

depending on the current number of active modules, $N_{fcm,\,k}$, and the module hydrogen consumption $\dot{m}_{\mathrm{H_2}}^{fcm}(P_{fcm,k})$. In this case, if no module is active, the fuel consumption is zero. On the contrary, under the assumption that the modules were always active in the previous chapters, there still was fuel consumption even if the net fuel cell system power was zero (see Figure 2.4).

The term $L_{fcm,\,k}$ expresses the sum of the degradation in both fuel cell modules. For this reason, it is divided by two in (5.11) to express the average degradation of the overall fuel cell system. In particular, the degradation stage cost is calculated similarly to (4.9), considering start-up/shut-down cycles, dynamic loading, low-power and high-power operations. Eventually, it is expressed as:

$$L_{fcm,\,k} = \delta_{ss}\ \Delta N^{+}_{fcm,\,k} + N_{fcm,\,k}\ (\delta_{lp}\ \Delta t_k^{fcm,lp} + \delta_{hp}\ \Delta t_k^{fcm,hp} + \delta_{dl}\ \frac{|\Delta P_{fcm,\,k}|}{2P_{fcm,nom}})\ , \tag{5.13}$$

where $\Delta N^{+}_{fcm,\,k}$ indicates positive increments in the number of active modules. Eventually, the sum of all these increments represents the total number of start-up cycles. The operating time at low-power is expressed as in (5.14), and the operating time at high-power as in (5.15).

$$\Delta t_k^{fcm,lp} = \begin{cases} \Delta t_k & \text{if} \quad P_{fcm,\,k} < 10\% \text{ of } P_{fcm,nom}\ , \\ 0 & \text{otherwise.} \end{cases} \tag{5.14}$$

$$\Delta t_k^{fcm,hp} = \begin{cases} \Delta t_k & \text{if} \quad P_{fcm,\,k} > 80\% \text{ of } P_{fcm,nom}\ , \\ 0 & \text{otherwise.} \end{cases} \tag{5.15}$$

Here, $P_{fcm,nom}$ is the nominal power of each fuel cell module (i.e. half of $P_{fcs,nom}$).

The models of the fuel cell modules derive from the one described in Section 2.1.2 for the overall system. In particular, the characteristic curves are scaled assuming that each module equally contributes to the heat generation and fuel consumption of the fuel cell system. Therefore, $P_{fcm,heat}$ is half of $P_{fcs,heat}$ and $\dot{m}_{\mathrm{H_2}}^{fcm}$ is half of $\dot{m}_{\mathrm{H_2}}$ (see Figure 2.4).

Moreover, assuming that the cooling system is common between the modules, the overall energy consumption due to fuel cell cooling is expressed as:

$$P_{fcs,cool} = P_{fcs,cool}(\, v\,, T_{amb}\,, N_{fcm}\, P_{fcm,heat}\,)\ , \tag{5.16}$$

considering the same performance as in Figure 2.6. Lastly, it is assumed that each fuel cell module has its own converter, which has the same efficiency characteristic curve depicted in Figure 2.5. Eventually, the battery power setpoint is calculated as follows:

$$P^*_{bat} = P_{el,des} - N_{fcm}\ (P_{fcm}\ \eta^{fcm}_{dc,dc}) + P_{fcs,cool}\ , \tag{5.17}$$

where $\eta^{fcm}_{dc,dc}$ indicates the converter efficiency of each module.

The predictive activation strategy for the multi-module fuel cell system proposed in this section is expected to be highly beneficial in short and low-demanding driving cycles. Indeed, if sufficiently charged, the battery system can sustain urban driving on its own for short periods (e.g. 30 minutes). Therefore, short driving cycles could be completed without fuel cells, entirely avoiding degradation.

However, it is not trivial to heuristically define how long the battery can sustain the driving cycle on its own because it depends on the truckload, initial SoC, route elevation, and external conditions. On the contrary, the proposed dynamic programming can consider all these factors and optimize the activation strategy depending on the desired trade-off between fuel consumption and fuel cell degradation.

The optimization results are analyzed below to demonstrate the benefits of the proposed strategy for mitigating fuel cell degradation. Here, the trivial results where the fuel cell modules are not active in very short driving cycles are not analyzed, although they significantly contribute to mitigating the degradation due to start-up/shut-down cycles.

Figure 5.4 shows the simulation results for a 54 minutes-long real-world driving cycle recorded on a rural-urban-rural route, considering a total vehicle mass of 20 tons. In this case, α is set to a low value so that fuel consumption has priority over fuel cell degradation in the optimization. On the right side, the figure shows the overall fuel cell system power, the individual module power and hydrogen consumption. The fuel cell system power depends on the number of active modules, as defined in (5.4). Here, the sections with both modules active are highlighted in blue, and those with one module in green. The figure shows that one module is active most of the driving cycle and operating close to the maximum efficiency point. However, it shuts down to reduce fuel consumption and maximize regeneration during urban driving (between minutes 14 and 22) and the downhill section (between minutes 40 and 43). On the other hand, the second fuel cell module activates twice during the first rural section due to higher loads, improving the overall system efficiency.

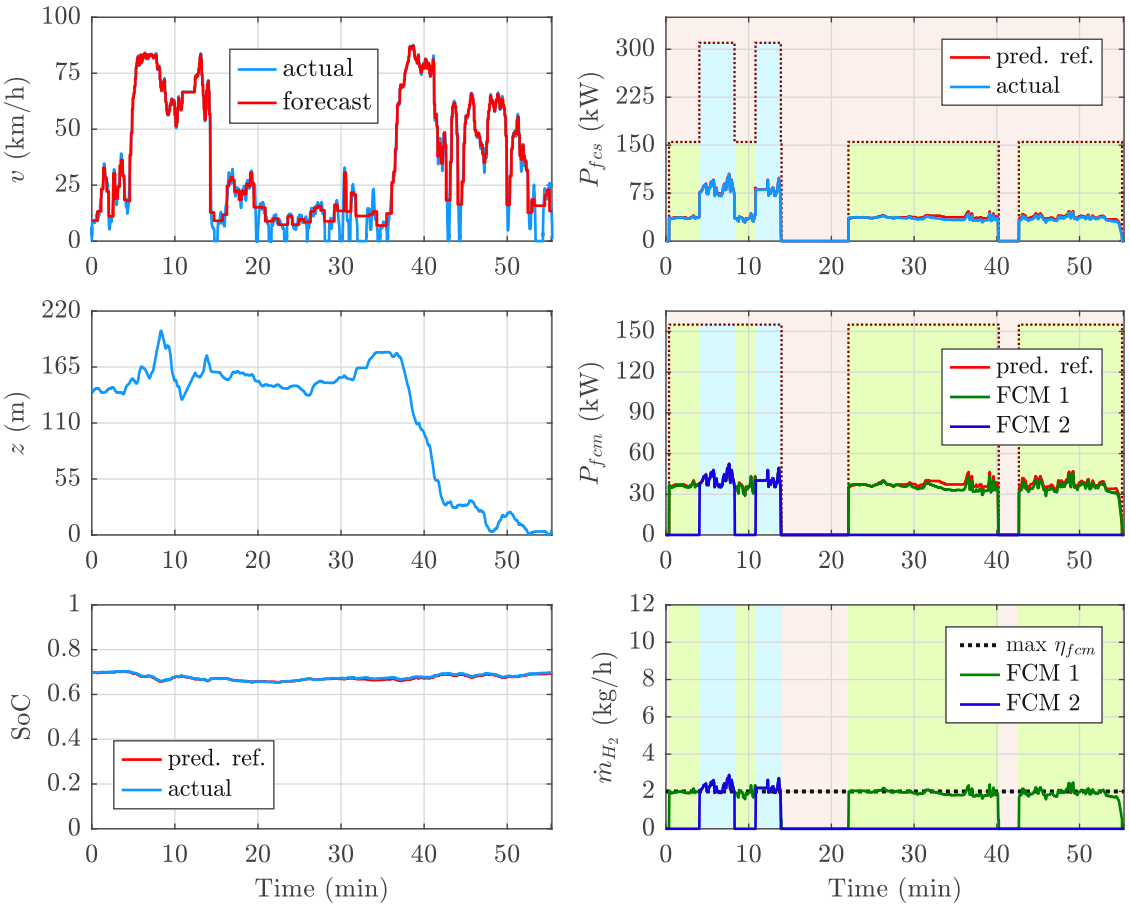

Figure 5.4: Simulation results for a short driving cycle on urban and rural roads showing the multi-module operation of the fuel cell system.

The weighting parameter α in the multi-objective function can move the optimization towards fuel consumption or fuel cell degradation. Figure 5.5 compares four different cases of multi-module fuel cell system operation on the same driving cycle as before.

- The results in Figure 5.5a are obtained with the method of Section 4.3 with $\alpha = 0.5$ and $\beta = 0$. Both modules are always active in this case, and the fuel cell system operates for a significant amount of time at low power, causing high degradation.
- The results in Figure 5.5b are obtained with $\alpha = 0$ in the predictive activation strategy. Here, the modules frequently start and shut down to minimize fuel consumption regardless of degradation.
- Figure 5.5c shows the one-module operation, obtained with a relatively low α, i.e. 0.05. In this case, the fuel cell module operates much more stationary around the maximum efficiency operating point.

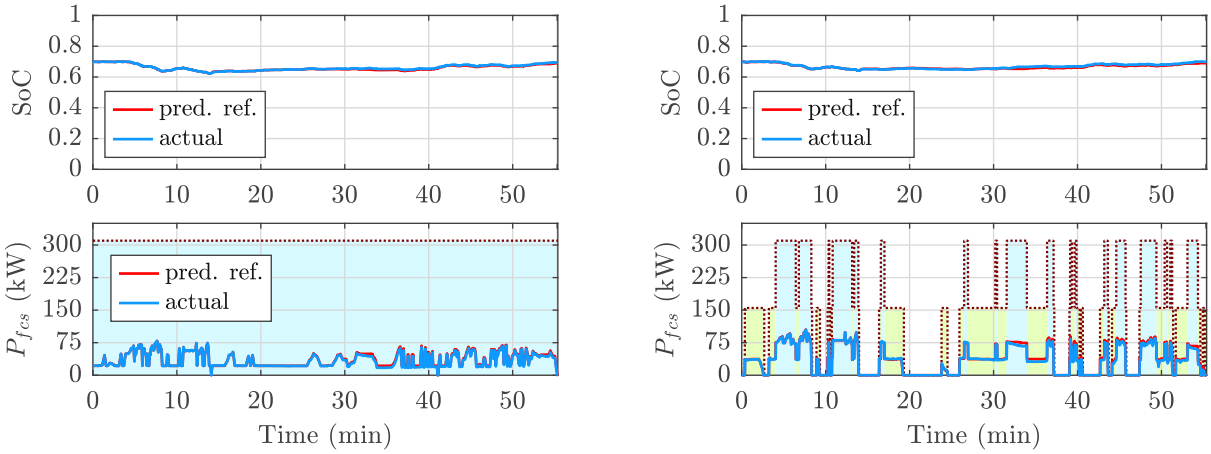

(a) Two-module operation.

(b) Optimal fuel consumption.

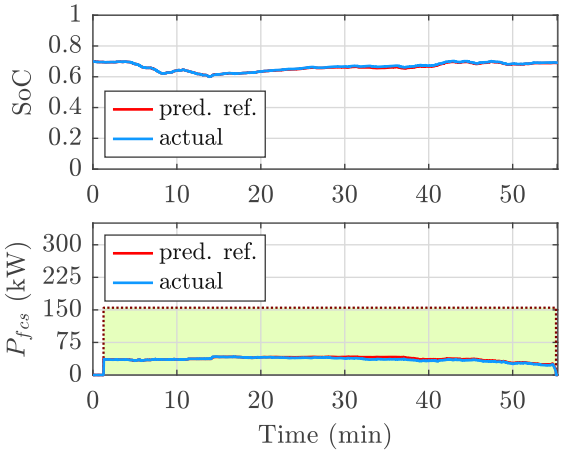

(c) One-module operation.

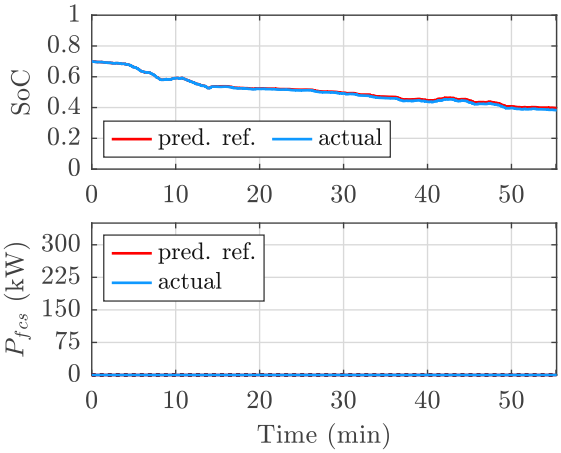

(d) Battery-only operation.

Figure 5.5: Comparison of different cases for the multi-module operation of the fuel cell system.

- Lastly, Figure 5.5d shows the battery-only operation. Here, the fuel cell modules are not activated at all to completely avoid degradation. It is interesting to note that the SoC drops from 70% to 40% to sustain the driving cycle in the battery-only operation.

Table 5.2 compares the performances of the different cases presented above in terms of fuel consumption and degradation rate.

- The minimum fuel consumption is obtained with the solutions in Figure 5.4 and Figure 5.5b, showing that the same result can be obtained without frequently shutting down the modules (which causes extremely high degradation). Moreover,

Table 5.2: Performance comparison of different cases for the multi-module operation of the fuel cell system.

SFC (kg/100 km)	final SoC	ΔSoD_{fcs} (10^{-6}/km)			No. of starts	
		average	FCM 1	FCM 2	FCM 1	FCM 2
5.49	0.70	15.6	18.8	12.4	3	2
5.91	0.70	8.9	8.9	8.9	1	1
5.49	0.70	101.9	92.7	111.0	15	18
5.57	0.70	3.1	6.2	0	1	0
0	0.40	0	0	0	0	0

the fuel consumption is 8% higher for the two-module operation and only 1% higher for the one-module operation.

- Excluding the battery-only case, the one-module operation leads to the lowest fuel cell degradation. It is interesting to compare the results with the two-module operation, where the average degradation is almost three times higher. Therefore, in the one-module operation, not only the fuel cell degradation is reduced because of one less start-up/shut-down cycle, but also because low-power operation is avoided. Nevertheless, even if only one module is used, the degradation rate is significantly higher than the ones reported in Section 4.3, because the driving cycle is significantly shorter (i.e. 32 kilometers).

Additional simulation results are reported in Figure 2.12 to demonstrate that the one-module operation is also possible for the flat-route and mountain-route driving cycles. In this case, the simulations consider a total vehicle mass of 20 tons to create low-demanding driving scenarios. Figure 5.6 shows the results of the one-module operation for both driving cycles. From the SoC and fuel cell power profiles, it is evident that one module is sufficient to sustain a low-demanding driving cycle also for long distances.

Table 5.3 compares the performances between one-module and two-module operations of the fuel cell system for the flat-route and mountain-route driving cycles. In both cases, adopting the one-module operation, the fuel degradation is 50% lower than the two-module one. On the other hand, the fuel consumption is 14% and 8% higher because the individual fuel cell module works at lower efficiency in the high-power operating region.

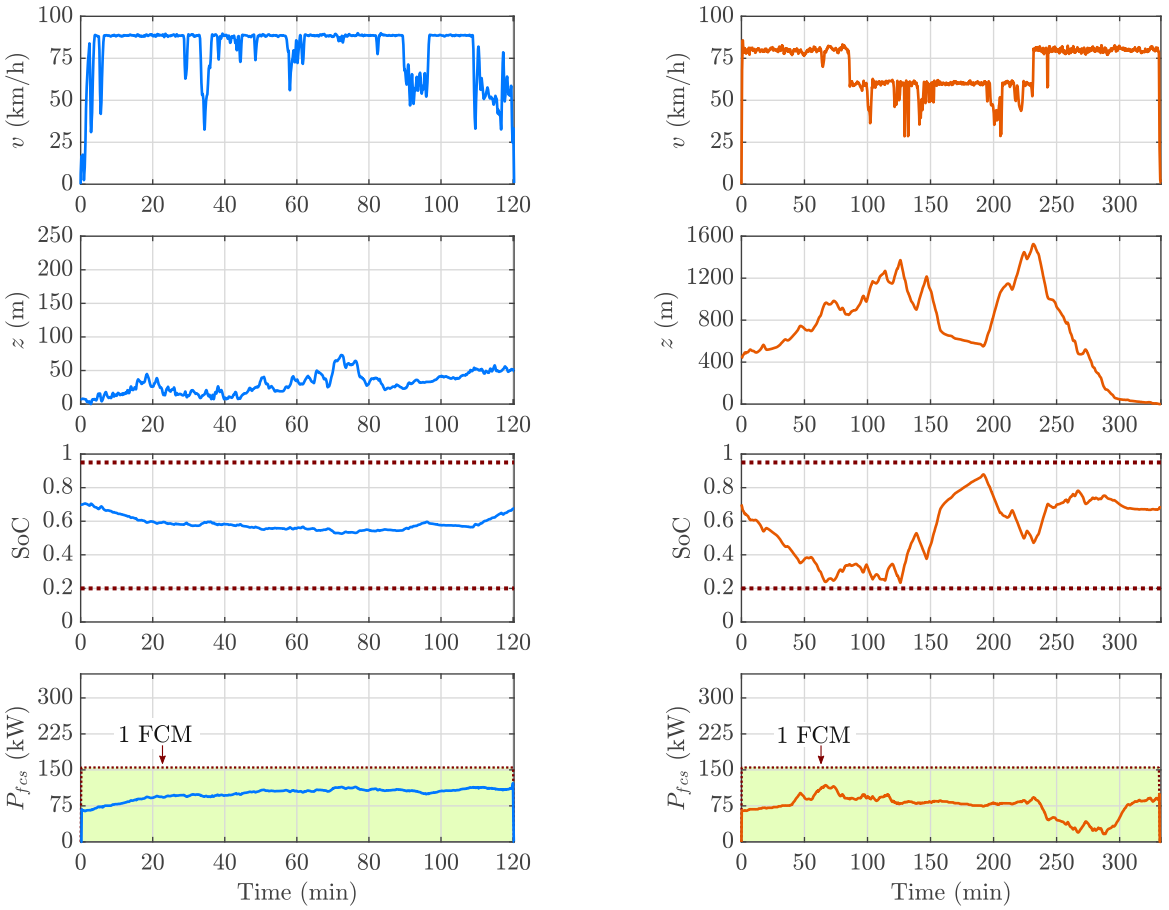

(a) Flat-route driving cycle

(b) Mountain-route driving cycle.

Figure 5.6: Simulation results for motorway driving cycles showing the one-module operation of the fuel cell system.

Table 5.3: Performance comparison between one-module and two-module operations of the fuel cell system for motorway driving cycles.

Driving cycle	SFC (kg/100 km)	final SoC	ΔSoD_{fcs} (10^{-6}/km)			No. of starts	
			average	FCM 1	FCM 2	FCM 1	FCM 2
flat	6.96	0.68	1.25	1.25	1.25	1	1
route/20t	7.98	0.68	0.64	1.28	0	1	0
mountain	5.98	0.68	0.55	0.55	0.55	1	1
route/20t	6.45	0.68	0.28	0.56	0	1	0

In conclusion, this section proposed a predictive strategy based on dynamic programming for the health-conscious activation of multi-module fuel cell systems. The significant benefits for the mitigation of fuel cell degradation have been demonstrated for short and low-demanding driving cycles and motorway ones. The next logical research direction is to address the robustness to speed forecast uncertainties to fully demonstrate the benefits in realistic driving scenarios and promote the implementation of the strategy in vehicles.

5.3 Speed planning and energy management co-optimization for eco-driving of fuel cell electric trucks

An increasingly popular idea to reduce the carbon footprint of the transport sector is eco-driving: i.e. adopting an energy-aware driving style that improves the vehicle performance. In conventional vehicles, eco-driving aims at saving fuel and reducing emissions. Similarly, in electric vehicles, eco-driving can significantly improve the overall powertrain efficiency and, thus, extend the driving range, fastening their advancement and commercialization.

Background and state of the art

A simple eco-driving application is truck driver training to follow heuristic guidelines, such as avoiding braking, anticipating traffic flow, and maintaining a constant speed [136]. However, the sophistication of advanced driver assistance systems (ADAS) has reached a maturity level that allows implementing eco-driving as online advice systems or intelligent cruise controllers in autonomous vehicles [137]. Therefore, studying eco-driving as an optimal control problem has become an appealing research topic with the goal, for example, of developing new methods to optimize the vehicle speed plan for a given route elevation profile. This topic is especially interesting for long-haul trucks driving in motorway driving scenarios, where the energy demand is high, and traffic is typically negligible (meaning that the optimal speed plan can be closely followed).

In hybrid vehicles, there is a strong interaction between the speed planning and energy management tasks. For example, driving too fast on an uphill road might determine a complete battery discharge. Therefore, the co-optimization of speed planning and energy management can significantly benefit fuel consumption and SoC control. However, the co-optimization problem has a much higher complexity than the hierarchical optimization of the individual problems [137].

Literature reviews on optimal eco-driving studies are proposed in [137, 138]. The first work also includes a rigorous formulation of the optimal control problem for the eco-driving of conventional, hybrid, and electric vehicles. The eco-driving of trucks has been studied for conventional vehicles in [139]–[141], always including the route elevation in the optimal control problem due to the heavy loads. The literature on eco-driving of passenger cars is more extensive, and some relevant works are [142]–[144] for hybrid electric vehicles, and [145]–[147] for fuel cell electric vehicles. In general, the energy management strategy is always included in the optimal control problem for the eco-driving of hybrid vehicles. Moreover, most works adopt dynamic programming or Pontryagin's minimum principle to solve the optimal control problem.

The author's work [64] focuses on the eco-driving of fuel cell electric trucks, optimizing the speed plan based on the route elevation and studying the trade-off between driving

time and range. In particular, the optimization method is inspired by [142] and relies on a combination of dynamic programming and Pontryagin's minimum principle to reduce the complexity of the problem. Typically, the co-optimization problem of speed planning and energy management involves two state variables (i.e. speed and battery SoC) and two input variables (e.g. acceleration and fuel cell power). Dynamic programming can be implemented to solve such a problem but with a high computational cost, making a real-time application of the method impractical. On the other hand, the approach proposed in [64] decouples the speed planning and energy management tasks by using PMP to derive the optimal power-split policy. This way, the optimal control problem is reduced to speed planning only (with one state variable and one input variable) and can be solved with DP in a reasonable computational time for real-time applications. The main limitation of this approach is that it does not include SoC constraints in the optimization.

To the author's knowledge, the work [145] represents the only study in the literature that uses dynamic programming to co-optimize the speed planning and energy management tasks. However, the main limitation is that PMP is adopted to reduce the number of decision variables in the dynamic programming implementation, which does not ensure global optimality and is only a valid approach under several simplifying assumptions. Still, the dynamic programming co-optimization required 50-55.000 ms/km for computational time, proving that the curse of dimensionality makes the method not well suited for real-time control. Nevertheless, the work demonstrates that the co-optimization approach can significantly benefit fuel consumption on hilly routes compared with a hierarchical/decoupled optimization approach, which first optimizes the speed plan and then the energy management strategy.

Contribution and formulation

This section proposes a novel formulation for the co-optimization of speed planning and energy management for eco-driving of fuel cell electric trucks. Ultimately, the goal of this co-optimization approach is to extend drastically reduce fuel consumption and, thus, to extend driving range.

The optimal control problem investigated in this section considers driving time, fuel consumption, and driving comfort as the main optimization targets. At the same time, it also includes constraints on speed, acceleration, SoC, and fuel cell power. Unlike other works, this study adopts dynamic programming to solve the co-optimization problem and ensures global optimality.

In general, there are several ways to formulate the optimal control problem for speed planning. However, the main distinction is between time-based and position-based problems. The first class has higher complexity because the position is a system state, and it is usually adopted to study urban driving scenarios, for example, when the vehicle needs to stop at a red light. On the other hand, if the vehicle never stops, there is bijective relation between time and position. For this reason, distance-based optimal

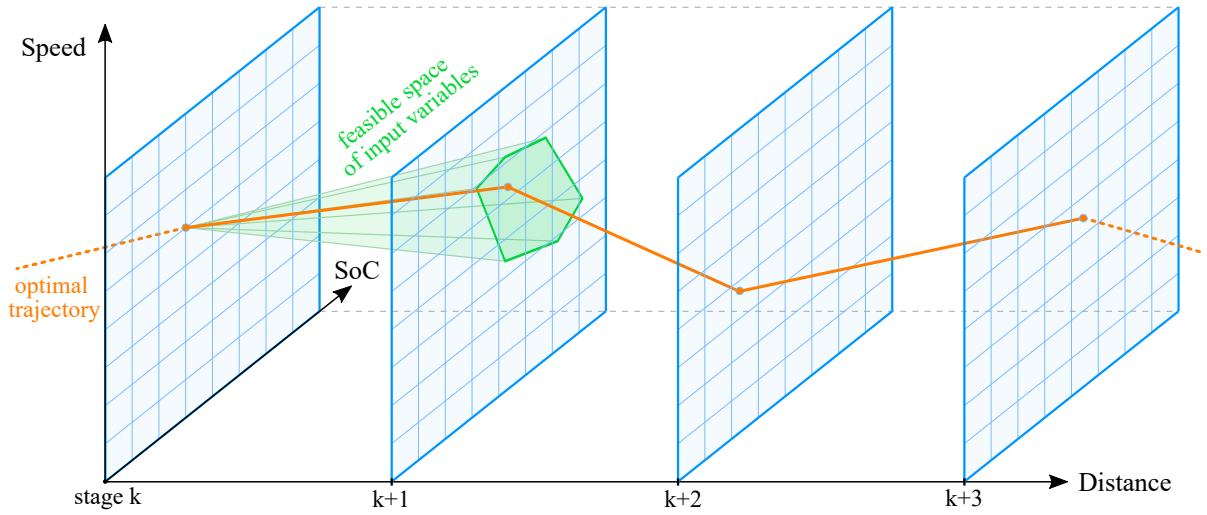

Figure 5.7: Representation of dynamic programming principle for speed planning and energy management co-optimization.

control problems are perfect for motorway driving scenarios. This work considers a distance-based optimal control problem because it focuses on a motorway route, the typical driving scenario for long-haul transportation. In this sense, motorway routes are the best application for eco-driving because of the significant energy demand and because traffic is typically negligible (meaning that the optimal speed plan can be closely followed).

Figure 5.7 offers a visual representation of the dynamic programming principle for the speed planning and energy management co-optimization, showing the higher complexity due to more state and input variables (compared with Figure 2.14).

In general, the individual problem for speed planning can be formulated by adopting the speed v as the state variable and the acceleration $\dot{v}$ as the input one. In this case, the power at wheels is calculated inverting (2.5). Moreover, considering (2.6), the electric motor power can be expressed as a function of speed, acceleration, and road slope as:

$$P_m = f(v, \dot{v}, \theta) \ . \tag{5.18}$$

Since the problem is distance-based and the speed is a state variable, the time must be calculated with adequate accuracy. For this reason, the time interval Δt_k to drive the segment Δs is calculated using Heun's integration method as:

$$\Delta t^* = \Delta s / v_k \tag{5.19a}$$
$$v^* = v_k + \dot{v}_k \ \Delta t^* \tag{5.19b}$$
$$v^{**} = (v_k + v^*)/2 \tag{5.19c}$$
$$\Delta t_k = \Delta s / v^{**} \tag{5.19d}$$

where $\dot{v}_k$ is the acceleration at the stage k. In the optimal control problem for energy management, the battery SoC was adopted as the state variable and P_{fcs} as the input one (see Section 3.2.1).

Eventually, the speed planning and energy management co-optimization problem is formulated considering two state variables (i.e. v and SoC) and two input variables (i.e. $\dot{v}$ and P_{fcs}). The multi-objective function for the co-optimization consists of three terms: driving time, fuel consumption, and driving comfort. Therefore, the optimal control problem is written as follows:

$$\min_{\left\{\begin{bmatrix}\dot{v}_1\\ P_{fcs,1}\end{bmatrix},\dots,\begin{bmatrix}\dot{v}_N\\ P_{fcs,N}\end{bmatrix}\right\}} \sum_{k=1}^{N} w_t\ \Delta t_k + w_f\ \dot{m}_{\mathrm{H_2}}(P_{fcs,k})\ \Delta t_k + w_c\ |\dot{v}_k| + \phi_k \tag{5.20}$$

where w_t is the weighting parameter for driving time, w_f for fuel consumption, and w_c for driving comfort. Dynamic programming must find the optimal sequence of acceleration and fuel cell power that minimizes the multi-objective function. The following constraints on the initial and final values are imposed for the speed and SoC:

$$v_1 = v_{in} \tag{5.21a}$$
$$\mathrm{SoC}_1 = \mathrm{SoC}_{in} \tag{5.21b}$$
$$v_N = v_{fin} \tag{5.21c}$$
$$\mathrm{SoC}_N = \mathrm{SoC}_{fin} \tag{5.21d}$$

where v_{in} is the initial speed, and v_{fin} the final one. The maximum and minimum values of speed, acceleration, SoC, and fuel cell power are constrained as:

$$v_{min} \leq v_k \leq v_{max} \tag{5.22a}$$
$$\dot{v}_{min} \leq \dot{v}_k \leq \dot{v}_{max} \tag{5.22b}$$
$$\mathrm{SoC}_{min} \leq \mathrm{SoC}_k \leq \mathrm{SoC}_{max} \tag{5.22c}$$
$$0 \leq P_{fcs,k} \leq P_{fcs,max} \tag{5.22d}$$

where $\dot{v}_{min}$ is the minimum acceleration, and $\dot{v}_{max}$ the maximum one. The discrete battery dynamics are expressed as in (3.6), whereas the speed dynamics as:

$$v_{k+1} = v_k + \Delta t_k\ \dot{v}_k\ . \tag{5.23}$$

The additive penalty function ψ_k allows to implement soft constraints on speed, SoC, and electric motor power. The function is defined as:

$$\psi_k = \begin{cases} \psi^* & \text{if} \quad \mathrm{SoC}_k < \mathrm{SoC}_{min,soft} \quad \text{or} \quad \mathrm{SoC}_k > \mathrm{SoC}_{max,soft} \\ \psi^* & \text{if} \quad v_k < v_{min,soft} \quad \text{or} \quad v_k > v_{max,soft} \\ \psi^* & \text{if} \quad P_{m,k} > P_{m,max} \\ 0 & \text{otherwise} \end{cases} \tag{5.24}$$

Table 5.4: Parameters of co-optimization problem.

Parameter	Symbol	Value	Parameter	Symbol	Value
Distance grid spacing	Δs	50 m	Min speed	v_{min}	25 km/h
Time weighting	w_t	variable	Min speed (soft)	$v_{min,soft}$	30 km/h
Consumption weighting	w_f	1	Max speed (soft)	$v_{max,soft}$	90 km/h
Comfort weighting	w_c	0.001	Max speed	v_{max}	95 km/h
Initial speed	v_{in}	70 km/h	Min SoC	SoC_{min}	0.20
Final speed	v_{fin}	70 km/h	Min SoC (soft)	$\text{SoC}_{min,soft}$	0.25
Initial SoC	SoC_{in}	0.70	Max SoC (soft)	$\text{SoC}_{max,soft}$	0.90
Final SoC	SoC_{fin}	0.70	Max SoC	SoC_{max}	0.95
Max motor power	$P_{m,max}$	500 kW	Min acceleration	$\dot{v}_{min}$	-0.20 m/s^2
Max FCS power	$P_{fcs,max}$	310 kW	Max acceleration	$\dot{v}_{max}$	0.20 m/s^2

where $\psi^* = 100$. The values of all the parameters in the co-optimization problem are listed in Table 5.4. Changing the weight w_t allows exploring different trade-offs between the driving time and fuel consumption. On the other hand, the weight on the driving comfort is constant to ensure that the speed profile is always sufficiently smooth and with limited jerk.

As already discussed in the previous sections, dynamic programming finds a solution to the control problem that is optimal up to the error introduced by the discretization of the distance, state, and input variables. The results presented below refer to a DP implementation with 150 elements in the speed grid, 40 for the acceleration, 61 for the SoC, and 16 for the fuel cell power. Notice that for the energy management variables, the number of elements is significantly lower than the one adopted in Section 3.2.1 to mitigate the curse of dimensionality. Even so, the computational time required for the co-optimization is 7500 ms/km, which is a hundredfold higher than the one for the energy management optimization.

Optimization results

The optimal speed planning is studied for a segment of the route shown in Figure 2.12c to investigate the most convenient way to overcome a mountain. The results in this section refer to a vehicle at full truckload (i.e. 42 tons) and with a 100 kWh battery system. The fuel cell and battery systems are assumed at 50% of state of degradation, and the ambient temperature is set at 35°C.

The proposed approach for the speed planning and energy management co-optimization is compared with three different methods to demonstrate its benefits. To ensure a fair performance comparison, the different methods are only used to obtain the speed plan for the defined route. Afterward, the energy management strategy is optimized for fuel consumption as described in Section 4.3. For clarity, the co-optimization approach is denoted with **co-optimization DP**. Below, the other approaches are listed and briefly described.

- **DP+PMP** denotes the optimization method adapted from [64], which uses Pontryagin's minimum principle to derive the optimal power-split policy and decouple the speed planning and energy management tasks. This way, the computational complexity is significantly reduced, but the main limitation of this approach is that it does not include SoC constraints in the optimization.
- **Decoupled DP** denotes the approach that does not include energy management at all in the optimization. In this case, dynamic programming is used to minimize the energy consumption of the electric motor. In particular, the motor power (5.18) replaces the hydrogen consumption in (5.20). Since the energy management strategy is optimized after the speed plan is created, this approach is equivalent to the sequential optimization procedure described in [145].
- **Cruising DP** denotes a dynamic programming optimization that aims at maintaining a constant speed for motorway cruising. In particular, the stage cost of the objective function in (5.20) is rewritten as: $w_v(v_k - v_{ref})^2 + w_c|\dot{v}_k|$, where w_v is a weighting parameter and v_{ref} is the cruising speed. Comparing eco-driving with constant speed cruising will demonstrate its general benefits against a conventional driving habit.

As initial analysis, Figure 5.8 shows the comparison between the co-optimization and decoupled approaches in terms of speed, motor power, fuel cell power, and SoC. In both cases, the driving time is 93 minutes. However, the signals are plotted versus the distance to demonstrate the effect of the different speed plans on fuel cell power and SoC in the same spots along the route. With the co-optimization approach, the vehicle drives essentially at maximum speed (i.e. 90 km/h) until kilometer 34 and after kilometer 71. On the contrary, using the decoupled approach, the vehicle drives slower in those sections and faster between them (i.e. during the uphill section of the route). The different speed plans have an enormous impact on energy management, as evident from the fuel cell and SoC profiles. In particular, using the decoupled approach, the SoC cannot be kept within the desired operating range (i.e. 0.25-0.90) even though the fuel cell power is at its maximum for the entire uphill section of the route. On the contrary, with the proposed co-optimization approach, the SoC stays within the desired range without requiring maximum fuel cell power operation, significantly improving fuel consumption.

The driving time significantly impacts the overall vehicle performance. Naturally, slow driving determines lower loads and fuel consumption. Therefore, when comparing different approaches for speed planning, it is essential to ensure that the driving time is the same for a fair comparison. Figure 5.9 shows the effect of driving time on the key performance indicators, comparing the different optimization approaches. The figure demonstrates that the proposed co-optimization approach results in significant fuel consumption improvements compared with the other approaches. Moreover, co-optimization is the only method that maintains the SoC within the desired range in

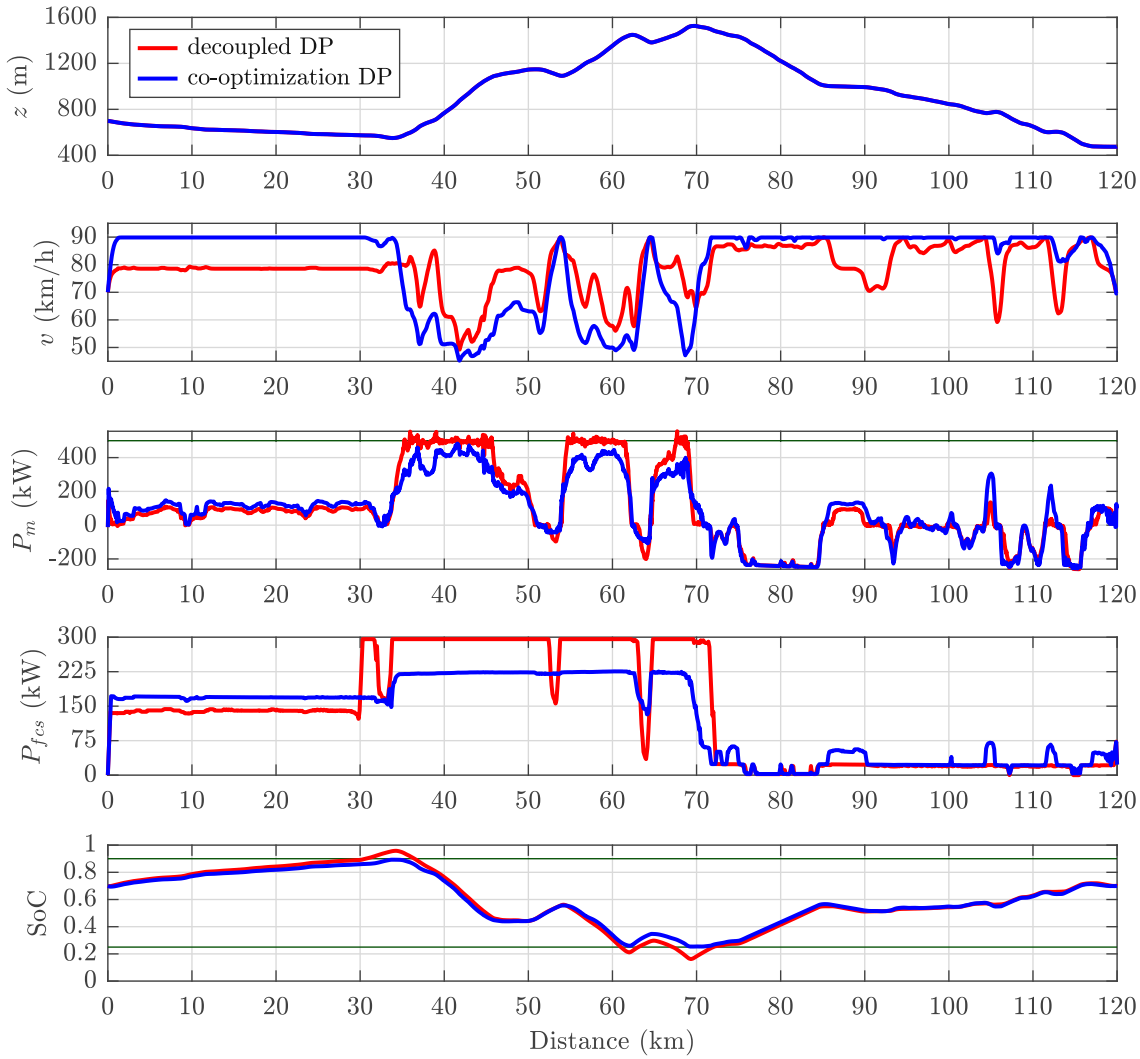

Figure 5.8: Comparison between two methods for optimal speed planning.

fast driving conditions. Interestingly, the motor energy is always higher with the co-optimization DP because of the lower regenerative braking energy. This aspect is also evident from the speed plans in Figure 5.8, where the decoupled DP slows down during the final descent to maximize the regenerative braking energy. On the contrary, the co-optimization DP essentially results in cruising at maximum speed.

The decoupled DP yields the minimum motor energy as it is expected due to its objective function formulation. On the other hand, its fuel consumption is generally higher than the other approaches because it completely neglects the energy management task. In this sense, the DP+PMP approach yields better fuel consumption because it also considers the energy management strategy within the optimization. However, this is only for driving times higher than 103 minutes, whereas for lower values, the decoupled

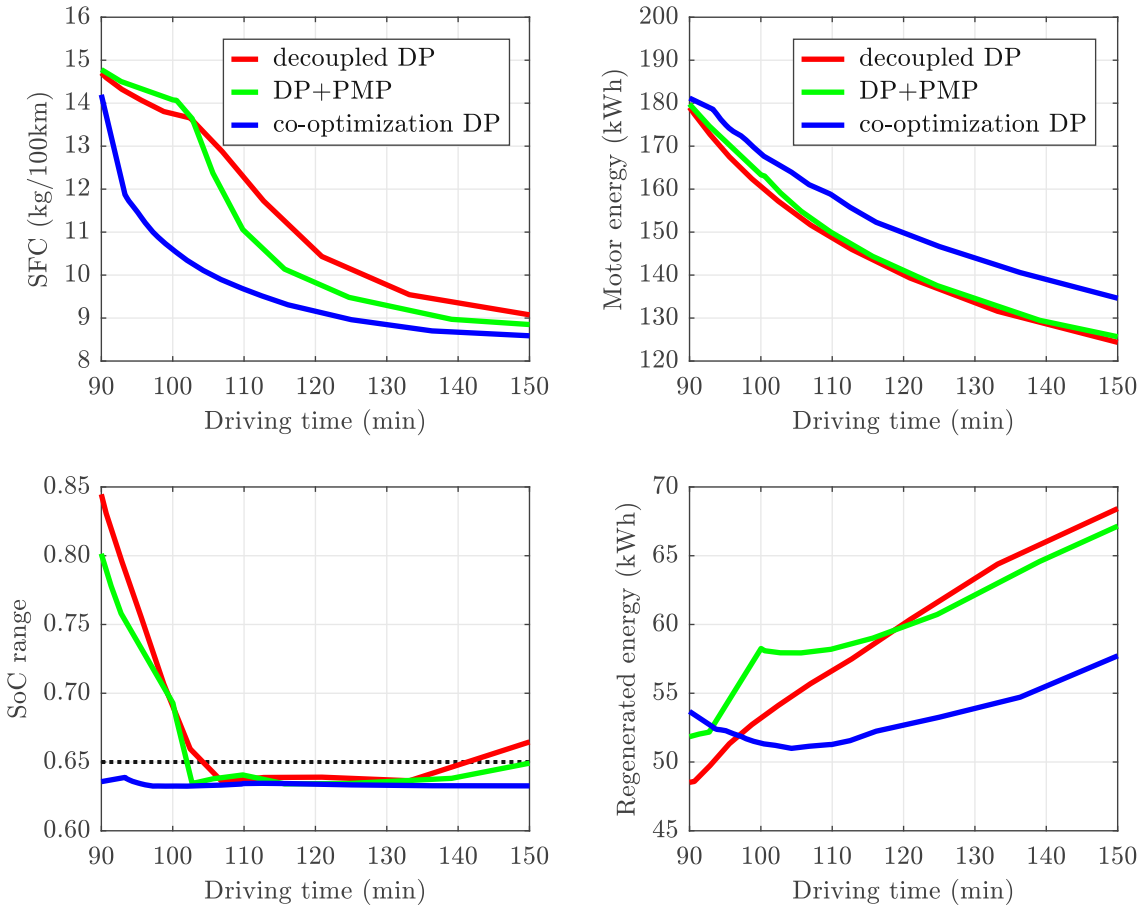

Figure 5.9: Effect of driving time on the key performance indicators for the different optimization approaches.

DP performs better. The reason is that DP+PMP does not consider the SoC constraints on the battery system. Indeed, the fuel consumption performance worsens for fast driving cycles when the SoC operating range cannot be kept within the desired operating range.

Table 5.5 compares the fuel consumption resulting from each optimization approach against the one obtained with the co-optimization DP for different driving time scenarios. The relative increase compared with the co-optimization is indicated with ΔSFC. In particular, the DP+PMP method has 5-33% higher fuel consumption than the co-optimization approach, the decoupled DP 10-32%, and the cruising DP 18-40%. These numbers demonstrate that the co-optimization of speed planning and energy management holds considerable potential for improving the fuel consumption of the vehicle and, consequently, its driving range. The benefits are generally higher at low driving times, i.e. for fast driving cycles, due to the higher electric load demand.

Table 5.5: Fuel consumption comparison between the investigated methods for at different driving times.

Driving time (min)	co-optimization DP	DP+PMP	decoupled DP	cruising DP
	SFC (kg/100 km)	ΔSFC (%)	ΔSFC (%)	ΔSFC (%)
95	11.48	25	23	24
100	10.60	33	30	31
105	10.05	26	32	37
110	9.67	14	27	40
115	9.37	9	21	38
120	9.16	7	15	31
125	8.96	6	13	25
130	8.85	5	10	18

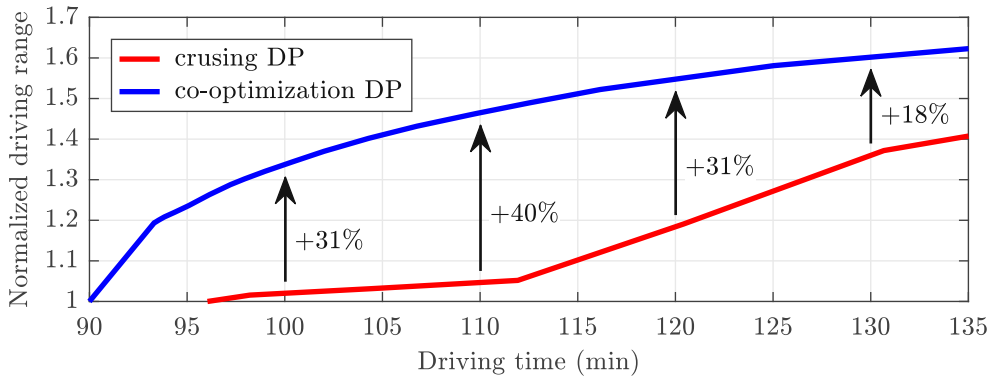

Figure 5.10: Comparison of driving range between the co-optimization DP and cruising DP.

Figure 5.10 reveals two compelling findings:

- First, it shows how the co-optimization DP increases the driving range if longer driving times are accepted. For example, going from 90 to 95 minutes (i.e. 5.6% longer driving time), the driving range is extended by 23%, which is an excellent improvement. The improvement is 60% for a driving time of 130 minutes. Therefore, considering that the hydrogen refueling infrastructure is currently undeveloped, the speed plan optimization holds considerable potential for the advancement of fuel cell electric trucks because it might make the difference between reaching the next closest refueling station or not.

- The second finding evident from Figure 5.10 is the enormous driving range improvement of the co-optimization approach compared with the constant-speed driving style. In particular, when the driving time is 110 minutes, the driving range is 40% higher for the co-optimization approach. It is particularly striking

that the cruising DP has a minimum improvement in driving range until the driving time reaches 112 minutes. This aspect demonstrates the enormous benefits of eco-driving for fuel cell electric trucks compared with the constant-speed driving style.

In conclusion, this section proposed a co-optimization approach for speed planning and energy management for fuel cell electric trucks on motorways routes. The significant benefits of the novel co-optimization compared with other approaches in the literature have been demonstrated. The next logical research direction is to include the fuel cell and battery degradation in the multi-objective function to exploit the advantages of the co-optimization approach even more. Additionally, the robustness against traffic conditions must be addressed to enable the real-world implementation of optimal eco-driving speed plans.

Chapter 6

Conclusion and Outlook

This thesis collects the most relevant methods and findings on predictive energy management of fuel cell electric trucks developed by the author during his doctoral studies. Even though the literature on energy management strategies for fuel cell electric vehicles is vast, the author conducted state-of-the-art investigations to address the significant research gap in studies focused on long-haul fuel cell trucks.

The results presented here confirm the enormous impact of energy management on fuel consumption and component degradation. Therefore, the thesis proposes innovative strategies that can foster the market penetration of fuel cell electric trucks by achieving better performance and lower ownership costs. The proposed strategies rely on dynamic programming, the only method that can ensure global optimal solutions to energy management problems.

The vehicle model described in Chapter 2 represents the basis for the optimal energy management strategies developed in this thesis. The component models derive from measurements available in literature or performed within the projects HyTruck and FC4HD, in which the author has been directly involved. Moreover, the real-world driving cycles described in this chapter enable a robust energy management design by representing realistic and diverse scenarios for performance validation.

Chapter 3 proposed a predictive energy management strategy based on dynamic programming, with the dual-stage control structure described in the author's works [60] and [65]. The methods and results presented in the works [57] and [58] are also included here as a basis for the robust design of the predictive energy management strategy. Eventually, the proposed strategy yields optimal performance even in challenging route topographies by considering the entire elevation profile for energy management optimization. Moreover, it favors the implementation of dynamic programming for real-time control, overcoming the well-known barriers of non-causality and high computational complexity.

Chapter 4 introduces a novel health-conscious energy management strategy that considers fuel cell and battery degradation as additional optimization targets. The results demonstrate that energy management can enormously reduce component degradation,

which is why the proposed strategy holds considerable potential for fostering the advancement of fuel cell electric trucks. The recent findings presented in this section will be collected in a future research article. Moreover, the high flexibility of the health-conscious energy management strategy in shifting between the optimization targets opens research directions on how to manage the degradation of the powertrain components to minimize the total cost of ownership of the vehicle.

Chapter 5 presents three innovative concepts to fully exploit the benefits of predictive energy management by establishing synergies with other control functions. These concepts aim at three major issues that are limiting the advancement of fuel cell electric trucks: low battery life due to poor thermal management, low fuel cell life due to start-up/shut-down cycles, and limited driving range due to high fuel consumption.

In particular, Section 5.1 described an energy management strategy that adapts to the battery temperature to improve its thermal management, adding considerable benefits in avoiding temperature peaks that accelerate degradation. The concept was already presented in the author's work [62] for a different battery thermal management system. Future research will be focused on predictive energy and thermal management co-optimization, continuing the work started here and in [72].

Section 5.2 presented a novel predictive strategy for the health-conscious activation of multi-module fuel cell systems, demonstrating significant benefits for mitigating fuel cell degradation in short, low-demanding, and even motorway driving cycles. This strategy can play a critical role in developing intelligent fuel cell electric trucks that optimally decide between battery-only, one-module, or two-module operation, depending on the expected driving scenarios. The findings presented in this section will be collected in a research article, also addressing the robustness against speed forecast uncertainties.

Section 5.3 described a novel method for speed planning and energy management co-optimization in fuel cell electric trucks. This new approach significantly improves the eco-driving strategy proposed in the author's work [64], where the optimization problem was simplified to reduce complexity. Here, the optimization results demonstrate that the eco-driving strategy can extend the driving range enormously compared with a standard constant-speed motorway cruising, which might be a solution to foster the advancement of fuel cell electric trucks. The findings presented in this section will be collected in a research article, including component degradation within the co-optimization targets and addressing the robustness against traffic conditions.

The main limitation of this thesis is that the proposed strategies were validated only in a simulation environment, meaning that the robustness to modeling uncertainties was not assessed. This limitation is dictated by the fact that significant financial investments and costs are required to test energy management strategies in fuel cell electric trucks. This issue is challenging to overcome because only a few companies have surpassed the prototype stages and are now on the market, meaning there are few opportunities for testing in actual vehicles. However, some of the predictive strategies presented in

this doctoral thesis will be validated on the fuel cell electric truck prototype under development in project FC4HD, finally overcoming the mentioned limitation.

Eventually, this thesis demonstrated that predictive and health-conscious energy management strategies could significantly contribute to the development of intelligent fuel cell electric trucks, holding considerable potential for performance improvements and cost reductions. The author proposed several innovative solutions to fully exploit the potential of energy management strategies, but there are still vast research prospects to further contribute to the advancement of fuel cell electric trucks and, thus, to the decarbonization of the long-haul transport sector.

Appendix A

Additional methods from the optimal control theory

This appendix is a supplement to Section 2.3. It continues the overview of optimal control theory, describing two methods widely used in the literature on energy management strategies: i.e. Pontryagin's minimum principle and model predictive control.

A.1 Pontryagin's minimum principle

Pontryagin's minimum principle is a set of necessary (but not sufficient) conditions for optimality. A control policy that meets these conditions is called *extremal*. Even though all optimal solutions are also extremal, the opposite is generally not true. Therefore, contrary to DP, PMP does not ensure the global optimality of the control law, which is why it is usually considered a sub-optimal solution. However, if the Hamiltonian is convex, there is a unique extremal solution, which is then also optimal [95].

The Hamiltonian of the optimal control problem (2.31) is defined as:

$$H(x(t), u(t), z(t), \lambda(t)) = L(x(t), u(t), z(t)) + \lambda(t) \cdot f(x(t), u(t), z(t)) \ , \tag{A.1}$$

where λ is usually referred to as co-state or adjoint state variable, and $f(\cdot)$ expresses the state dynamics. Pontryagin's minimum principle states that the control law $u^*(t)$ is extremal if it minimizes the Hamiltonian at each instant. Therefore:

$$u^*(t) = \arg\min_{u(t)} \ H(x(t), u(t), z(t), \lambda(t)) \quad , \quad \forall t \in [0, t_{fin}] \quad . \tag{A.2}$$

Moreover, the state dynamics must satisfy the condition:

$$\dot{x}(t) = \left. \frac{\partial H}{\partial \lambda} \right|_{u^*} = f(x(t), u^*(t), z(t)) \ , \tag{A.3}$$

and the co-state dynamics:

$$\dot{\lambda}(t) = -\frac{\partial H}{\partial x}\bigg|_{u^*} = -\frac{\partial L}{\partial x} - \lambda \frac{\partial f}{\partial x} \ . \tag{A.4}$$

From a practical point of view, PMP can be used to design optimal controllers by minimizing the Hamiltonian to generate extremal controls as in (A.2).
The state variable follows the dynamics of (A.3) and must satisfy the boundary conditions included in (2.31) on the initial and final values. However, one of the main issues with implementing PMP is that the initial condition of the co-state variable, $\lambda(0)$, is unknown. This value significantly impacts the optimization results and, in particular, the final value of the state variable. A common approach in the literature [95] is to use a shooting method to solve the boundary value problem by iteratively changing $\lambda(0)$ until $x(t_{fin}) = x_{fin}$ is satisfied.

A.2 Model predictive control

In general, model predictive control refers to control strategies that optimize the control policy over a finite time horizon using a model of the system to predict its future outputs. For example, in Figure A.1, the inputs are manipulated before the output reference step to improve the system response. However, only the first element of the optimal control sequence is implemented. In the next timestep, the predictive horizon moves forward, and the optimization repeats. For this reason, MPC is also known as receding horizon control.

A standard MPC formulation considers a discrete linear state-space model, a quadratic cost function, and linear constraints. Such formulation has proven suitable to overcome the main drawback of MPC for real-time control applications: the high computational requirements to solve the optimization problem at each step. This thesis adopts the formulation from [148]. The discrete linear state-space model is:

$$x_{k+1} = Ax_k + B\Delta u_k + E\Delta z_k \ , \tag{A.5a}$$
$$y_k = Cx_k \ , \tag{A.5b}$$

where A, B, C, and E are the system matrices. The predictive outputs over the horizon can be expressed as a function of the control and disturbance increments, ΔU and ΔZ, as:

$$Y = Fx_k + \Phi_u \Delta U + \Phi_u \Delta Z \ , \tag{A.6}$$

where the matrices F, Φ_u, and Φ_z are defined as in [148]. Eventually, the quadratic cost function can be expressed as a function of ΔU:

$$J_h = (Y_{ref} - Y)^T Q (Y_{ref} - Y) + \Delta U^T R \ \Delta U, \tag{A.7}$$

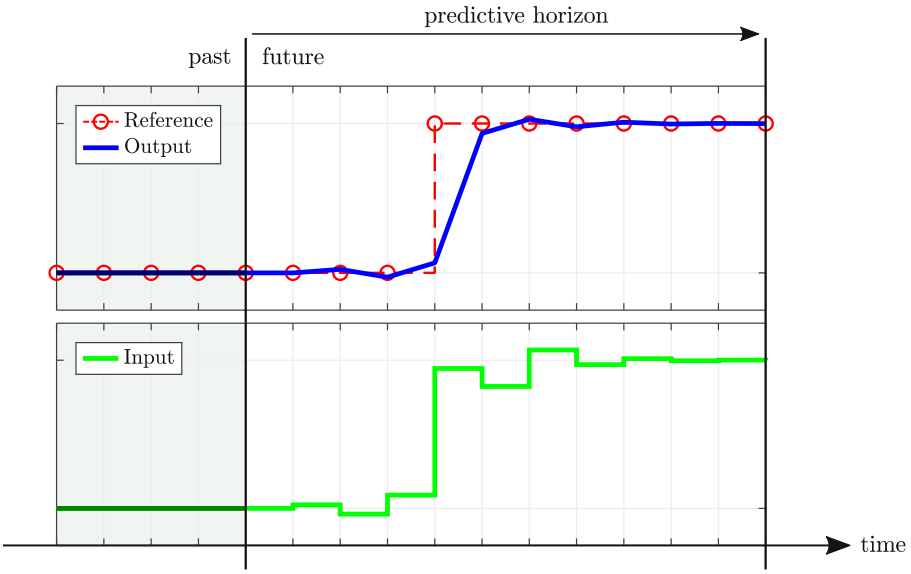

Figure A.1: Representation of the model predictive control principle.

where Y_{ref} are the output references over the horizon, Q and R are semi-positive defined weighting matrices. The optimization problem resulting can be solved using quadratic programming to minimize the horizon cost J_h:

$$\Delta U_{opt} = \arg\min_{\Delta U} \; J_h \quad , \quad \text{s.t.} \quad M\Delta U \leq \gamma \; . \tag{A.8}$$

where ΔU_{opt} defines the optimal control sequence, and M and γ express the linear constraints on outputs and inputs.

An important conclusion is that predictive energy management strategies with short-term horizons cannot yield optimal results. On the other hand, increasing the predictive horizon exceeds the real-time computational requirements for on-board vehicle control.

Appendix B

Additional results of offline and online strategies

This section describes supplementary energy management strategies to Chapter 3 for optimal fuel consumption and SoC control. First, it describes offline strategies based on dynamic programming and Pontryagin's minimum principle. Then, it describes online strategies based on simple heuristics and model predictive control.

B.1 Offline strategies for performance benchmark

The most used methods for offline energy management strategies are dynamic programming and Pontryagin's minimum principle. The literature has shown that for hybrid electric vehicles, PMP has similar performance to DP for fuel consumption optimization but has the advantage of being computationally faster [95].

This section shows that for optimal fuel consumption and SoC control of the fuel cell electric truck under investigation, the strategies are equivalent when the driving requirements are low. However, for high requirements (e.g. due to heavy loads on hilly routes), PMP does not yield global optimality as DP and cannot intrinsically deal with the SoC constraints.

B.1.1 Dynamic programming for energy management

Implementing dynamic programming for the energy management strategy requires complete and apriori knowledge of the driving cycle. Indeed, the electric load required to drive a specific driving cycle (deriving from the speed and elevation profiles) represents a disturbance in the optimal control problem for energy management and can be calculated following a backward-facing modeling approach.

In the energy management problem for fuel cell electric vehicles, there is only one state variable: the battery SoC. Moreover, assuming (3.1), the fuel cell system power is the only input variable. Therefore, to minimize the fuel consumption expressed in (3.2),

the optimal control problem (2.32) is rewritten as:

$$\min_{\{P_{fcs,1},\dots P_{fcs,N}\}} \sum_{k=1}^{N} \dot{m}_{\mathrm{H_2}}(P_{fcs,k})\ \Delta t \tag{B.1}$$

with the same constraints as in (3.5), but with discrete system dynamics expressed as:

$$\mathrm{SoC}_{k+1} = \mathrm{SoC}_k - \Delta t\ \frac{V_{oc,k} - \sqrt{V_{oc,k}^2 - 4\,P^*_{bat,k}\,R_{int,k}}}{2\ R_{int,k}\ Q_{bat,max}}\ . \tag{B.2}$$

The main difference compared to the optimization problem (3.5) is that the time interval and electric load in each stage are exactly known. Here, Δt is the spacing of the time grid of dynamic programming and is set to 0.2 seconds. The battery power in (B.2) depends on the fuel cell power (input variable) and the electric load (disturbance variable) as in (3.1). The open circuit voltage and internal resistance have the time subscript k because they depend on the SoC.

B.1.2 Pontryagin's minimum principle for energy management

Pontryagin's minimum principle is used to find the extremal controls that minimize the Hamiltonian. Following the theory described in Appendix A.1, the Hamiltonian of objective function (3.2) is expressed as:

$$H = \dot{m}_{\mathrm{H_2}} + \lambda \cdot \dot{\mathrm{SoC}}\ . \tag{B.3}$$

At each time step, the fuel cell power setpoint is the one that minimizes the Hamiltonian:

$$P^*_{fcs} = \arg\min_{P_{fcs}} H\ . \tag{B.4}$$

This method can consider the minimum and maximum limits on the fuel cell power during the minimization of the Hamiltonian (B.4). On the other hand, PMP cannot intrinsically deal with the SoC constraints but only artificially by augmenting the Hamiltonian with an additive penalty function [95, 149]. However, this thesis does not implement the penalty because it significantly hinders the fuel consumption optimization.

From a physical standpoint, the Hamiltonian can be interpreted as the sum of hydrogen consumption and the equivalent battery consumption, with the co-state variable representing an equivalence factor. The co-state variable dynamics are expressed as:

$$\dot{\lambda} = -\frac{\partial H}{\partial \mathrm{SoC}}\bigg|_{P^*_{fcs}}\ . \tag{B.5}$$

Note that the SoC rate of change in the Hamiltonian (B.3) depends on the SoC because of the open circuit voltage and the internal resistance (2.18), which have the characteristics depicted Figure 2.7b. The initial value of the co-state variable influences the final SoC. Usually, the initial co-state is iteratively changed until the SoC reaches the desired value at the end of the cycle. To do that, PMP requires complete and apriori knowledge of the driving cycle, which is why it is categorized as an offline strategy.

The energy management strategies based on Pontryagin's minimum principle and dynamic programming are compared considering two driving cycles. The first one has lower performance requirements because it is on a flat route and with a vehicle mass of 30 tons. In contrast, the second cycle is significantly more demanding because it is on a hilly route and with a vehicle mass of 35 tons. The simulation results are summarized in Table B.1 in terms of fuel consumption, average fuel cell efficiency, and final, minimum and maximum SoC values. It is important to note that the fuel consumption comparison is fair because PMP and DP yield the same final SoC. Moreover, the SoC and fuel cell power profiles are compared in Figures B.1 and B.2.

The strategies yield equivalent fuel consumption, SoC, and fuel cell power profiles for the flat route driving cycle. In this case, the SoC battery operating range is narrow because the route is flat. On the other hand, for the driving cycle on the hilly route, PMP results in 0.46% higher fuel consumption than DP. Thus, it does not correspond to the optimal solution. Moreover, the SoC operating range is significantly wider because of the hilly elevation profile. The higher fuel consumption is due to the battery operation at a lower SoC on average, where its efficiency is low.

It is important to note that the final SoC is 0.94 for the strategy based on PMP because of its incapability to deal with the SoC constraints. Indeed, using a different initial co-state value to obtain a lower final SoC leads to the complete discharge of the battery (SoC $= 0$), which is unfeasible. On the contrary, DP could be used to reach any final SoC because it can deal with the maximum and minimum constraints intrinsically within the optimization (as shown later).

Table B.1: Performance comparison between DP and PMP.

Driving cycle	EMS	Fuel consumption		Fuel cell	SoC		
		(kg/100 km)	deviation (%)	efficiency	final	min	max
flat route/30t	DP	8.73	-	0.530	0.76	0.58	0.76
	PMP	8.73	0.02	0.530	0.76	0.57	0.76
hilly route/35t	DP	9.73	-	0.524	0.94	0.30	0.94
	PMP	9.77	0.46	0.523	0.94	0.10	0.94

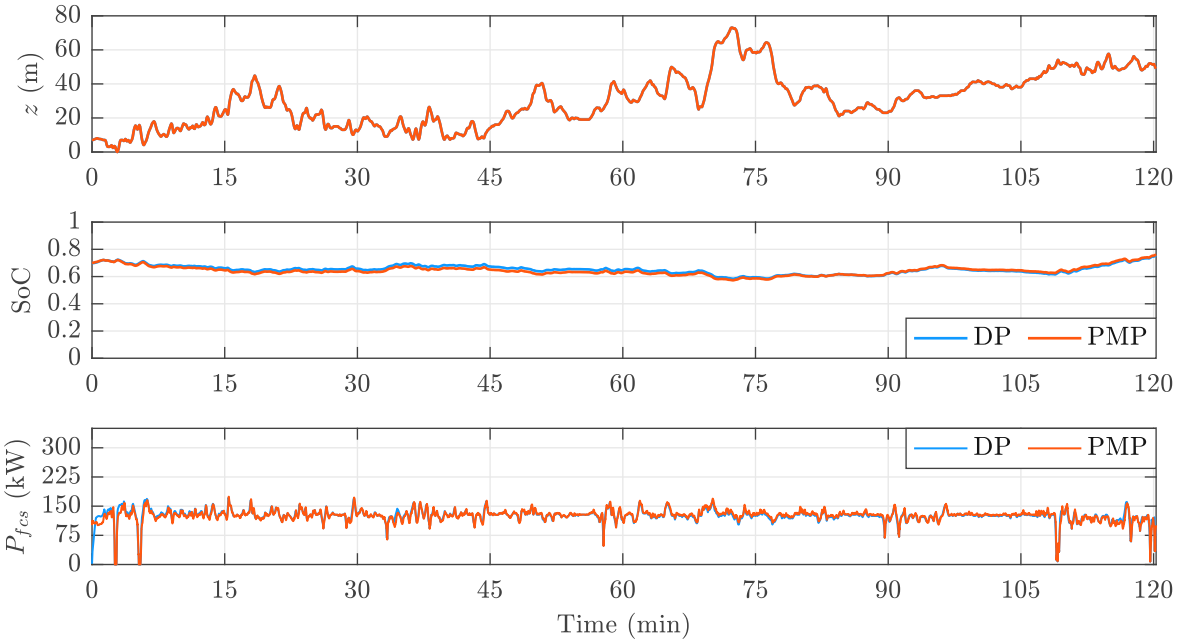

Figure B.1: Comparison of the energy management results between PMP and DP on the flat route driving cycle with vehicle mass of 30 tons.

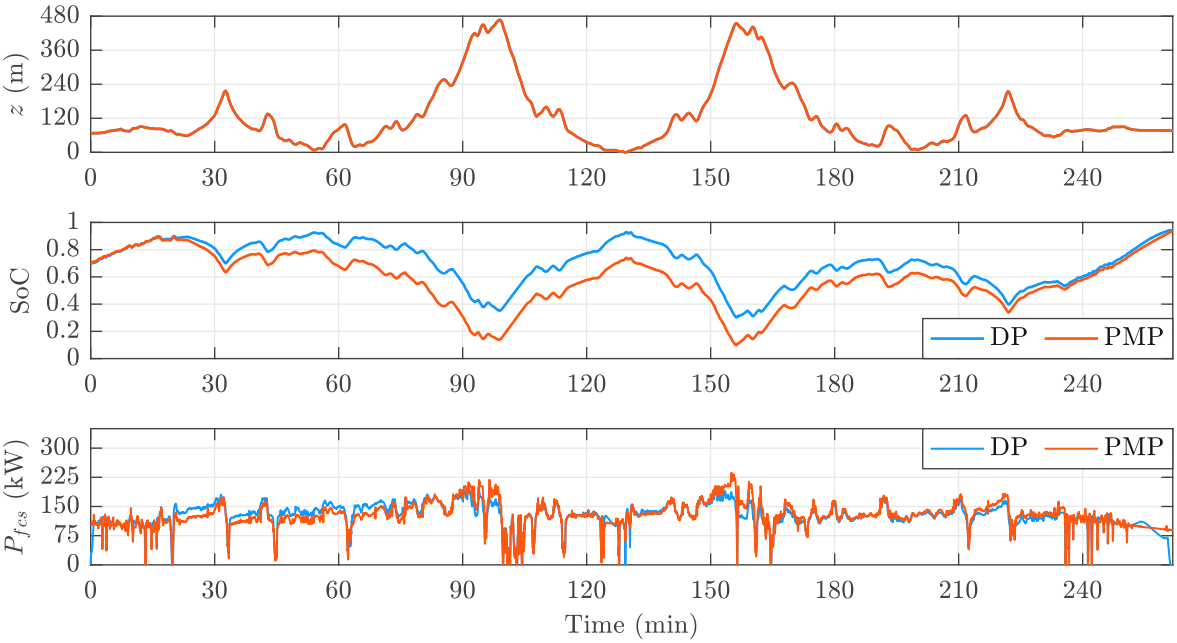

Figure B.2: Comparison of the energy management results between PMP and DP on the hilly route driving cycle with vehicle mass of 35 tons.

Eventually, dynamic programming is adopted in this thesis as the offline strategy for the performance benchmarks because it ensures optimal results for fuel consumption and SoC control.

B.2 Strategies for on-board control

This section describes and compares online two strategies with opposite characteristics: the first is a rule-based strategy based on simple heuristics, whereas the second is a model predictive control strategy deriving from the optimal control theory. The simulation results indicate that both strategies yield similar fuel consumption, even though their complexity is entirely different. Moreover, the comparison with DP shows that both strategies are close to optimality for the low-demanding driving cycle, but the results are significantly worse for the more challenging one.

B.2.1 Rule-based strategy

The principle adopted for designing the heuristic control strategy is to operate the fuel cell as close as possible to the maximum efficiency point, which corresponds to the power: $P_{fcs,\eta} = 74$ kW (see Figure 2.4). However, if the fuel cell system always operates at that operating point, the battery would be completely depleted because the average load of heavy-duty vehicles is significantly higher. To cope with this issue, the rule-based energy management strategy defines the fuel cell power setpoint as:

$$P^*_{fcs} = P_{fcs,\eta} + r_1 \left(P_{el,des} - P_{fcs,\eta}\right) + r_2 \left(\mathrm{SoC}_{des} - \mathrm{SoC}\right) . \tag{B.6}$$

The second term on the right-hand side considers the deviation between the desired load and the maximum efficiency power. The third term considers the deviation between the SoC and its desired value. In this way, if the battery charge is too low, the fuel cell increases its power to recharge it. Additionally, the fuel cell power setpoint is subject to the following constraints:

$$|\dot{P}^*_{fcs}| \leq r_3 , \tag{B.7a}$$

$$0 \leq P^*_{fcs} \leq P_{fcs,max} . \tag{B.7b}$$

The parameters r_1, r_2, and r_3 largely influence the performance of the RB strategy. For example, if $r_1 = 1$, the fuel cell operates in *power-following* mode, which generally results in high fuel consumption. On the other hand, if $r_1 = 0$ and the electric loads are high, there is a higher risk of complete battery charge depletion. For high values of r_2, the EMS will try to keep the battery charge as close as possible to the desired value, generally resulting in high fuel consumption. However, if r_2 is too low, there is a higher risk that the battery overcharges or completely depletes. The parameter r_3 serves as a filter for the high-frequency loads, which are generally detrimental to

fuel cell degradation and efficiency. Here, it is assumed that $\mathrm{SoC}_{des} = 0.70$, $r_1 = 0.2$, $r_2 = 400$ kW, and $r_3 = 9$ kW/s.

B.2.2 Model predictive control strategy with short-term forecasts

Over the last decades, several model predictive control applications have been implemented in the industry achieving substantial performance improvement, especially in process engineering. The standard MPC formulation considers a discrete linear state-space model, a quadratic cost function, and linear constraints, as described in Appendix A.2. This section formulates an MPC for optimal energy management, similar to the author's previous works in [57] and [58].

Since the MPC relies on receding horizon optimizations, ensuring a suitably low complexity for real-time control is usually challenging. For this reason, the strategy proposed here considers short-term electric load forecasts. In particular, it is assumed that the sampling time of the system is 1 second and that the predictive horizon is 10 seconds. Under these assumptions, there is an optimization instance every second, requiring a computational time of 10 ms to be solved. On the other, if the predictive horizon was 300 seconds, each optimization instance would require 10 seconds, which would violate real-time control requirements. For simplicity, it is assumed that the electric load forecast is certain.

The objective function of the MPC is expressed considering quadratic terms as follows:

$$J_{mpc} = \sum_{k=1}^{10} m_1 \left(\mathrm{SoC}_{des} - \mathrm{SoC}_{k+1}\right)^2 + m_2 \left(P_{fcs,\eta} - P_{fcs,\,k}\right)^2 + m_3 \, \Delta P_{fcs,\,k}^2 \ , \tag{B.8}$$

where the first term aims at being close to the desired SoC reference, the second at maximizing fuel cell efficiency, and the third at limiting the fuel cell transients. Here, m_1, m_2, and m_3 are weighting parameters set as 10^2, 10^{-11}, and 10^{-11}, respectively.

The discrete linear state-space model is expressed as:

$$\underbrace{\begin{bmatrix} \mathrm{SoC}_{k+1} \\ P_{fcs,\,k} \\ P_{bat,\,k} \end{bmatrix}}_{x^*_{k+1}} = \underbrace{\begin{bmatrix} 1 & 0 & 0 \\ 0 & 0 & 0 \\ 0 & 0 & 0 \end{bmatrix}}_{A_m} \underbrace{\begin{bmatrix} \mathrm{SoC}_{k} \\ P_{fcs,\,k-1} \\ P_{bat,\,k-1} \end{bmatrix}}_{x^*_{k}} + \underbrace{\begin{bmatrix} \theta \\ 1 \\ -1 \end{bmatrix}}_{B_m} \underbrace{\begin{bmatrix} P_{fcs,\,k} \end{bmatrix}}_{u_k} + \underbrace{\begin{bmatrix} -\theta \\ 0 \\ 1 \end{bmatrix}}_{E_m} \underbrace{\begin{bmatrix} P_{el,des,\,k} \end{bmatrix}}_{z_k} \tag{B.9}$$

considering the SoC, fuel cell power, and battery power as state variables. In this case, the discrete SoC dynamics shown in (B.2) are expressed in linear form by defining: $\theta = (V_{oc,k}\ Q_{bat,max})^{-1}$. Moreover, linear constraints on the maximum and minimum values are applied for all the states.

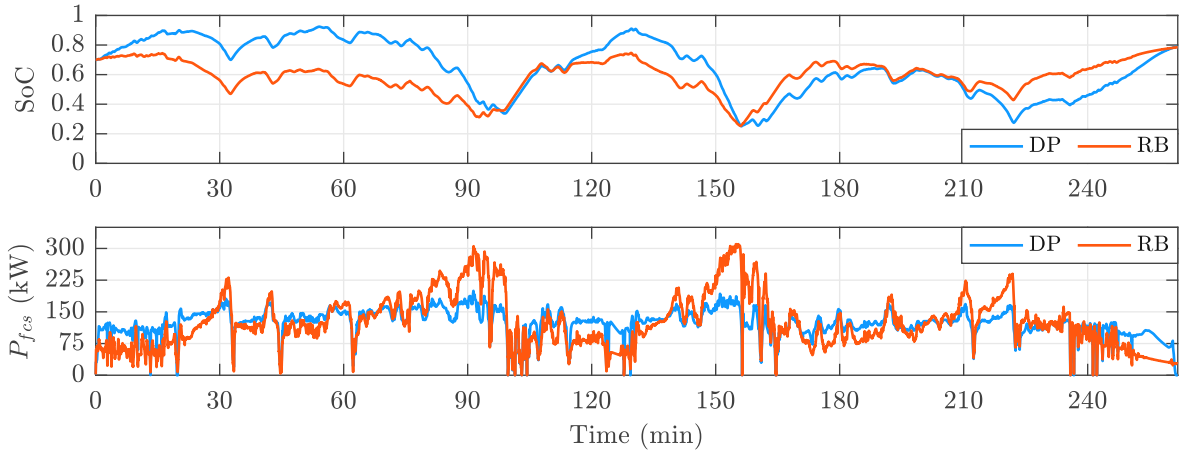

Figure B.3: Comparison between RB and DP on the hilly route driving cycle.

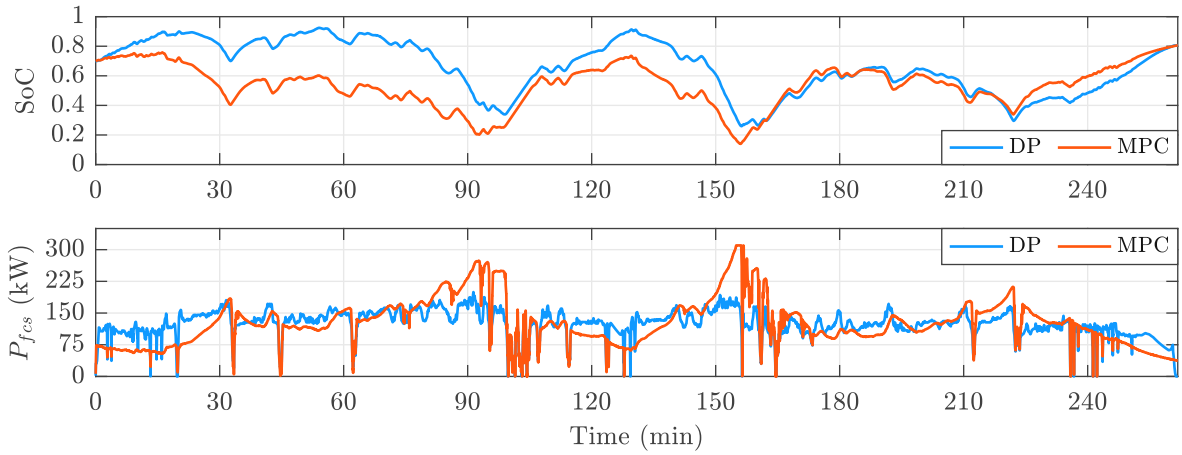

Figure B.4: Comparison between MPC and DP on the hilly route driving cycle.

The RB and MPC energy management strategies are analyzed considering the hilly-route driving cycle with a vehicle mass of 35 tons. Each strategy is compared against the dynamic programming solution that yields the same final SoC. The SoC and fuel cell power profiles are compared in Figures B.3 and B.4. Contrary to dynamic programming, both strategies operate the FCS at maximum power after minute 150 to restore the desired SoC after the uphill section of the route, greatly hindering fuel cell efficiency. The main difference between the RB and MPC strategies is that the latter has a much smoother fuel cell power profile due to the last term in the objective function (B.8).

The simulation results are summarized in Table B.2 in terms of fuel consumption, average fuel cell efficiency, and final, minimum and maximum SoC values. The table also includes the simulation results for the flat-route driving cycle. The table indicates that both strategies yield similar fuel consumption, even though their complexity is en-

Table B.2: Performance comparison between RB and MPC strategies.

Driving cycle	EMS	Fuel consumption		Fuel cell	SoC		
		(kg/100 km)	deviation (%)	efficiency	final	min	max
flat route/30t	DP	8.67	-	0.532	0.65	0.51	0.72
	MPC	8.72	0.58	0.531	0.65	0.49	0.71
	DP	8.68	-	0.532	0.68	0.52	0.72
	RB	8.71	0.34	0.529	0.68	0.55	0.71
hilly route/35t	DP	9.69	-	0.525	0.80	0.26	0.92
	MPC	10.13	4.59	0.507	0.80	0.14	0.81
	DP	9.68	-	0.525	0.79	0.25	0.92
	RB	10.15	4.82	0.501	0.79	0.25	0.79

tirely different. Moreover, the comparison with dynamic programming shows that both strategies yield close-to-optimal results on the flat route because it is a low-demanding driving cycle. On the other hand, the results are significantly worse for the more challenging driving cycle on the hilly route.

Bibliography

[1] World Health Organization. Climate change and health. Online at: https://www.who.int/news-room/fact-sheets/detail/climate-change-and-health, October 2021.

[2] Marissa Moultak, Nic Lutseyand, and Dale Hall. Transitioning to zero-emission heavy-duty freight vehicles. In *The international council on clean transportation*. ICCT, September 2017.

[3] Eamonn Mulholland, Jacob Teter, Pierpaolo Cazzola, Zane McDonald, and Brian P. Ó Gallachóir. The long haul towards decarbonising road freight – a global assessment to 2050. *Applied Energy*, 216:678–693, April 2018.

[4] Zachary P. Cano, Dustin Banham, Siyu Ye, Andreas Hintennach, Jun Lu, Michael Fowler, and Zhongwei Chen. Batteries and fuel cells for emerging electric vehicle markets. *Nature Energy*, 3(4):279–289, April 2018.

[5] Ballard. Fuel cell electric trucks, solutions for zero-emission freight transport (brochure). Online at: https://online.flippingbook.com/view/933520, September 2022.

[6] David A. Cullen, K. C. Neyerlin, Rajesh K. Ahluwalia, Rangachary Mukundan, Karren L. More, Rodney L. Borup, Adam Z. Weber, Deborah J. Myers, and Ahmet Kusoglu. New roads and challenges for fuel cells in heavy-duty transportation. *Nature Energy*, 6(5):462–474, March 2021.

[7] James Kast, Ram Vijayagopal, John J. Gangloff, and Jason Marcinkoski. Clean commercial transportation: Medium and heavy duty fuel cell electric trucks. *International Journal of Hydrogen Energy*, 42(7):4508–4517, February 2017.

[8] James Kast, Geoffrey Morrison, John J. Gangloff, Ram Vijayagopal, and Jason Marcinkoski. Designing hydrogen fuel cell electric trucks in a diverse medium and heavy duty market. *Research in Transportation Economics*, 70:139–147, October 2018.

[9] Jiaze Yan, Ge Wang, Siyuan Chen, He Zhang, Jiaqi Qian, and Yuxuan Mao. Harnessing freight platforms to promote the penetration of long-haul heavy-duty hydrogen fuel-cell trucks. *Energy*, 254:124225, September 2022.

[10] Dong-Yeon Lee, Amgad Elgowainy, Andrew Kotz, Ram Vijayagopal, and Jason Marcinkoski. Life-cycle implications of hydrogen fuel cell electric vehicle technology for medium- and heavy-duty trucks. *Journal of Power Sources*, 393:217–229, July 2018.

[11] Lei Ren, Sheng Zhou, Tianduo Peng, and Xunmin Ou. Greenhouse gas life cycle analysis of china's fuel cell medium- and heavy-duty trucks under segmented usage scenarios and vehicle types. *Energy*, 249:123628, June 2022.

[12] María de las Nieves Camacho, Daniel Jurburg, and Martín Tanco. Hydrogen fuel cell heavy-duty trucks: Review of main research topics. *International Journal of Hydrogen Energy*, 47(68):29505–29525, August 2022.

[13] Christoph Küffner. Multi-level perspective for the development and diffusion of fuel cell heavy-duty trucks. *Transportation Research Part D: Transport and Environment*, 111:103460, October 2022.

[14] Kate Forrest, Michael Mac Kinnon, Brian Tarroja, and Scott Samuelsen. Estimating the technical feasibility of fuel cell and battery electric vehicles for the medium and heavy duty sectors in california. *Applied Energy*, 276:115439, October 2020.

[15] S. Mojtaba Lajevardi, Jonn Axsen, and Curran Crawford. Simulating competition among heavy-duty zero-emissions vehicles under different infrastructure conditions. *Transportation Research Part D: Transport and Environment*, 106:103254, May 2022.

[16] Romain Sacchi, Christian Bauer, and Brian L. Cox. Does size matter? the influence of size, load factor, range autonomy, and application type on the life cycle assessment of current and future medium- and heavy-duty vehicles. *Environmental Science & Technology*, 55(8):5224–5235, March 2021.

[17] California Fuel Cell Partnership. Fuel cell electric trucks: A vision for freight movement in california and beyond. Online at: https://www.prnewswire.com, July 2021.

[18] Scania. Scania takes part in hydrogen project. Online at: `https://www.scania.com/group/en/home/newsroom/news/2022/Scania-takes-part-in-hydrogen-project.html`, April 2022.

[19] Nikola Motor. Nikola announces strategic agreements with Bosch for fuel-cell manufacturing. Online at: https://nikolamotor.com, September 2021.

[20] Quantron. QHM FCEV: New standards in heavy long-distance transport. Online at: `https://www.quantron.net/en/q-truck/q-heavy/qhm-fcev/`, November 2022.

[21] Hyzon Motors. Hyzon hymax series: Built for your operations, without the emissions. Online at: https://www.hyzonmotors.com/vehicles/hyzon-hymax-series, November 2022.

[22] Hyundai. XCIENT fuel cell: Eco-friendly and still energy-efficient solution for transportation. Online at: https://trucknbus.hyundai.com/global/en/products/truck/xcient-fuel-cell, November 2022.

[23] Torsten Seibt. Mercedes GENH2 truck brennstoffzellen-lkw. Online at: https://www.auto-motor-und-sport.de, July 2022.

[24] Scania. Norwegian whole-saler ASKO puts hydrogen powered fuel cell electric scania trucks on the road. Online at: https://www.scania.com, January 2020.

[25] Volvo Trucks. Volvo Trucks showcases new zero-emissions truck. Online at: https://www.volvotrucks.com/en-en/news-stories/press-releases/2022/jun/volvo-trucks-showcases-new-zero-emissions-truck.html, June 2022.

[26] Project FC4HD. Heavy-Duty Fuel Cell Road Demonstrator founded by the Austrian Research Promotion Agency (FFG). Online at: https://www.wiva.at/project/fc4hd, 2021.

[27] Project HyTruck. Hydrogen Truck Austria founded by the Austrian Research Promotion Agency (FFG). Online at: https://www.wiva.at/project/hytruck, 2019.

[28] Lino Guzzella and Antonio Sciarretta. *Vehicle Propulsion Systems*. Springer Berlin Heidelberg, 2013.

[29] Wisdom Enang and Chris Bannister. Modelling and control of hybrid electric vehicles (a comprehensive review). *Renewable and Sustainable Energy Reviews*, 74:1210–1239, July 2017.

[30] Xueqin Lü, Yinbo Wu, Jie Lian, Yangyang Zhang, Chao Chen, Peisong Wang, and Lingzheng Meng. Energy management of hybrid electric vehicles: A review of energy optimization of fuel cell hybrid power system based on genetic algorithm. *Energy Conversion and Management*, 205:112474, February 2020.

[31] Teng Teng, Xin Zhang, Han Dong, and Qicheng Xue. A comprehensive review of energy management optimization strategies for fuel cell passenger vehicle. *International Journal of Hydrogen Energy*, February 2020.

[32] M. Kandidayeni, J.P. Trovão, M. Soleymani, and L. Boulon. Towards health-aware energy management strategies in fuel cell hybrid electric vehicles: A review. *International Journal of Hydrogen Energy*, 47(17):10021–10043, February 2022.

[33] Venkata KoteswaraRao Kasimalla, Naga Srinivasulu G., and Venkateswarlu Velisala. A review on energy allocation of fuel cell/battery/ultracapacitor for hybrid electric vehicles. *International Journal of Energy Research*, 42(14):4263–4283, July 2018.

[34] A. Ravey, B. Blunier, and A. Miraoui. Control strategies for fuel-cell-based hybrid electric vehicles: From offline to online and experimental results. *IEEE Transactions on Vehicular Technology*, 61(6):2452–2457, July 2012.

[35] K. Ettihir, L. Boulon, and K. Agbossou. Optimization-based energy management strategy for a fuel cell/battery hybrid power system. *Applied Energy*, 163:142–153, February 2016.

[36] Tom Fletcher, Rob Thring, and Martin Watkinson. An energy management strategy to concurrently optimise fuel consumption & PEM fuel cell lifetime in a hybrid vehicle. *International Journal of Hydrogen Energy*, 41(46):21503–21515, December 2016.

[37] Philipp Kemper, Philipp Rehlaender, Ulf Witkowski, and Andreas Schwung. Competitive evaluation of energy management strategies for hybrid electric vehicle based on real world driving. In *2017 European Modelling Symposium (EMS)*, pages 151–156. IEEE, November 2017.

[38] Daming Zhou, Alexandre Ravey, Ahmed Al-Durra, and Fei Gao. A comparative study of extremum seeking methods applied to online energy management strategy of fuel cell hybrid electric vehicles. *Energy Conversion and Management*, 151:778–790, November 2017.

[39] Ke Song, Huan Chen, Peimin Wen, Tao Zhang, Boqiang Zhang, and Tong Zhang. A comprehensive evaluation framework to evaluate energy management strategies of fuel cell electric vehicles. *Electrochimica Acta*, 292:960–973, December 2018.

[40] Meiling Yue, Samir Jemei, Rafael Gouriveau, and Noureddine Zerhouni. Review on health-conscious energy management strategies for fuel cell hybrid electric vehicles: Degradation models and strategies. *International Journal of Hydrogen Energy*, 44(13):6844–6861, March 2019.

[41] Yongqiang Wang, Scott J. Moura, Suresh G. Advani, and Ajay K. Prasad. Power management system for a fuel cell/battery hybrid vehicle incorporating fuel cell and battery degradation. *International Journal of Hydrogen Energy*, 44(16):8479–8492, March 2019.

[42] Zhumu Fu, Longlong Zhu, Fazhan Tao, Pengju Si, and Lifan Sun. Optimization based energy management strategy for fuel cell/battery/ultracapacitor hybrid

vehicle considering fuel economy and fuel cell lifespan. *International Journal of Hydrogen Energy*, 45(15):8875–8886, March 2020.

[43] Mehroze Iqbal, Haitham S. Ramadan, and Mohamed Becherif. Health-aware frequency separation method for online energy management of fuel cell hybrid vehicle considering efficient urban utilization. *International Journal of Hydrogen Energy*, 46(29):16030–16047, April 2021.

[44] Robert Luca, Michael Whiteley, Toby Neville, Paul R. Shearing, and Dan J.L. Brett. Comparative study of energy management systems for a hybrid fuel cell electric vehicle - a novel mutative fuzzy logic controller to prolong fuel cell lifetime. *International Journal of Hydrogen Energy*, 47(57):24042–24058, July 2022.

[45] Xiyun Li, Yujie Wang, Duo Yang, and Zonghai Chen. Adaptive energy management strategy for fuel cell/battery hybrid vehicles using pontryagin's minimal principle. *Journal of Power Sources*, 440:227105, November 2019.

[46] Xiaohua Wu, Xiaosong Hu, Xiaofeng Yin, Yiqiang Peng, and Volker Pickert. Convex programming improved online power management in a range extended fuel cell electric truck. *Journal of Power Sources*, 476:228642, November 2020.

[47] Yanbiao Feng, Qiang Liu, Yong Li, Jue Yang, and Zuomin Dong. Energy efficiency and CO2 emission comparison of alternative powertrain solutions for mining haul truck using integrated design and control optimization. *Journal of Cleaner Production*, 370:133568, October 2022.

[48] G. Di Ilio, P. Di Giorgio, L. Tribioli, G. Bella, and E. Jannelli. Preliminary design of a fuel cell/battery hybrid powertrain for a heavy-duty yard truck for port logistics. *Energy Conversion and Management*, 243:114423, September 2021.

[49] Kyle Simmons, Yann Guezennec, and Simona Onori. Modeling and energy management control design for a fuel cell hybrid passenger bus. *Journal of Power Sources*, 246:736–746, January 2014.

[50] Cong Geng, Xiaofei Jin, and Xin Zhang. Simulation research on a novel control strategy for fuel cell extended-range vehicles. *International Journal of Hydrogen Energy*, 44(1):408–420, January 2019.

[51] Qiuyi Guo, Zhiguo Zhao, Peihong Shen, and Peidong Zhou. Optimization management of hybrid energy source of fuel cell truck based on model predictive control using traffic light information. *Control Theory and Technology*, 17(4):309–324, November 2019.

[52] Xiaosong Hu, Changfu Zou, Xiaolin Tang, Teng Liu, and Lin Hu. Cost-optimal energy management of hybrid electric vehicles using fuel cell/battery health-aware

predictive control. *IEEE Transactions on Power Electronics*, 35(1):382–392, January 2020.

[53] Jinglai Wu, Nong Zhang, Dongkui Tan, Jiujian Chang, and Weilong Shi. A robust online energy management strategy for fuel cell/battery hybrid electric vehicles. *International Journal of Hydrogen Energy*, 45(27):14093–14107, May 2020.

[54] Qian Xun, Nikolce Murgovski, and Yujing Liu. Joint component sizing and energy management for fuel cell hybrid electric trucks. *IEEE Transactions on Vehicular Technology*, pages 1–1, 2022.

[55] Qian Xun, Nikolce Murgovski, and Yujing Liu. Chance-constrained robust co-design optimization for fuel cell hybrid electric trucks. *Applied Energy*, 320:119252, August 2022.

[56] Xiaokai Guo, Xianguo Yan, Zhi Chen, and Zhiyu Meng. Research on energy management strategy of heavy-duty fuel cell hybrid vehicles based on dueling-double-deep q-network. *Energy*, 260:125095, December 2022.

[57] Alessandro Ferrara, Michael Okoli, Stefan Jakubek, and Christoph Hametner. Energy management of heavy-duty fuel cell electric vehicles: Model predictive control for fuel consumption and lifetime optimization. *IFAC-PapersOnLine*, 53(2):14205–14210, 2020.

[58] Alessandro Ferrara, Stefan Jakubek, and Christoph Hametner. Energy management of heavy-duty fuel cell vehicles in real-world driving scenarios: Robust design of strategies to maximize the hydrogen economy and system lifetime. *Energy Conversion and Management*, 232:113795, March 2021.

[59] Alessandro Ferrara, Saeid Zendegan, Hans-Michael Koegeler, Sajin Gopi, Martin Huber, Johannes Pell, and Christoph Hametner. Calibration of adaptive energy management strategies for fuel cell trucks using real-world driving scenarios. In *International Simulation Conference*. AVL, June 2021.

[60] Saeid Zendegan, Alessandro Ferrara, Stefan Jakubek, and Christoph Hametner. Predictive battery state of charge reference generation using basic route information for optimal energy management of heavy-duty fuel cell vehicles. *IEEE Transactions on Vehicular Technology*, 70(12):12517–12528, December 2021.

[61] Alessandro Ferrara, Saeid Zendegan, Hans-Michael Koegeler, Sajin Gopi, Martin Huber, Johannes Pell, and Christoph Hametner. Optimal calibration of an adaptive and predictive energy management strategy for fuel cell electric trucks. *Energies*, 15(7):2394, March 2022.

[62] Alessandro Ferrara, Matthias Hütter, and Christoph Hametner. Adaptive energy management strategy to avoid battery temperature peaks in fuel cell electric trucks. *IFAC-PapersOnLine*, 55(24):311–316, 2022.

[63] Julian Kölbl, Alessandro Ferrara, and Christoph Hametner. Impact of energy management strategy calibration on component degradation and fuel economy of heavy-duty fuel cell vehicles. *IFAC-PapersOnLine*, 55(24):317–322, 2022.

[64] Alessandro Ferrara and Christoph Hametner. Eco-driving of fuel cell electric trucks: optimal speed planning combining dynamic programming and pontryagin's minimum principle. In *2022 IEEE 96th Vehicular Technology Conference (VTC2022-Fall)*. IEEE, September 2022.

[65] Alessandro Ferrara and Christoph Hametner. Cost-optimal design and energy management of fuel cell electric trucks. *International Journal of Hydrogen Energy*, January 2023.

[66] D. Ambuhl and L. Guzzella. Predictive reference signal generator for hybrid electric vehicles. *IEEE Transactions on Vehicular Technology*, 58(9):4730–4740, November 2009.

[67] Yongchang Du, Yue Zhao, Qinpu Wang, Yuanbo Zhang, and Huaicheng Xia. Trip-oriented stochastic optimal energy management strategy for plug-in hybrid electric bus. *Energy*, 115:1259–1271, November 2016.

[68] Daliang Shen, Liting Lu, and Steffen Müller. Utilization of predictive information to optimize driving and powertrain control of series hybrid vehicles. *Automotive and Engine Technology*, 2(1-4):39–47, March 2017.

[69] Huiying Liu, Yongming Yao, Jie Wang, Yutong Qin, and Tianyu Li. A control architecture to coordinate energy management with trajectory tracking control for fuel cell/battery hybrid unmanned aerial vehicles. *International Journal of Hydrogen Energy*, March 2022.

[70] Alessandro Ferrara and Christoph Hametner. Rule-based energy management strategy of fuel cell/ultracapacitor/battery vehicles: winner of the IEEE VTS motor vehicles challenge 2020. In *2020 IEEE Vehicle Power and Propulsion Conference (VPPC)*. IEEE, November 2020.

[71] Alessandro Ferrara and Christoph Hametner. Impact of energy management strategies on hydrogen consumption and start-up/shut-down cycles in fuel cell-ultracapacitor-battery vehicles. *IEEE Transactions on Vehicular Technology*, 71(6):5692–5703, June 2022.

[72] Banu Cicek Büyüker, Alessandro Ferrara, and Christoph Hametner. Predictive battery cooling in heavy-duty fuel cell electric vehicles. *IFAC-PapersOnLine*, 55(24):304–310, 2022.

[73] G. Mohan, F. Assadian, and S. Longo. Comparative analysis of forward-facing models vs backward-facing models in powertrain component sizing. In *Hybrid and Electric Vehicles Conference 2013 (HEVC 2013)*. Institution of Engineering and Technology, 2013.

[74] Jay T. Pukrushpan, Huei Peng, and Anna G. Stefanopoulou. Control-oriented modeling and analysis for automotive fuel cell systems. *Journal of Dynamic Systems, Measurement, and Control*, 126(1):14–25, March 2004.

[75] Linhao Fan, Guobin Zhang, and Kui Jiao. Characteristics of PEMFC operating at high current density with low external humidification. *Energy Conversion and Management*, 150:763–774, October 2017.

[76] Julio Luna, Elio Usai, Attila Husar, and Maria Serra. Enhancing the efficiency and lifetime of a proton exchange membrane fuel cell using nonlinear model-predictive control with nonlinear observation. *IEEE Transactions on Industrial Electronics*, 64(8):6649–6659, August 2017.

[77] Bowen Wang, Kangcheng Wu, Zirong Yang, and Kui Jiao. A quasi-2d transient model of proton exchange membrane fuel cell with anode recirculation. *Energy Conversion and Management*, 171:1463–1475, September 2018.

[78] Dominik Murschenhofer, Dominik Kuzdas, Stefan Braun, and Stefan Jakubek. A real-time capable quasi-2d proton exchange membrane fuel cell model. *Energy Conversion and Management*, 162:159–175, April 2018.

[79] Mohamed H.S. Bargal, Mohamed A.A. Abdelkareem, Qi Tao, Jing Li, Jianpeng Shi, and Yiping Wang. Liquid cooling techniques in proton exchange membrane fuel cell stacks: A detailed survey. *Alexandria Engineering Journal*, 59(2):635–655, April 2020.

[80] Peng Ren, Pucheng Pei, Yuehua Li, Ziyao Wu, Dongfang Chen, and Shangwei Huang. Degradation mechanisms of proton exchange membrane fuel cell under typical automotive operating conditions. *Progress in Energy and Combustion Science*, 80:100859, September 2020.

[81] Jian Zhao and Xianguo Li. A review of polymer electrolyte membrane fuel cell durability for vehicular applications: Degradation modes and experimental techniques. *Energy Conversion and Management*, 199:112022, November 2019.

[82] Rod Borup, Jeremy Meyers, Bryan Pivovar, Yu Seung Kim, Rangachary Mukundan, Nancy Garland, Deborah Myers, Mahlon Wilson, Fernando Garzon, David Wood, Piotr Zelenay, Karren More, Ken Stroh, Tom Zawodzinski, James Boncella, James E. McGrath, Minoru Inaba, Kenji Miyatake, Michio Hori, Kenichiro Ota, Zempachi Ogumi, Seizo Miyata, Atsushi Nishikata, Zyun Siroma, Yoshiharu Uchimoto, Kazuaki Yasuda, Ken ichi Kimijima, and Norio Iwashita. Scientific aspects of polymer electrolyte fuel cell durability and degradation. *Chemical Reviews*, 107(10):3904–3951, October 2007.

[83] Pucheng Pei, Qianfei Chang, and Tian Tang. A quick evaluating method for automotive fuel cell lifetime. *International Journal of Hydrogen Energy*, 33(14):3829–3836, July 2008.

[84] Josef C Meier, Carolina Galeano, Ioannis Katsounaros, Jonathon Witte, Hans J Bongard, Angel A Topalov, Claudio Baldizzone, Stefano Mezzavilla, Ferdi Schüth, and Karl J J Mayrhofer. Design criteria for stable pt/c fuel cell catalysts. *Beilstein Journal of Nanotechnology*, 5:44–67, January 2014.

[85] Alessandro Ferrara, Pierpaolo Polverino, and Cesare Pianese. Analytical calculation of electrolyte water content of a proton exchange membrane fuel cell for on-board modelling applications. *Journal of Power Sources*, 390:197–207, June 2018.

[86] Jorn M. Reniers, Grietus Mulder, and David A. Howey. Review and performance comparison of mechanical-chemical degradation models for lithium-ion batteries. *Journal of The Electrochemical Society*, 166(14):A3189–A3200, 2019.

[87] Christoph R. Birkl, Matthew R. Roberts, Euan McTurk, Peter G. Bruce, and David A. Howey. Degradation diagnostics for lithium ion cells. *Journal of Power Sources*, 341:373–386, February 2017.

[88] Ahmad Alyakhni, Loic Boulon, Jean-Michel Vinassa, and Olivier Briat. A comprehensive review on energy management strategies for electric vehicles considering degradation using aging models. *IEEE Access*, 9:143922–143940, 2021.

[89] Ying Wang, Zhi Zhou, Audun Botterud, Kaifeng Zhang, and Qia Ding. Stochastic coordinated operation of wind and battery energy storage system considering battery degradation. *Journal of Modern Power Systems and Clean Energy*, 4(4):581–592, October 2016.

[90] Bolun Xu, Alexandre Oudalov, Andreas Ulbig, Goran Andersson, and Daniel S. Kirschen. Modeling of lithium-ion battery degradation for cell life assessment. *IEEE Transactions on Smart Grid*, 9(2):1131–1140, March 2018.

[91] Alan Millner. Modeling lithium ion battery degradation in electric vehicles. In *2010 IEEE Conference on Innovative Technologies for an Efficient and Reliable Electricity Supply*. IEEE, September 2010.

[92] Richard E. Bellman. *Dynamic Programming*. Princeton University Press, December 2010.

[93] Simona Onori, Lorenzo Serrao, and Giorgio Rizzoni. Dynamic programming. In *SpringerBriefs in Electrical and Computer Engineering*, pages 41–49. Springer London, December 2015.

[94] Olle Sundstrom and Lino Guzzella. A generic dynamic programming matlab function. In *2009 IEEE International Conference on Control Applications*. IEEE, July 2009.

[95] Lorenzo Serrao, Simona Onori, and Giorgio Rizzoni. A comparative analysis of energy management strategies for hybrid electric vehicles. *Journal of Dynamic Systems, Measurement, and Control*, 133(3), March 2011.

[96] M. D. McKay, R. J. Beckman, and W. J. Conover. A comparison of three methods for selecting values of input variables in the analysis of output from a computer code. *Technometrics*, 21(2):239, May 1979.

[97] Sanyapong Petchrompo, David W. Coit, Alexandra Brintrup, Anupong Wannakrairot, and Ajith Kumar Parlikad. A review of pareto pruning methods for multi-objective optimization. *Computers & Industrial Engineering*, 167:108022, May 2022.

[98] Sanyapong Petchrompo, Anupong Wannakrairot, and Ajith Kumar Parlikad. Pruning pareto optimal solutions for multi-objective portfolio asset management. *European Journal of Operational Research*, 297(1):203–220, February 2022.

[99] Thomas Rudolf, Tobias Schurmann, Stefan Schwab, and Soren Hohmann. Toward holistic energy management strategies for fuel cell hybrid electric vehicles in heavy-duty applications. *Proceedings of the IEEE*, 109(6):1094–1114, June 2021.

[100] Liangfei Xu, Clemens David Mueller, Jianqiu Li, Minggao Ouyang, and Zunyan Hu. Multi-objective component sizing based on optimal energy management strategy of fuel cell electric vehicles. *Applied Energy*, 157:664–674, November 2015.

[101] M. Jain, C. Desai, and S.S. Williamson. Genetic algorithm based optimal powertrain component sizing and control strategy design for a fuel cell hybrid electric bus. In *2009 IEEE Vehicle Power and Propulsion Conference*. IEEE, September 2009.

[102] E. Tazelaar, Y. Shen, P.A. Veenhuizen, T. Hofman, and P.P.J. van den Bosch. Sizing stack and battery of a fuel cell hybrid distribution truck. *Oil & Gas Science and Technology – Revue d'IFP Energies nouvelles*, 67(4):563–573, July 2012.

[103] Xiaosong Hu, Nikolce Murgovski, Lars Mardh Johannesson, and Bo Egardt. Optimal dimensioning and power management of a fuel cell/battery hybrid bus via convex programming. *IEEE/ASME Transactions on Mechatronics*, 20(1):457–468, February 2015.

[104] Zunyan Hu, Jianqiu Li, Liangfei Xu, Ziyou Song, Chuan Fang, Minggao Ouyang, Guowei Dou, and Gaihong Kou. Multi-objective energy management optimization and parameter sizing for proton exchange membrane hybrid fuel cell vehicles. *Energy Conversion and Management*, 129:108–121, December 2016.

[105] Xiaohua Wu, Xiaosong Hu, Xiaofeng Yin, Lei Li, Zhaowei Zeng, and Volker Pickert. Convex programming energy management and components sizing of a plug-in fuel cell urban logistics vehicle. *Journal of Power Sources*, 423:358–366, May 2019.

[106] Tom Fletcher and Kambiz Ebrahimi. The effect of fuel cell and battery size on efficiency and cell lifetime for an l7e fuel cell hybrid vehicle. *Energies*, 13(22):5889, November 2020.

[107] Yanbiao Feng and Zuomin Dong. Integrated design and control optimization of fuel cell hybrid mining truck with minimized lifecycle cost. *Applied Energy*, 270:115164, July 2020.

[108] Shrihari D. Gaikwad and Prakash C. Ghosh. Sizing of a fuel cell electric vehicle: A pinch analysis-based approach. *International Journal of Hydrogen Energy*, 45(15):8985–8993, March 2020.

[109] Sebastian Wolff, Moritz Seidenfus, Matthias Brönner, and Markus Lienkamp. Multi-disciplinary design optimization of life cycle eco-efficiency for heavy-duty vehicles using a genetic algorithm. *Journal of Cleaner Production*, 318:128505, October 2021.

[110] Kyuhyun Sim, Ram Vijayagopal, Namdoo Kim, and Aymeric Rousseau. Optimization of component sizing for a fuel cell-powered truck to minimize ownership cost. *Energies*, 12(6):1125, March 2019.

[111] Niklas. How much does a tesla battery weigh? Online at: `https://weightofstuff.com/how-much-does-a-tesla-battery-weigh`, May 2022.

[112] Jeremy Diez. Advanced vehicle testing – baseline vehicle testing results: 2014 tesla model s 85 kwh. `https://avt.inl.gov/sites/default/files/pdf/fsev/fact2014teslamodels.pdf`, November 2015.

[113] Capgemini. FIT FOR NET-ZERO: 55 Tech Quests to accelerate Europe's recovery and pave the way to climate neutrality. https://www.capgemini.com/wp-content/uploads/2020/10/Net-zero-main-report-2020.pdf, October 2020.

[114] Adria Wilson, Gregory Kleen, and Dimitrios Papageorgopoulos. Fuel cell system cost - 2017. https://www.hydrogen.energy.gov/pdfs/17007_fuel_cell_system_cost_2017.pdf, November 2017.

[115] Logan Goldie-Scot. A behind the scenes take on lithium-ion battery prices. Online at: https://about.bnef.com, March 2019.

[116] Long Lam and Pavol Bauer. Practical capacity fading model for li-ion battery cells in electric vehicles. *IEEE Transactions on Power Electronics*, 28(12):5910–5918, December 2013.

[117] Muhammad Fahad Zia, Elhoussin Elbouchikhi, and Mohamed Benbouzid. Optimal operational planning of scalable DC microgrid with demand response, islanding, and battery degradation cost considerations. *Applied Energy*, 237:695–707, March 2019.

[118] M.A. Hannan, M.S.H. Lipu, A. Hussain, and A. Mohamed. A review of lithium-ion battery state of charge estimation and management system in electric vehicle applications: Challenges and recommendations. *Renewable and Sustainable Energy Reviews*, 78:834–854, October 2017.

[119] Weiping Diao, Saurabh Saxena, Bongtae Han, and Michael Pecht. Algorithm to determine the knee point on capacity fade curves of lithium-ion cells. *Energies*, 12(15):2910, July 2019.

[120] Zhen Song, Yue Pan, Huicui Chen, and Tong Zhang. Effects of temperature on the performance of fuel cell hybrid electric vehicles: A review. *Applied Energy*, 302:117572, November 2021.

[121] Thomas Miro Padovani, Maxime Debert, Guillaume Colin, and Yann Chamaillard. Optimal energy management strategy including battery health through thermal management for hybrid vehicles. *IFAC Proceedings Volumes*, 46(21):384–389, 2013.

[122] Mohammad Reza Amini, Jing Sun, and Ilya Kolmanovsky. Two-layer model predictive battery thermal and energy management optimization for connected and automated electric vehicles. In *2018 IEEE Conference on Decision and Control (CDC)*. IEEE, December 2018.

[123] Rajath Kantharaj and Amy M. Marconnet. Heat generation and thermal transport in lithium-ion batteries: A scale-bridging perspective. *Nanoscale and Microscale Thermophysical Engineering*, 23(2):128–156, February 2019.

[124] Manlio Valerio Morganti, Stefano Longo, Marko Tirovic, Chiu-Yueh Blaise, and Gregory Forostovsky. Multi-scale, electro-thermal model of NMC battery cell. *IEEE Transactions on Vehicular Technology*, 68(11):10594–10606, November 2019.

[125] Tianhong Wang, Qi Li, Xiaotong Wang, Weirong Chen, Elena Breaz, and Fei Gao. A power allocation method for multistack PEMFC system considering fuel cell performance consistency. *IEEE Transactions on Industry Applications*, 56(5):5340–5351, September 2020.

[126] Tianhong Wang, Qi Li, Liangzhen Yin, Weirong Chen, Elena Breaz, and Fei Gao. Hierarchical power allocation method based on online extremum seeking algorithm for dual-PEMFC/battery hybrid locomotive. *IEEE Transactions on Vehicular Technology*, 70(6):5679–5692, June 2021.

[127] Yu Yan, Qi Li, Weirong Chen, Wenqiang Huang, and Jiawei Liu. Hierarchical management control based on equivalent fitting circle and equivalent energy consumption method for multiple fuel cells hybrid power system. *IEEE Transactions on Industrial Electronics*, 67(4):2786–2797, April 2020.

[128] Tianhong Wang, Qi Li, Liangzhen Yin, and Weirong Chen. Hydrogen consumption minimization method based on the online identification for multi-stack PEMFCs system. *International Journal of Hydrogen Energy*, 44(11):5074–5081, February 2019.

[129] Su Zhou, Gang Zhang, Lei Fan, Jianhua Gao, and Fenglai Pei. Scenario-oriented stacks allocation optimization for multi-stack fuel cell systems. *Applied Energy*, 308:118328, February 2022.

[130] Mohammadreza Moghadari, Mohsen Kandidayeni, Loic Boulon, and Hicham Chaoui. Operating cost comparison of a single-stack and a multi-stack hybrid fuel cell vehicle through an online hierarchical strategy. *IEEE Transactions on Vehicular Technology*, pages 1–13, 2022.

[131] Alvaro Macias Fernandez, Mohsen Kandidayeni, Loic Boulon, and Hicham Chaoui. An adaptive state machine based energy management strategy for a multi-stack fuel cell hybrid electric vehicle. *IEEE Transactions on Vehicular Technology*, 69(1):220–234, January 2020.

[132] Jianhao Zhou, Jun Liu, Yuan Xue, and Yuhui Liao. Total travel costs minimization strategy of a dual-stack fuel cell logistics truck enhanced with artificial

potential field and deep reinforcement learning. *Energy*, 239:121866, January 2022.

[133] Xin Li, Zhiyu Shang, Fei Peng, Liwei Li, Yuanzhe Zhao, and Zhixiang Liu. Increment-oriented online power distribution strategy for multi-stack proton exchange membrane fuel cell systems aimed at collaborative performance enhancement. *Journal of Power Sources*, 512:230512, November 2021.

[134] Caizhi Zhang, Tao Zeng, Qi Wu, Chenghao Deng, Siew Hwa Chan, and Zhixiang Liu. Improved efficiency maximization strategy for vehicular dual-stack fuel cell system considering load state of sub-stacks through predictive soft-loading. *Renewable Energy*, 179:929–944, December 2021.

[135] Arash Khalatbarisoltani, Mohsen Kandidayeni, Loic Boulon, and Xiaosong Hu. Power allocation strategy based on decentralized convex optimization in modular fuel cell systems for vehicular applications. *IEEE Transactions on Vehicular Technology*, 69(12):14563–14574, December 2020.

[136] J. I. Huertas, J. Díaz, M. Giraldo, D. Cordero, and L. M. Tabares. Eco-driving by replicating best driving practices. *International Journal of Sustainable Transportation*, 12(2):107–116, June 2017.

[137] Antonio Sciarretta, Giovanni De Nunzio, and Luis Leon Ojeda. Optimal Ecodriving Control: Energy-Efficient Driving of Road Vehicles as an Optimal Control Problem. *IEEE Control Systems*, 35(5):71–90, 2015.

[138] Nan Xu, Xiaohan Li, Qiao Liu, and Di Zhao. An overview of eco-driving theory, capability evaluation, and training applications. *Sensors*, 21(19):6547, September 2021.

[139] Erik Hellström, Maria Ivarsson, Jan äslund, and Lars Nielsen. Look-ahead control for heavy trucks to minimize trip time and fuel consumption. *IFAC Proceedings Volumes*, 40(10):439–446, 2007.

[140] Benjamin Passenberg, Peter Kock, and Olaf Stursberg. Combined time and fuel optimal driving of trucks based on a hybrid model. In *2009 European Control Conference (ECC)*. IEEE, August 2009.

[141] Nalin Kumar Sharma, Ahad Hamednia, Nikolce Murgovski, Esteban R. Gelso, and Jonas Sjoberg. Optimal eco-driving of a heavy-duty vehicle behind a leading heavy-duty vehicle. *IEEE Transactions on Intelligent Transportation Systems*, 22(12):7792–7803, December 2021.

[142] Dac Viet Ngo, Theo Hofman, Maarten Steinbuch, and Alex F A Serrarens. An optimal control-based algorithm for hybrid electric vehicle using preview route

information. In *Proceedings of the 2010 American Control Conference*. IEEE, June 2010.

[143] D. Maamria, K. Gillet, G. Colin, Y. Chamaillard, and C. Nouillant. Computation of eco-driving cycles for hybrid electric vehicles: Comparative analysis. *Control Engineering Practice*, 71:44–52, February 2018.

[144] Di Chen, Youngki Kim, Mike Huang, and Anna Stefanopoulou. An iterative and hierarchical approach to co-optimizing the velocity profile and power-split of plug-in hybrid electric vehicles. In *2020 American Control Conference (ACC)*. IEEE, July 2020.

[145] Youngki Kim, Miriam Figueroa-Santos, Niket Prakash, Stanley Baek, Jason B. Siegel, and Denise M. Rizzo. Co-optimization of speed trajectory and power management for a fuel-cell/battery electric vehicle. *Applied Energy*, 260:114254, February 2020.

[146] Zhigen Nie, Yuan Jia, Wanqiong Wang, Zheng Chen, and Rachid Outbib. Co-optimization of speed planning and energy management for intelligent fuel cell hybrid vehicle considering complex traffic conditions. *Energy*, 247:123476, May 2022.

[147] Xiaodong Wei, Jianghao Leng, Chao Sun, Weiwei Huo, Qiang Ren, and Fengchun Sun. Co-optimization method of speed planning and energy management for fuel cell vehicles through signalized intersections. *Journal of Power Sources*, 518:230598, January 2022.

[148] Liuping Wang. *Model Predictive Control System Design and Implementation Using MATLAB®*. Springer London, 2009.

[149] Simona Onori and Laura Tribioli. Adaptive pontryagin's minimum principle supervisory controller design for the plug-in hybrid GM chevrolet volt. *Applied Energy*, 147:224–234, June 2015.